




Fast QSC solver: tool for systematic study of $\mathcal{N} = 4$ Super-Yang-Mills spectrum

Nikolay Gromov ^a, Árpád Hegedűs,^b Julius Julius ^a and Nika Sokolova ^a

^a*Department of Mathematics, King's College London,
Strand, London WC2R 2LS, U.K.*

^b*Institute for Particle and Nuclear Physics, HUN-REN Wigner Research Centre for Physics,
H-1525 Budapest 114, P.O.B. 49, Hungary*

E-mail: nikolay.gromov@kcl.ac.uk, hegedus.arpad@wigner.hun-ren.hu,
julius.julius@kcl.ac.uk, nika.sokolova@kcl.ac.uk

ABSTRACT: Integrability methods give us access to a number of observables in the planar $\mathcal{N} = 4$ SYM. Among them, the Quantum Spectral Curve (QSC) governs the spectrum of anomalous dimensions. Low lying states were successfully studied in the past using the QSC. However, with the increased demand for a systematic study of a large number of states for various applications, there is a clear need for a fast QSC solver which can easily access a large number of excited states. Here, we fill this gap by developing a new algorithm and applied it to study all 219 states with the bare dimension $\Delta_0 \leq 6$ in a wide range of couplings.

The new algorithm has an improved performance at weak coupling and allows to glue numerics smoothly the available perturbative data, resolving the previous obstruction. Further ~ 8 -fold efficiency gain comes from C++ implementation over the best available `Mathematica` implementation. We have made the code and the data to be available via a [GitHub](#) repository.

The method is generalisable for non-local observables as well as for other theories such as deformations of $\mathcal{N} = 4$ SYM and ABJM. It may find applications in the separation of variables and bootstrability approaches to the correlation functions. Some applications to correlators at strong coupling are also presented.

KEYWORDS: Integrable Field Theories, Nonperturbative Effects, Scale and Conformal Symmetries, Supersymmetric Gauge Theory

ARXIV EPRINT: [2306.12379](https://arxiv.org/abs/2306.12379)

Contents

1	Introduction	1
2	Local operators and quantum numbers	4
3	QSC: A practical user's manual	7
3.1	Generalities	8
3.2	Types of states and discrete symmetries	13
4	Setting up the numerical problem	14
4.1	Basics	14
4.2	Closing the system: Newton method for harmonics on the cut	17
4.3	Details of the numerical procedure for different types of states	19
5	C++ implementation	23
5.1	Fast QSC solver: user manual	23
5.2	Management of the parameters, precision control and extrapolation	29
5.3	Examples of parameters and benchmarking	30
6	Data analysis at strong coupling	31
6.1	Strong coupling analysis of the numerical data	33
6.2	Counting of states and Kaluza-Klein towers	37
6.3	Bootstrability	39
7	Conclusion	44
A	Spectral data for all states in planar $\mathcal{N} = 4$ SYM with $\Delta_0 \leq 6$	45
B	Conversion to the left-right symmetric form	51
C	One-loop spectrum of $\mathfrak{sl}(2)$ sector and mode numbers	53
D	Counting of states at higher δ	55
D.1	States with $\delta = 2$	55
D.2	States with $\delta = 3$	56

1 Introduction

The spectrum of planar $\mathcal{N} = 4$ Super-Yang-Mills (SYM) theory is the most studied non-protected observable. Yet only a handful of states are available in the literature [1–11]. Recently, new methods became available which utilise a combination of the conformal bootstrap techniques with the insights from integrability to obtain observables beyond the spectrum [12–15]. The information about the non-perturbative spectrum combined with the conformal bootstrap method is already shown to give very accurate bounds on the structure constants in some examples [12, 13].

The non-perturbative spectrum can only be studied numerically, except for some limiting cases, such as in the near-BPS regime [2, 3, 8, 16] or in the limit of infinitely long operators, using the Asymptotic Bethe Ansatz (ABA) [17, 18]. There is very little chance of an exact analytic expression for all states in the theory, which is already quite clear from the cumbersome structure of the weak coupling expansion for the states which are tractable analytically [10, 11].

The numerical methods to tackle the non-perturbative spectrum of short operators was pioneered in [1] on the example of the simplest non-trivial Konishi operator, and was based on the infinite set of integral equations called the Thermodynamic Bethe Ansatz (TBA). The TBA based approach has a number of problems: the linear convergence rate, high computational cost, and finally going beyond the simplest set of operators was proven to be complicated [19]. With the discovery of the Quantum Spectral Curve (QSC) [20, 21], which is a finite system of equations, both analytic techniques [10, 11, 22–25] and numerical methods [9, 26] were developed to go well beyond the state of the art of what was possible at the level of TBA.

In this paper we take the previous developments of the numerical approaches to the non-perturbative spectrum to an industrial level. By adding new ideas to improve its performance at weak coupling, where the perturbative data is readily available [11], to start up the numerics for a huge number of states, and by using fast C++ implementation of our new algorithm. We computed all 219 states with bare dimension $\Delta_0 \leq 6$ on one PC (with two multi-core CPUs) in a timescale of a few months, which also included the time for adjusting our algorithm.

We make the data and the code available via [GitHub](#) keeping in mind that it can be modified to be applicable for a variety of situations: this may include the Regge complex-spin trajectories [16, 27], boundary problems such as Wilson defects [12, 28–34], other theories such as ABJM [35–40] or AdS₃ — where the QSC was recently proposed [41, 42] and solved numerically for some type of states [43], as well as various deformations, such as β -deformation [44, 45], γ -deformation [46, 47] or η -deformation [48, 49], or to calculate the Hagedorn temperature non-perturbatively [50–52]. We hope our code would be beneficial for the communities studying these systems.

Details on the results. In addition to making the source code available via [GitHub](#) on <https://GitHub.com/julius-julius/qsc> alongside the additional tools to test the C++ compilation, to generate the starting points and to control the parameters during the run. We also generated and share the following data: for the 45 states with additional symmetries we computed the spectrum in the range $g = [0, 5]$ ($\lambda \in [0, \sim 4000]$). Their spectral plot is given in figure 2. For some selected states in a wider range e.g. for Konishi operator we have the data in much wider range $g \in [0, 13]$. Then for 92 the operators with less symmetries we considered smaller range $g \in [0, 2]$. These are plotted in figure 3(a). Finally for the most complicated 82 operators we currently have $g \in [0, 1]$,¹ which we plan to expand later. They are plotted in figure 3(b). The full spectrum of planar $\mathcal{N} = 4$ SYM, for all states with bare dimension $\Delta_0 \leq 6$, in the range $g \in [0, 1]$ is plotted in figure 1.

¹The state ${}_6[0\ 2\ 2\ 2\ 2\ 2\ 2\ 0]_{6,7}$ is computed in the range $g = [0, 0.746875]$. This state will be updated.

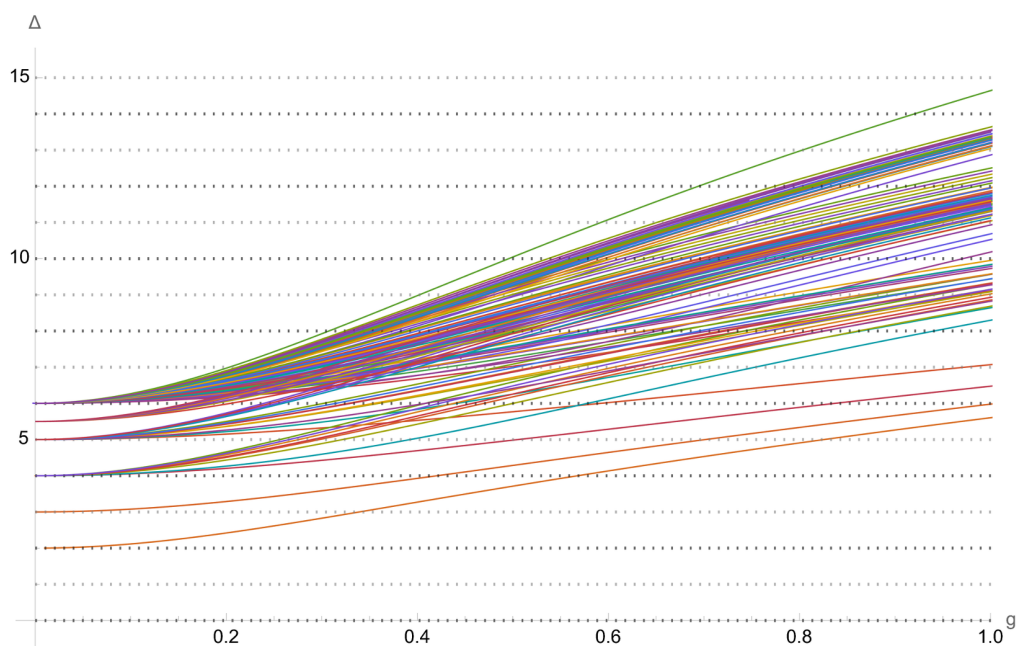


Figure 1. The scaling dimension of all 219 states in $\mathcal{N} = 4$ SYM, with bare dimension $\Delta_0 \leq 6$ in the range $g \in [0, 1]$ or 't Hooft coupling $\lambda \in [0, 16 \pi^2] \sim [0, 158]$.

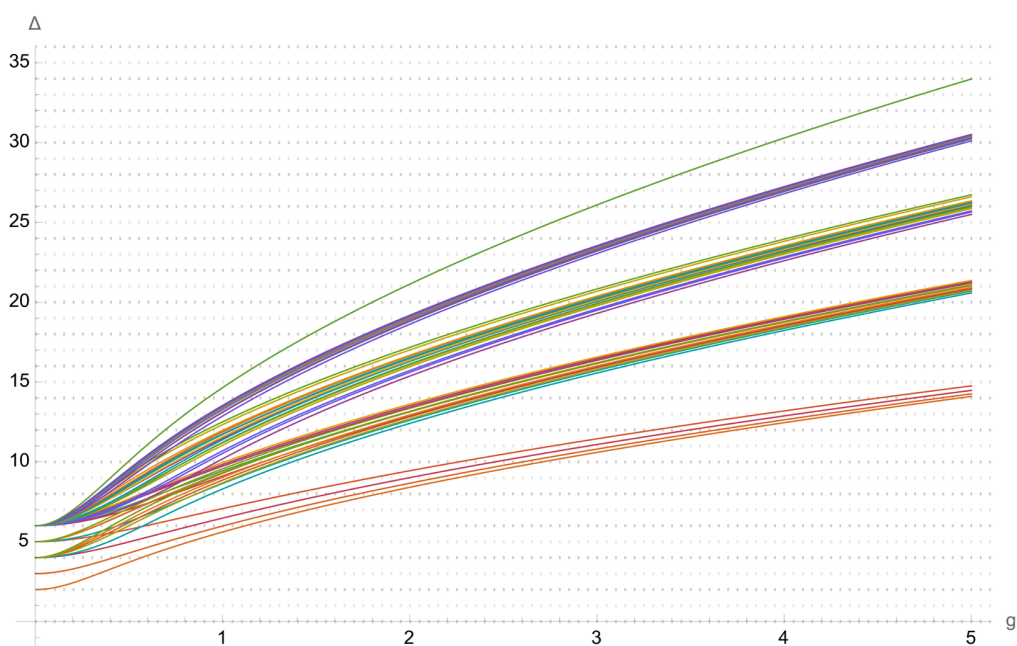


Figure 2. The scaling dimension of 45 states in $\mathcal{N} = 4$ SYM, with bare dimension $\Delta_0 \leq 6$, that have additional symmetries (cf. type I states, discussed in section 4.3.1) which make them amicable to more efficient numerical computation thereby allowing us to achieve higher range in the 't Hooft coupling. We provide their scaling dimensions in the range $g \in [0, 5] = \lambda \in [0, 400 \pi^2] \sim [0, 4000]$.

In the paper we also analyse the strong coupling behaviour by fitting of our data. When the accuracy allows, we determine analytic numbers or provide numerical expression for the strong coupling expansion otherwise.

Finally, we use the strong coupling data to find the structure constants large g coefficients, which were studied recently using conformal bootstrap [53, 54], by boosting these results with the spectral data.

Structure of the paper. In section 2 we introduce the general notations for the local operator in $\mathcal{N} = 4$ SYM and introduce notations for their quantum numbers; in section 3 we review the key aspect of the QSC needed for the introduction of the numerical algorithm for the QSC solver in section 4. Then in section 5 we describe the C++ implementation with the installation and usage instructions as well as the benchmarking of the performance. In section 6 we present the data for the spectrum and its detailed analysis followed by a conclusion in section 7.

2 Local operators and quantum numbers

In this section we describe the notations we use through this paper for the states and for their quantum numbers.

$\mathcal{N} = 4$ SYM is a superconformal field theory with $PSU(2, 2|4)$ symmetry group [55–61]. As such, a state in this theory is characterised by six quantum numbers. Namely, the scaling dimension: Δ , the Dynkin labels of the Lorentz group $SO(3, 1)$: $(\ell_1 \ell_2)$ (a.k.a. Lorentz spin labels), and the Dynkin labels of the R -symmetry group $SO(6)$: $(q_1 p q_2)$ (a.k.a. R -symmetry labels).

The Lagrangian of $\mathcal{N} = 4$ SYM depends on two parameters: the Yang-Mills coupling g_{YM} , and the rank of the gauge group $SU(N)$ [55, 56]. The integrable structure of the theory manifests itself [62] in the planar, or large- N limit, where we take $g_{YM} \rightarrow 0$ and $N \rightarrow \infty$ in such a way that the 't Hooft coupling $\lambda \equiv g_{YM}^2 N$, is held fixed. Another scaling of the 't Hooft coupling is $g \equiv \frac{\sqrt{\lambda}}{4\pi}$, which is a standard notation in the integrability literature. We use both g and λ , preferring g for weak and finite coupling, and λ for strong coupling.

In this paper, we work exclusively with planar $\mathcal{N} = 4$ SYM. As such, due to large- N factorisation [63, 64] one can focus entirely on linear combinations of the single trace operators

$$\text{tr } \mathcal{W}_1 \dots \mathcal{W}_L, \tag{2.1}$$

where \mathcal{W}_I are “fields” of $\mathcal{N} = 4$ SYM, defined as²

$$\mathcal{W}_I \in \left\{ \mathcal{D}^i \Phi, \mathcal{D}^j \Psi, \mathcal{D}^k \bar{\Psi}, \mathcal{D}^l \mathcal{F} \right\}. \tag{2.2}$$

Here, \mathcal{D} is the covariant derivative, and Φ is a scalar, Ψ and $\bar{\Psi}$ are gluinos, and \mathcal{F} is the gluon field strength.³ The trace is over the $SU(N)$ colour indices, under which all fields transform in the adjoint representation. The number of fields entering under the trace is called the length of the operator and is denoted by L , which is only well defined at zero 't Hooft coupling.

²Here, the superscript on \mathcal{D} is used to denote multiple applications of the covariant derivative, rather than an index associated to the symmetry group.

³Strictly speaking, each of these have Lorentz and/or R -symmetry indices, which we have suppressed for convenience. The form of these fields with their associated indices is given in table 1.

In general, the scaling dimension Δ of a state in this theory is a non-trivial function of the 't Hooft coupling λ . As $\mathcal{N} = 4$ SYM is a conformal field theory (CFT) [57, 65], the scaling dimension of an operator \mathcal{O} can be extracted from its two-point function^{4,5}

$$\langle \mathcal{O}(x)\mathcal{O}(y) \rangle = \frac{1}{|x - y|^{2\Delta}}, \tag{2.3}$$

where x and y are coordinates in the 4D space. We can separate the scaling dimension Δ into the bare/engineering/classical dimension — denoted by Δ_0 , which is the sum of the bare dimensions of its constituent fields — and its quantum corrections, called the anomalous dimension. The bare dimension Δ_0 of an operator may be obtained by setting the 't Hooft coupling $g = \lambda = 0$.

Due to supersymmetry, operators organise themselves into supermultiplets which comprise all operators with the same anomalous dimension. Supermultiplets are denoted by the quantum numbers of the highest weight state (we choose the convention/grading where the state with the lowest dimension Δ [10]) in the multiplet. All primary members of the multiplet are superdescendants of the superprimary, obtained by acting with a set of 16 supercharges on the highest weight state. Each time we act with the supercharge we either get zero or an operator with a dimension increased by 1/2.

Superconformal multiplets can be short, semi-short and long [70–74]. Here we focus on long multiplets as for them the scaling dimension is not protected. Semi-short multiplets require fine-tuning of the parameters and as a result are only known to exist at $g = 0$ [74].

To classify weak coupling solutions of the QSC, it is convenient to switch to the notation which uses the oscillator numbers following [10, 75–78]. The reason for this is that at $g = 0$ there is an additional “quantum number” (or rather a label): the length of a single-trace operator L . In addition to the Lorentz spin labels, and the R -symmetry labels, these quantum numbers parameterise the length L as well [10]. Therefore, we use the following set of oscillator numbers:

$$\{n_{\mathbf{b}_1}, n_{\mathbf{b}_2}, n_{\mathbf{f}_1}, n_{\mathbf{f}_2}, n_{\mathbf{f}_3}, n_{\mathbf{f}_4}, n_{\mathbf{a}_1}, n_{\mathbf{a}_2}\}. \tag{2.4}$$

These are directly related to Lorentz spin labels and R -symmetry labels as

$$\ell_1 = n_{\mathbf{b}_2} - n_{\mathbf{b}_1}, \ell_2 = n_{\mathbf{a}_1} - n_{\mathbf{a}_2}, q_1 = n_{\mathbf{f}_1} - n_{\mathbf{f}_2}, p = n_{\mathbf{f}_2} - n_{\mathbf{f}_3}, q_2 = n_{\mathbf{f}_3} - n_{\mathbf{f}_4}, \tag{2.5}$$

and parameterise the bare dimension Δ_0 and length L of single-trace operators as

$$\begin{aligned} \Delta_0 &= \sum_{i=1}^4 \frac{n_{\mathbf{f}_i}}{2} + \sum_{i=1}^2 n_{\mathbf{a}_i}, \\ L &= \sum_{i=1}^4 \frac{n_{\mathbf{f}_i}}{2} + \sum_{i=1}^2 \left(\frac{n_{\mathbf{a}_i}}{2} - \frac{n_{\mathbf{b}_i}}{2} \right). \end{aligned} \tag{2.6}$$

At finite coupling, the symmetry group reduces to $\text{PSU}(2, 2|4)$ and a multiplet is described by the usual set of 6 quantum numbers $\{\Delta, \ell_1, \ell_2, q_1, p, q_2\}$ (2.5), mixing operators with

⁴Assuming the correct normalisation.

⁵Note that operators dressed with more indices that furnish non-trivial representations of the symmetry group $\text{PSU}(2, 2|4)$ will have a more complicated expression for their two-point function, which are available in the standard references on CFT [66–69].

Type of Field	Field interpretation	Oscillator Content	Δ_0	L
Scalar	Φ_{ab}	$\mathbf{f}_a^\dagger \mathbf{f}_b^\dagger 0\rangle$	1	1
Glino/Fermion	$\Psi_{a\alpha}$	$\mathbf{f}_a^\dagger \mathbf{a}_\alpha^\dagger 0\rangle$	$\frac{3}{2}$	1
	$\bar{\Psi}_{\dot{a}\dot{\alpha}}$	$\epsilon_{abcd} \mathbf{f}_b^\dagger \mathbf{f}_c^\dagger \mathbf{f}_d^\dagger \mathbf{b}_{\dot{\alpha}}^\dagger 0\rangle$	$\frac{3}{2}$	1
Gluon Field Strength	$\mathcal{F}_{\alpha\beta}$	$\mathbf{a}_\alpha^\dagger \mathbf{a}_\beta^\dagger 0\rangle$	2	1
	$\bar{\mathcal{F}}_{\dot{\alpha}\dot{\beta}}$	$\mathbf{f}_1^\dagger \mathbf{f}_2^\dagger \mathbf{f}_3^\dagger \mathbf{f}_4^\dagger \mathbf{b}_{\dot{\alpha}}^\dagger \mathbf{b}_{\dot{\beta}}^\dagger 0\rangle$	2	1
Covariant Derivative	$\mathcal{D}_{\alpha\dot{\alpha}}$	$\mathbf{a}_\alpha^\dagger \mathbf{b}_{\dot{\alpha}}^\dagger 0\rangle$	1	0

Table 1. The map between fundamental fields of $\mathcal{N} = 4$ SYM and action of different types of oscillators on a Fock vacuum $|0\rangle$. The fields have the following indices: the Greek letters α, β, \dots and $\dot{\alpha}, \dot{\beta}, \dots$ are SU(2) spinor indices, take values 1, 2, and together furnish representations of the Lorentz algebra. The Latin letters a, b, \dots are SU(4) \cong SO(6) spinor indices, take values 1, \dots , 4, and furnish a representations of the R -symmetry algebra. Content of the table taken from [10, 78].

different length L [79]. Even though the integer L is no longer associated with any symmetry at finite coupling, we still can use it to label the states by tracing them back to $g = 0$. Similarly, the bare dimension Δ_0 is not a quantum number, but rather a useful label which can be used to distinguish different states.

Even though the oscillator numbers contain more information than the Dynkin labels, we will still find several operators sharing the same oscillator numbers. In order to distinguish them we introduce an additional label which we call the multiplicity label, it is a positive integer and denoted as `sol`. Therefore, in order to identify each superprimary state/operator in planar $\mathcal{N} = 4$ SYM uniquely, we introduce the `State ID`, which comprises the set of oscillator numbers, the bare dimension and solution number. We have

$$\text{State ID} : \Delta_0 [n_{\mathbf{b}_1} \ n_{\mathbf{b}_2} \ n_{\mathbf{f}_1} \ n_{\mathbf{f}_2}, n_{\mathbf{f}_3} \ n_{\mathbf{f}_4} \ n_{\mathbf{a}_1} \ n_{\mathbf{a}_2}]_{\text{sol}} . \tag{2.7}$$

Another reason why oscillator numbers are particularly convenient is because they enable us to immediately associate a state/operator with its possible field content at zero coupling. Below, we present the map between oscillator numbers and “fundamental fields”.⁶ We have In table 1, the fermionic creation operators \mathbf{f}_a^\dagger increase the corresponding fermionic oscillator number $n_{\mathbf{f}_a}$, $\mathbf{a}_\alpha^\dagger$ are counted by $n_{\mathbf{a}_\alpha}$ and $n_{\mathbf{b}_{\dot{\alpha}}}$ counts the number of $\mathbf{b}_{\dot{\alpha}}^\dagger$, cf. (2.4). Below, we present some examples, to illustrate this.

Konishi multiplet. To denote this multiplet, we need the oscillator content of its highest weight state $\mathcal{O}_{\text{h.w.}}$, which is⁷

$$\mathcal{O}_{\text{h.w.}} = \text{tr}(\mathcal{X}\bar{\mathcal{X}}) + \text{tr}(\mathcal{Y}\bar{\mathcal{Y}}) + \text{tr}(\mathcal{Z}\bar{\mathcal{Z}}) = \text{tr} \Phi_I \Phi_I . \tag{2.8}$$

In table 2, we present the 6 scalar fields of $\mathcal{N} = 4$ SYM with their respective oscillator content. Using it we can construct $\mathcal{O}_{\text{h.w.}}$, and therefore write down the `State ID` of the

⁶The difference between fundamental fields and fields used in equation (2.2) is that we consider the covariant derivative as a separate fundamental field, rather than it being a constituent of another field [10].

⁷The indices used in the r.h.s. of the second equality, are SO(6) vector indices, and take the values $I = 1, \dots, 6$.

Scalar field	Oscillator Content	Δ_0	L
$\mathcal{Z} \equiv \Phi_{12} = \Phi_1 + i\Phi_2$	[0 0 1 1 0 0 0 0]	1	1
$\mathcal{X} \equiv \Phi_{13} = \Phi_3 + i\Phi_4$	[0 0 1 0 1 0 0 0]	1	1
$\mathcal{Y} \equiv \Phi_{14} = \Phi_5 + i\Phi_6$	[0 0 1 0 0 1 0 0]	1	1
$\bar{\mathcal{Z}} \equiv \Phi_{34} = \Phi_1 - i\Phi_2$	[0 0 0 0 1 1 0 0]	1	1
$\bar{\mathcal{X}} \equiv \Phi_{24} = \Phi_3 - i\Phi_4$	[0 0 0 1 0 1 0 0]	1	1
$\bar{\mathcal{Y}} \equiv \Phi_{23} = \Phi_5 - i\Phi_6$	[0 0 0 1 1 0 0 0]	1	1

Table 2. The six polarisations of Φ_{ab} and their respective oscillator content. We also display how they can be re-expressed in terms of the vector representation of $SO(6)$, which capture the six real scalar fields of $\mathcal{N} = 4$ SYM.

Konishi multiplet as

$$\text{Konishi} : {}_2[0\ 0\ 1\ 1\ 1\ 1\ 0\ 0]_1. \tag{2.9}$$

The superprimary of this multiplet has the bare dimension 2 (the left subscript) and as it is the only multiplet with these quantum numbers it has unit multiplicity, and therefore $\text{so1} = 1$ (the right subscript).

SL(2) sector. Consider another important example of multiplets in the $SL(2)$ sector. Each such multiplet contains an operator that is constructed out of L scalars \mathcal{Z} , with S covariant derivatives, that can schematically⁸ be represented as $\text{tr } \mathcal{D}^S \mathcal{Z}^L$.⁹ These operators are not the highest weight states in the multiplet by our choice of convention/grading (see [10] for the details). In our notation $SL(2)$ sector multiplets can be identified by the following form of their **State ID**. We have

$$\mathfrak{sl}(2) \text{ sector} : {}_{L+S-2}[0\ S-2\ L-1\ L-1\ 1\ 1\ S-2\ 0]_{\text{so1}}. \tag{2.10}$$

These states have quantum numbers

$$\mathfrak{sl}(2) \text{ sector} : [\ell\ \ell\ 0\ p\ 0] = [S-2\ S-2\ 0\ L-2\ 0]. \tag{2.11}$$

Finally, we assign to each state an integer number **State Number** or **St. No.** which is just a useful label to enumerate all states in the database.

3 QSC: A practical user’s manual

Here we describe the Quantum Spectral Curve (QSC) [20, 21] a method to solve the spectral problem for planar $\mathcal{N} = 4$ SYM for both analytical and numerical applications. In this section we cover the basics of the QSC and introduce key notations.

⁸Concretely, such operators are $\text{tr}(\mathcal{D}^{n_1} \mathcal{Z}) \dots (\mathcal{D}^{n_1} \mathcal{Z})$, with $\sum_k^L n_k = S$.

⁹Indeed, the Konishi multiplet contains the operator $\text{tr } \mathcal{D}^2 \mathcal{Z}^2$ of this form and thus the Konishi multiplet is also an $\mathfrak{sl}(2)$ multiplet.

3.1 Generalities

Each state in this theory is associated with 2^8 Q-functions of a complex *spectral parameter* u , associated with the PSU(2,2|4) symmetry of the theory. The Q-functions are not all independent and are related by the QQ-relations described below. In the well studied cases of the spin-chains the Q-functions (or Baxter polynomials for the compact symmetry group) are the building blocks for the wave-functions of the states in a separation of variables basis (for recent developments see [80–90]). In particular, they contain all the quantum numbers of the state in the large- u asymptotic, which includes, in particular, the exact scaling dimension Δ .

In addition to the large- u asymptotic, injecting the information about the quantum numbers, one has to impose additional analyticity constraints on the Q-functions. As functions of the complex variable u they may have branch cuts with the branch points at $\pm 2g + in/2$ for an integer n and $g = \frac{\sqrt{\lambda}}{4\pi}$ related to the 't Hooft coupling λ .

The monodromy of the Q-functions through branch cuts is linked to a symmetry of the QQ-relations, which can be traced back to the crossing symmetry and which allows to constrain them to a discrete set of solutions, corresponding to the local states of the theory [21]. We describe this property below in more detail.

3.1.1 Algebraic properties

A Q-function is labelled by up to 8 indices, with a bar separating up to four indices from the rest. The Q-functions are absolutely anti-symmetric for each of two groups of indexes. It is easy to see that this labelling accounts for all 2^8 Q-functions.

The advantage of this labelling of the Q-function is that the QQ-relations (a.k.a. Wronskian identities) can be written in a compact form (in the conventions of [21]):

$$Q_{A|I}Q_{Aab|I} = Q_{Aa|I}^+Q_{Ab|I}^- - Q_{Aa|I}^-Q_{Ab|I}^+, \tag{3.1}$$

$$Q_{A|I}Q_{A|Iij} = Q_{A|Ii}^+Q_{A|Ij}^- - Q_{A|Ii}^-Q_{A|Ij}^+, \tag{3.2}$$

$$Q_{Aa|I}Q_{A|Ii} = Q_{Aa|Ii}^+Q_{A|I}^- - Q_{Aa|I}^-Q_{A|I}^+. \tag{3.3}$$

Here we use the notation $f^\pm \equiv f(u \pm i/2)$, lower case indices denote single indices, and upper case indices denote sets of indexes.

Additionally, we have the following determinant-type relations [21]:

$$Q_{a_1\dots a_{k+n}|i_1\dots i_k} = \frac{(n+k)!}{n!k!} Q_{[a_1\dots a_n|\emptyset} Q_{[a_{n+1}\dots a_{n+k}]|i_1\dots i_k}^{[\pm n]}, \tag{3.4}$$

$$Q_{a_1\dots a_k|i_1\dots i_{k+n}} = (-1)^{nk} \frac{(n+k)!}{n!k!} Q_{a_1\dots a_k|[i_1\dots i_k} Q_{\emptyset|i_{k+1}\dots i_{k+n}}^{[\pm n]}, \tag{3.5}$$

where $[\dots]$ stands for the standard anti-symmetrisation of the indices.

The Q-function with no indices, i.e. $Q_{\emptyset|\emptyset}$, is set to unity. The eight single index Q-functions $\mathbf{P}_a \equiv Q_{a|\emptyset}$ and $\mathbf{Q}_i \equiv Q_{\emptyset|i}$, are distinguished, since starting with them and using the QQ-relations (3.1), (3.2) and (3.3), we can construct all 2^8 Q-functions. A special case of the equation (3.3) with $A = \emptyset, I = \emptyset$, allows us to relate the distinguished Q-functions, with two-index Q-functions, and is very useful practically

$$Q_{a|i}^+ - Q_{a|i}^- = \mathbf{P}_a \mathbf{Q}_i. \tag{3.6}$$

One defines Hodge-dual Q-functions with upper indices in the following way [21, 91]:

$$Q^{a_1 a_2 \dots a_n | i_1, i_2 \dots i_m} \equiv (-1)^{nm} \epsilon^{a_1 a_2 \dots a_n b_1 b_2 \dots b_{4-n}} \epsilon^{i_1, i_2 \dots i_m j_1, j_2 \dots j_{4-m}} Q_{b_1 b_2 \dots b_{4-n} | j_1 j_2 \dots j_{4-m}}, \quad (3.7)$$

with $b_1 < \dots < b_{4-n}$ and $j_1 < \dots < j_{4-m}$. Then, we see that $Q^{\emptyset|\emptyset} = Q_{1234|1234}$, which we further require to be equal to unity as well.¹⁰ We can also define distinguished Q-functions with single upper-indices:

$$\mathbf{P}^a \equiv Q^{a|\emptyset} = Q^{a|i}(u + i/2)\mathbf{Q}_i, \quad (3.8)$$

$$\mathbf{Q}^i \equiv Q^{\emptyset|i} = Q^{a|i}(u + i/2)\mathbf{P}_a. \quad (3.9)$$

Using the determinant relations (3.4) and (3.5) to write $Q_{1234|1234}$ as a 4×4 determinant of various $Q_{a|i}$, one gets

$$Q_{1234|1234} = \begin{vmatrix} Q_{1|1} & Q_{1|2} & Q_{1|3} & Q_{1|4} \\ Q_{2|1} & Q_{2|2} & Q_{2|3} & Q_{2|4} \\ Q_{3|1} & Q_{3|2} & Q_{3|3} & Q_{3|4} \\ Q_{4|1} & Q_{4|2} & Q_{4|3} & Q_{4|4} \end{vmatrix} = 1. \quad (3.10)$$

Now, since we know that $Q_{1234|1234} = 1$, we see that $Q_{1234|1234}^+ - Q_{1234|1234}^- = 0$. At the same time, the r.h.s. of (3.10) gives a non-trivial constraint:

$$\mathbf{Q}_i \mathbf{P}_a Q^{a|i} = 0. \quad (3.11)$$

Combining with (3.8) and (3.9), we get

$$\mathbf{P}_a \mathbf{P}^a = \mathbf{Q}_i \mathbf{Q}^i = 0. \quad (3.12)$$

Expanding the determinant (3.10) on the first row, and repackaging the 3×3 sub-determinants as $Q^{a|i}$, we get

$$Q_{i|a} Q^{j|a} = -\delta_i^j. \quad (3.13)$$

From equations (3.8) and (3.13), we get

$$\mathbf{P}_a = -\mathbf{Q}^i Q_{a|i}^+, \quad (3.14)$$

$$\mathbf{Q}_i = -\mathbf{P}^a Q_{a|i}^+. \quad (3.15)$$

Combining equations (3.6) and (3.15), we obtain

$$Q_{a|i}^+ - Q_{a|i}^- = -\mathbf{P}_a \mathbf{P}^b Q_{b|i}^+. \quad (3.16)$$

Equations (3.6), (3.8), (3.9) (3.12)–(3.16) will play the central role in the description of the numerical algorithm, as we describe in section 4.

The Q-functions are further constrained by the analyticity conditions, which we describe below.

¹⁰This can be linked with the P in PSU [91].

3.1.2 Symmetries of the Q-system

The subset of the QQ-relations above (3.6)–(3.16) is invariant under the following Λ -transformation [11]

$$\mathbf{P}_a \rightarrow x^{+\Lambda} \mathbf{P}_a, \quad \mathbf{Q}_i \rightarrow x^{-\Lambda} \mathbf{Q}_i, \quad Q_{a|i} \rightarrow Q_{a|i} \quad (3.17)$$

and

$$\mathbf{P}^a \rightarrow x^{-\Lambda} \mathbf{P}^a, \quad \mathbf{Q}^i \rightarrow x^{+\Lambda} \mathbf{Q}^i, \quad Q^{a|i} \rightarrow Q^{a|i} \quad (3.18)$$

where x is some function of the spectral parameter u . As we show below, in order for this symmetry to remain the symmetry of the QSC, which also includes the analyticity constraints one can conclude that $x(u)$ should be the Zhukovsky functions, defined in equation (3.30) (or its power). Note that other Q-functions outside the reduced set transform rather non-trivially under this map.

In addition one has the following linear transformation *H-symmetry* [21]

$$\mathbf{P}_a \rightarrow \hat{H}_a{}^b \mathbf{P}_b, \quad \mathbf{Q}_i \rightarrow \check{H}_i{}^j \mathbf{Q}_j \quad (3.19)$$

for some constant matrices \hat{H} and \check{H} . The transformation of other Q-functions can be deduced from (3.19) and can be found in [21]. We also impose $\det \hat{H} = \det \check{H} = 1$ in order to preserve $Q_{\emptyset|\emptyset} = 1$. We also have

$$\mathbf{P}^a \rightarrow \hat{H}^a{}_b \mathbf{P}^b, \quad \mathbf{Q}^i \rightarrow \check{H}^i{}_j \mathbf{Q}^j \quad (3.20)$$

where $\hat{H}^a{}_b$ and $\check{H}^i{}_j$ are inverse and transposed matrices of $\hat{H}_a{}^b$ and $\check{H}_i{}^j$.

3.1.3 Asymptotic properties

Like in the case of the simple spin chains, in the case of the planar $\mathcal{N} = 4$ SYM, the quantum numbers of the states are hidden in the large- u behaviour of the Q-functions. Since, we can build all the Q-functions starting from the distinguished single-index ones, it is sufficient to specify the asymptotic information only for these functions. The asymptotics of \mathbf{P}_a and \mathbf{Q}_i are related to the quantum numbers of the state that they characterise. Introduce the constants powP_a and powQ_i , so that as $u \rightarrow \infty$, we have

$$\mathbf{P}_a \simeq \mathbb{A}_a u^{\text{powP}_a}, \quad \mathbf{Q}_i \simeq \mathbb{B}_i u^{\text{powQ}_i}, \quad (3.21)$$

where \mathbb{A}_a and \mathbb{B}_i are constants, defined below. The large- u asymptotic is given by

$$\text{powP} = \{-n_{\mathbf{f}_1} - 2 - \Lambda, -n_{\mathbf{f}_2} - 1 - \Lambda, -n_{\mathbf{f}_3} - \Lambda, -n_{\mathbf{f}_4} + 1 - \Lambda\}, \quad (3.22)$$

$$\text{powQ} = \left\{ L + \frac{\gamma}{2} + n_{\mathbf{b}_1} + \Lambda, L + \frac{\gamma}{2} + n_{\mathbf{b}_2} + 1 + \Lambda, -\frac{\gamma}{2} - n_{\mathbf{a}_1} - 2 + \Lambda, -\frac{\gamma}{2} - n_{\mathbf{a}_2} - 1 + \Lambda \right\}, \quad (3.23)$$

where Λ is the ambiguity related to the symmetry (3.17), n 's are the oscillator numbers of the state and the anomalous dimension γ is defined as

$$\gamma \equiv \Delta - \Delta_0, \quad (3.24)$$

where Δ_0 and L can be written in terms of the oscillator numbers via (2.6). Furthermore, the asymptotics of the single-upper-index Q-functions are

$$\mathbf{P}^a \simeq \mathbb{A}^a u^{-\text{powP}_a-1}, \quad \mathbf{Q}^i \simeq \mathbb{B}^i u^{-\text{powQ}_i-1}. \quad (3.25)$$

The constants \mathbb{A}_a and \mathbb{B}_i contain certain freedom as they can be re-defined using H -symmetry (3.19). However the combinations $\mathbb{A}_a \mathbb{A}^a$ and $\mathbb{B}_i \mathbb{B}^i$ (for each a and i) are invariant under the subset of the H -symmetry, which preserves the asymptotic (3.21). Those 8 combinations can be also written explicitly in terms of the quantum numbers of the states [21]. In this paper we adopt the conventions of [11] where the individual \mathbb{A}_a and \mathbb{B}_i are fixed in terms of powP and powQ

$$\mathbb{A}_a = \frac{(\text{powP}_a + \text{powQ}_1 + 1)(\text{powP}_a + \text{powQ}_2 + 1)}{\prod_{b>a} i(\text{powP}_a - \text{powP}_b)}, \quad (3.26)$$

$$\mathbb{A}^a = \frac{(\text{powP}_a + \text{powQ}_3 + 1)(\text{powP}_a + \text{powQ}_4 + 1)}{\prod_{b<a} i(\text{powP}_a - \text{powP}_b)}, \quad (3.27)$$

$$\mathbb{B}_j = \begin{cases} \frac{1}{\prod_{k>j} i(-\text{powQ}_j + \text{powQ}_k)}, & \text{for } j = 1, 2, \\ \frac{\prod_k (\text{powP}_k + \text{powQ}_j + 1)}{\prod_{k>j} i(\text{powQ}_j - \text{powQ}_k)}, & \text{for } j = 3, 4, \end{cases} \quad (3.28)$$

$$\mathbb{B}^j = \begin{cases} \frac{\prod_k (\text{powP}_k + \text{powQ}_j + 1)}{\prod_{k<j} i(\text{powQ}_j - \text{powQ}_k)}, & \text{for } j = 1, 2, \\ \frac{1}{\prod_{k<j} i(-\text{powQ}_j + \text{powQ}_k)}, & \text{for } j = 3, 4. \end{cases} \quad (3.29)$$

3.1.4 Analytic constraints

We will mainly focus on the analytic properties of \mathbf{P}_a and \mathbf{Q}_i and the Hodge dual \mathbf{P}^a and \mathbf{Q}^i .

Firstly, on their main sheet, the \mathbf{P}_a and \mathbf{P}^a have only two branch points, which are located at $-2g$ and $+2g$, and joined by a short branch cut, *i.e.* a branch cut passing through zero. As such, they can be efficiently parameterised by the Zhukovsky variable $x(u)$ defined by

$$x(u) \equiv \frac{u + \sqrt{u - 2g}\sqrt{u + 2g}}{2g}. \quad (3.30)$$

As a result, we have the following *convergent* expansion for \mathbf{P} which parameterises it everywhere on the main sheet and even includes some area around the cut on the next sheet:

$$\mathbf{P}_a = (gx)^{\text{powP}_a} \left(\mathbb{A}_a + \sum_{n=1}^{\infty} \frac{c_{a,n}}{x^n} \right), \quad \mathbf{P}^a = (gx)^{-\text{powP}_a-1} \left(\mathbb{A}^a + \sum_{n=1}^{\infty} \frac{c^{a,n}}{x^n} \right). \quad (3.31)$$

Note that explicit dependence on Δ of the state enters through \mathbb{A}_a and \mathbb{A}^a to (3.26) and (3.27). The expansion coefficients $c_{a,n}$, $c^{a,n}$ and Δ are some functions of g for each particular state and contain complete information on all other Q-functions [26] as we also argue below. In particular one can reconstruct \mathbf{Q}_i and \mathbf{Q}^i .

The expansion (3.31) is also convergent near the branch cut $[-2g, 2g]$ on the second sheet, where the \mathbf{P} -functions contains infinite series of other cuts $[-2g + i\mathbb{Z}, 2g + i\mathbb{Z}]$. Denote the analytic continuation of \mathbf{P}_a on this sheet by $\tilde{\mathbf{P}}_a$. Due to the parametrisation (3.31) in terms of the Zhukovsky variable, we can obtain an expression for $\tilde{\mathbf{P}}_a$ by just sending $x \rightarrow 1/x$ in (3.31).

Note that the fact that the branch cut $[-2g, 2g]$, which becomes a unit circle in x variable, is inside the convergence domain of the Laurent series in x guarantees fast convergence with the coefficients $c_{a,n}$ decaying exponentially at sufficiently large n . For numerical applications this allows to truncate the series at finite n while keeping the high precision of the parametrisation in the vicinity of the branch-cut and the whole main sheet.

One should note, that due to the H -symmetry (3.19), partially fixed by the asymptotic (3.21), there is still some freedom in re-defining the coefficients $c_{a,n}$, which we fix below in a particular way, depending on a type of the state. We refer to this symmetry as *gauge symmetry*.

Finally, in order to constrain the infinite set of constraints $c_{a,n}$, $c^{a,n}$ and Δ we have to impose the following analytic conditions on the \mathbf{Q} 's:

- The \mathbf{Q}_i should be analytic in the upper half-plane, and have infinitely many branch points on the lower-half plane, located at $\pm 2g - in$, with $n \in \mathbb{Z}$ and $n \geq 0$, joined by short cuts. This property is guaranteed by construction and follows from the representation of \mathbf{P} in (3.31).
- Upon passing through the branch cut on the real axis, we obtain $\tilde{\mathbf{Q}}_i$, which are analytic in the lower half-plane, and have an infinite series of cuts on the upper half plane.

Note that the branch structure of $\tilde{\mathbf{Q}}_i$ is similar to that of $\bar{\mathbf{Q}}_i$ (i.e. complex conjugate function), the complex conjugate of \mathbf{Q}_i . In fact, we have to impose the following “gluing” conditions [21, 25, 27]:¹¹

$$\tilde{\mathbf{Q}}_i = G_{ij} \bar{\mathbf{Q}}^j, \quad \tilde{\mathbf{Q}}^i = G^{ij} \bar{\mathbf{Q}}_j, \tag{3.32}$$

where the most general form of them can be written as

$$G_{ij} = \begin{pmatrix} 0 & \alpha_1 & 0 & 0 \\ \alpha_2 & 0 & 0 & 0 \\ 0 & 0 & 0 & \beta_1 \\ 0 & 0 & \beta_2 & 0 \end{pmatrix}_{ij}, \quad G^{ij} = \begin{pmatrix} 0 & \alpha_3 & 0 & 0 \\ \alpha_4 & 0 & 0 & 0 \\ 0 & 0 & 0 & \beta_3 \\ 0 & 0 & \beta_4 & 0 \end{pmatrix}^{ij}, \tag{3.33}$$

which relate $\tilde{\mathbf{Q}}_i$ and $\bar{\mathbf{Q}}_i$. The coefficients in the gluing matrices are related as we should have \bar{G}^{ij} as an inverse matrix of G_{ij} . Furthermore, $G_{ij} = \bar{G}_{ji}$ [27]. Therefore, only two parameters are independent, i.e.

$$\alpha_1 = \bar{\alpha}_2 = 1/\alpha_3 = 1/\bar{\alpha}_4 = \alpha, \quad 1/\beta_1 = 1/\bar{\beta}_2 = \beta_3 = \bar{\beta}_4 = \beta. \tag{3.34}$$

¹¹This condition is essentially a reflection of the unitarity of the $\mathcal{N} = 4$ SYM. However, for some applications, such as complex 't Hooft coupling analytic continuation, complex spin or Fishnet limit this may not be general enough. In general one can always construct two sets of \mathbf{Q}_i with upper and lower half analyticity and glue those sets on the cut $[-2g, 2g]$ on the real axis. In the present case, when the coupling is real, the complex conjugation is simply a quick way to construct the lower-half-plane analytic set of the \mathbf{Q} -functions for numerical applications.

The gluing conditions (3.32) impose strong constraints on $\{\Delta, c_{a,n}, c^{a,n}\}$, giving a discrete set of solutions (up to the gauge symmetry). The way to impose and solve this constraint numerically was initially developed in [26], and it is generalised in section 4 for all types of states. Next we review our notation for the 4 types of states, classified according to some discrete symmetries of the system.

3.2 Types of states and discrete symmetries

Based on quantum numbers, we can divide the states of $\mathcal{N} = 4$ SYM into four broad groups according to additional symmetries of their \mathbf{P}_a functions. For that we will use two types of symmetries: *left-right symmetry* and *parity symmetry*, which we explore below.

Left-right Symmetry. There is an additional symmetry of interchanging Q functions with their Hodge dual. This symmetry interchanges two $SU(2|2)$ subgroups of the $PSU(2, 2|4)$ and is usually referred to as left-right Symmetry.

The state is invariant under the left-right symmetry if there exists a combination of H - and Λ -transformations which allows to relate \mathbf{P}_a and \mathbf{P}^a in the following way

$$\mathbf{P}_a = \chi_{ab} \mathbf{P}^b, \tag{3.35}$$

where

$$\chi_{ab} = -\chi^{ab} = \begin{pmatrix} 0 & 0 & 0 & 1 \\ 0 & 0 & -1 & 0 \\ 0 & 1 & 0 & 0 \\ -1 & 0 & 0 & 0 \end{pmatrix}. \tag{3.36}$$

The relation (3.35) implies, via the QQ-relations that one can also assume that $\mathbf{Q}_i = \chi_{ij} \mathbf{Q}^j$. Thus, the anti-symmetric tensors χ_{ab} and χ_{ij} identifies the two $PSU(2|2)$ subgroups reducing the symmetry to $OSp(4|4)$ (up to a real form).

In this case we do not need to use both set of \mathbf{P}_a and \mathbf{P}^a , and we have only one set of parameters $\{c_{a,n}\}$ corresponding to the lower index, which gives considerable acceleration of the numeric.

Parity Symmetry. Another Z_2 symmetry of the local operators of $\mathcal{N} = 4$ SYM is the symmetry of reversing the order of operators under the trace. In the language of the spectral parameter this corresponds to changing u to $-u$.

There is a distinct set of states which is invariant under this symmetry. In this case one can assume that \mathbf{P} 's have certain parity under $u \rightarrow -u$, so that it is possible to simplify the ansatz for \mathbf{P}_a as follows, skipping every second power of x

$$\mathbf{P}_a = (gx)^{\text{powP}_a} \left(\mathbb{A}_a + \sum_{n=1}^{+\infty} \frac{c_{a,2n}}{x^{2n}} \right). \tag{3.37}$$

Again this amounts to efficiently reducing the number of parameters in the system by a factor of two, considerably improving the numerical performance for these states.

Notation	LR-symmetry	$u \leftrightarrow -u$ symmetry	# of states related by the symmetries
Type I	x	x	1
Type II	x	o	2
Type III	o	x	2
Type IV	o	o	2 or 4

Table 3. Four types of the states. The type I states require the smallest number of parameters needed to reach a given accuracy and are the simplest to deal with numerically. At the same time the type IV states require roughly 4 times more parameters and are the “heaviest” to deal with numerically. Note that it is not always totally trivial to identify the specific type of a state, as that requires finding the H -symmetry transformation which maps Left to Right.

Types of states. As we explained above we have two types of Z_2 symmetries: *left-right symmetry* and *parity symmetry*. Each operator in SYM can be either in a singlet or doublet representation of each of the two symmetries. Accordingly, we have 4 types of states, which require slightly different numerical treatment, as the additional reflection symmetries are beneficial for the reduction of the parameters. At the same time if the state is not invariant under a reflection then there should be another state with exactly the same dimension Δ , which may also be used to save the computational time. We introduce the notation for the four type of states as shown in the table 3.¹²

4 Setting up the numerical problem

In this section we describe the main steps of the numerical algorithm. We setup our numerical problem essentially following [26]. The main novelty in our approach is elucidated in the next section, where we describe a method which considerably improves the performance at weak coupling, which is essential for highly excited states, that get more and more degenerate with increased bare dimension. As we describe below, this allows us to initialise the numerical procedure from weak coupling, using the perturbative QSC solver of [10, 11].

4.1 Basics

We describe the main steps of the algorithm for states with no additional symmetry (type IV or general states). There are some further simplifications to the procedure if we consider states with Z_2 symmetries (left-right symmetry or parity symmetry, cf. section 3.2), and some additional subtleties appear when we relax symmetries. Here for the most general states we describe the main steps of the algorithm and will comment on deviations, depending on the type of the states, in the section 4.3.

Step 1: Parameters of the problem. We begin with the ansatz (3.31). We truncate the infinite sum at some fixed value of n , which we denote as `cutP`:

$$\mathbf{P}_a = (g x)^{\text{powP}_a} \left(\mathbb{A}_a + \sum_{n=1}^{\text{cutP}} \frac{c_{a,n}}{x^n} \right), \tag{4.1}$$

¹²There could be states invariant only w.r.t. to both reflection performed simultaneously. As these states are quite rare we have not introduced a separate code for those and they are treated as general.

State type	# gauge conditions	# independent parameters
I	1	2 cutP
II	4	4 cutP - 4
III	2	7 cutP/2 - 1
IV	6	7 cutP - 7

Table 4. Number of independent parameters for each state type.

$$\mathbf{P}^a = (g x)^{-\text{powP}_a+1} \left(\mathbb{A}^a + \sum_{n=1}^{\text{cutP}} \frac{c^{a,n}}{x^n} \right). \tag{4.2}$$

Thus, the set of parameters of our problem is $\{\Delta, c_{a,n}, c^{a,n}\}$, with $a = 1, \dots, 4$, $n = 1, \dots, \text{cutP}$. However, there is a nontrivial condition, following from the QQ-relations (3.12), which we use to constrain a set of cutP parameters by setting

$$\mathbf{P}_a \mathbf{P}^a = 0 + \mathcal{O}(1/x^{\text{cutP}}). \tag{4.3}$$

Therefore, the total number of parameters to fix from the gluing conditions (3.32) is $7 \text{ cutP} + 1$ (which also includes Δ).

The gauge symmetry (i.e. left over H -symmetry) allows us to fix six coefficients

$$\begin{aligned} c_{2,\text{powP}_2-\text{powP}_1} = 0, & \quad c_{3,\text{powP}_3-\text{powP}_1} = 0, & \quad c_{3,\text{powP}_3-\text{powP}_2} = 0, \\ c_{4,\text{powP}_4-\text{powP}_1} = 0, & \quad c_{4,\text{powP}_4-\text{powP}_2} = 0, & \quad c_{4,\text{powP}_4-\text{powP}_3} = 0, \end{aligned} \tag{4.4}$$

which reduces the total number of free parameters to $7 \text{ cutP} - 5$. In the case of the most general operators there are two additional constraints on the parameters as described below in subsection 4.3.4. In cases of less symmetric states we have bigger gauge symmetry and thus more gauge conditions to impose. In table 4, we summarise the number of independent parameters for the different types of states.

Step 2: Finding $Q_{a|i}$ at large u . Having the ansatz for \mathbf{P} 's at hand, we firstly go to the large u limit. In this limit we can find the whole set of functions \mathbf{P}_a , \mathbf{Q}_i and $Q_{a|i}$ asymptotically.

For instance, given the asymptotics of \mathbf{P}_a and \mathbf{Q}_i , one can read the asymptotic for $Q_{a|i}$ from the QQ-relation (3.16). Therefore, one can approximate $Q_{a|i}$ at large u as the following asymptotic expansion

$$Q_{a|i} \simeq u^{\text{powP}_a+\text{powQ}_i+1} \sum_{n=0}^{\text{cutQai}} \frac{B_{a|i,n}}{u^n}, \tag{4.5}$$

introducing coefficients $B_{a|i,n}$ and the cut-off for the number of terms in the asymptotic expansion cutQai . Our goal is to find the set of coefficients $B_{a|i,n}$ in terms of $c_{a,n}$ and $c^{a,n}$. For that we use the QQ-relation (3.16) substituting the asymptotic expansions of all functions.¹³

¹³Note that due to the expected infinite series of branch-cuts in the lower half plane accumulating at $-i\infty$ the series above can only be asymptotic and has zero convergence radius. In practice this means that one should increase $\text{Im } u$ together with cutQai to get a better approximation for $Q_{a|i}$.

At the leading order, coefficients $B_{a|i,0}$ can be fixed in terms of \mathbb{A}_a , \mathbb{B}_i , powP_a and powQ_i :

$$B_{a|i,0} = -i \frac{\mathbb{A}_a \mathbb{B}_i}{\text{powP}_a + \text{powQ}_i + 1}. \quad (4.6)$$

Expanding the QQ-relation (3.16) in large u , we obtain a linear system of $16 \times \text{cutQai}$ equations to determine $B_{a|i,n}$ where $a = 1, \dots, 4$, $i = 1, \dots, 4$ and $n = 1 \dots \text{cutQai}$. We have

$$T_{a|i,n}^b B_{b|i,n} = F_{a|i,n}, \quad n = 1, \dots, \text{cutQai}, \quad (4.7)$$

where

$$T_{a|i,n}^b = i \delta_a^b (\text{powP}_a + \text{powQ}_j + 1 - n) + \mathbb{A}_a \mathbb{A}^b, \quad (4.8)$$

and $F_{a|i,n}$ is a function of all previously computed $\{B_{a|j,k} : k = 1, \dots, n-1\}$ and $\{c_{a,m}, c^{a,m} : m = 1, \dots, n\}$.

We can solve the linear system (4.7) to obtain the $B_{a|i,n}$ coefficients in terms $c_{a,k}$ and $c^{a,k}$, for $k = 1, \dots, n$, and the quantum numbers of the state. As we explain in section 4.3.4 this step should be taken with extra care, as the linear system may not have a solution. In some cases, as we will see in section 4.3, the linear system (4.7) may have zero-modes, which need to be handled with care. We explain how to do this in detail in section 4.3.

As a result of solving the linear system (4.7), we obtain $Q_{a|i}$ at large u up to cutQai orders in $1/u$. In the next steps, we need to explore $Q_{a|i}$ near the branch cut.

Step 3: Approaching the cut. Equipped with $Q_{a|i}$ at large u , we can proceed to approximating $Q_{a|i}$ numerically close to the branch cut. We start by evaluating (4.5) at some particular value of $u = u_0 + i \text{QaiShift} - i/2$, where QaiShift is a large positive integer, so that the expansion (4.5) is reliable at this point. Then we rewrite (3.16) as

$$Q_{a|k} \left(u - \frac{i}{2} \right) = \left[\delta_a^b + \mathbf{P}_a(u) \mathbf{P}^b(u) \right] Q_{b|k} \left(u + \frac{i}{2} \right) \equiv U_a^b(u) Q_{b|k} \left(u + \frac{i}{2} \right). \quad (4.9)$$

This allows us to recursively reduce the magnitude of the imaginary part of the argument of $Q_{a|i}$, until we reach just above the real axis. We have (with a matrix multiplication under the square brackets)

$$Q_{a|k} \left(u_0 + \frac{i}{2} \right) = \left[U(u_0 + i) \dots U(u_0 + (\text{QaiShift} - 1) i) \right]_a^b Q_{b|k} \left(u_0 + \text{QaiShift} i - \frac{i}{2} \right). \quad (4.10)$$

Notice that it is possible to do this because the ansatz for \mathbf{P}_a in (3.31) is convergent, and therefore we can evaluate the product $\mathbf{P}_a \mathbf{P}^b$ at any value of u in the upper-half plane, whereas the expansion (4.5) for $Q_{a|i}$ is asymptotic, and only gives a good approximation at large enough $\text{Im}(u)$.

We repeat the procedure for nPoints probe points on the cut. More precisely we use Chebyshev nodes in the interval $[-2g, 2g]$ i.e. $u_{0,k} = 2g \cos \left(\frac{2k-1}{2 \text{nPoints}} \pi \right)$ for $k = 1, \dots, \text{nPoints}$. The Chebyshev nodes are particularly convenient because: firstly, they are more dense near

the branch points, where the \mathbf{Q} -functions are the most unpredictable; secondly, they are mapped points with equal separation on the unit circle under the Zhukovsky map (3.30).

Having computed $Q_{a|i}^+$ we can easily find both \mathbf{Q}_i and its analytic continuation under the cut on the real axis $\tilde{\mathbf{Q}}_i$ from (3.15):

$$\mathbf{Q}_i = -Q_{a|i}^+ \mathbf{P}^a, \quad \tilde{\mathbf{Q}}_i = -Q_{a|i}^+ \tilde{\mathbf{P}}^a, \quad (4.11)$$

where we remember that $\tilde{\mathbf{P}}^a$ can be obtained from (4.1) \mathbf{P}^a , by sending $x \rightarrow \tilde{x} = 1/x$.

Here let us notice that one can find $Q^{a|i}$ directly from $Q_{a|i}$ by using (3.13), which states that $Q^{a|i}$ is minus inverse of the transpose of $Q_{a|i}$. Then one constructs \mathbf{Q}^i and $\tilde{\mathbf{Q}}^i$ in the same way, using

$$\mathbf{Q}^i = Q^{a|i,+} \mathbf{P}_a, \quad \tilde{\mathbf{Q}}^i = Q^{a|i,+} \tilde{\mathbf{P}}_a. \quad (4.12)$$

In the end, we obtain lists of \mathbf{Q} -functions: \mathbf{Q}_i , \mathbf{Q}^i , $\tilde{\mathbf{Q}}_i$ and $\tilde{\mathbf{Q}}^i$ evaluated at `nPoints` Chebyshev nodes on the cut. We denote the lists as `Qidownlist`, `Qiuplist`, `Qidowntlist` and `Qiuptlist` respectively. After we obtain the \mathbf{Q} -functions just above the branch cut, we can impose the gluing conditions (3.32).

In the next section, we will see how the gluing conditions are used to obtain a system of equations for the free parameters of our problem which is then solved using Newton's method.

4.2 Closing the system: Newton method for harmonics on the cut

Here we describe the main novelty of the current implementation.

First let us briefly summarise the previous method by [26]. We started from the \mathbf{P} -functions, solved the QQ-relations to construct $Q_{a|i}$ which by itself enabled us to compute the \mathbf{Q} -functions both above and below the branch cut. Basically for any set of parameters $\{c\} \equiv \{c_{a,n}, c^{a,n}\}$ and Δ , we would be able to conduct this procedure. In order to close the equations we have to impose the gluing condition, which relates $\mathbf{Q}_i(u \pm i0)$ to $\tilde{\mathbf{Q}}^i(u \mp i0)$ for $u \in [-2g, 2g]$. Schematically

$$\mathbf{P}_a, \mathbf{P}^a \rightarrow Q_{a|i} \rightarrow \mathbf{Q}_i(\{c\}, \Delta|u), \tilde{\mathbf{Q}}^i(\{c\}, \Delta|u) \quad (4.13)$$

where we added the parameters into arguments of the \mathbf{Q} -functions to emphasise that they can be constructed for given values of parameters.

The method of [26] consisted in using an optimisation algorithm to adjust parameters in order to minimise the mismatch in the gluing condition evaluated at the Chebyshev nodes u_m :

$$\min \sum_m \left| \mathbf{Q}^k(\{c\}, \Delta|u_m \pm i0) - G^{kj} \overline{\mathbf{Q}_j(\{c\}, \Delta|u_m \pm i0)} \right|^2. \quad (4.14)$$

This works well at finite g , but loses precision quickly at very small couplings. The reason for this is that the convergence radius of the expansion (3.31) of the \mathbf{P} -functions into inverse powers of x at weak coupling has the convergence radius $1/|x(\pm 2g \pm i)| \simeq g$, meaning that the expansion coefficients $c_{a,n} \sim g^n$ all vanish quickly but at a different rate. The fact that they vanish quickly of course allows for very efficient truncation, which becomes exact at a given order in small coupling, however, the difference in the scale makes the optimisation problem ill-conditioned.

In order to resolve this problem in this paper we propose an alternative method. Denoting

$$\mathbf{P}_a^{\text{Updated}} \equiv -Q_{a|k}^+ G^{kj} \overline{\mathbf{Q}_j(\{c\}, \Delta|u \pm i0)}, \quad u \in [-2g, 2g] \quad (4.15)$$

such that on the solution of the QSC we should have $\mathbf{P}_a^{\text{Updated}} = \mathbf{P}_a$, but “off-shell” it is a function with rather different analytic properties — it is almost guaranteed to have infinitely many cuts even on the defining sheet. Nevertheless, we can use the Zukovsky map to resolve the cut on the real axis, which produces an analyticity annulus, containing the unit circle where we can define the Laurent expansion

$$\mathbf{P}_a^{\text{Updated}} = (gx)^{\text{powP}_a} \sum_{n=-\infty}^{+\infty} \frac{c_{a,n}^{\text{Updated}}}{x^n} \quad (4.16)$$

the prefactor we introduced for convenience, without loss of generality. We notice that on-shell (i.e. when the gluing condition is satisfied) we should have all positive powers coefficients to vanish $c_{a,n}^{\text{Updated}} = 0$, $n < 0$, zero power coefficient should become 1 and the rest should coincide with the initial parameters $c_{a,n}$.

Technically, finding coefficients $c_{a,n}^{\text{Updated}}$ is identical to the Fourier transformation in the angle ϕ going around the unit circle $x = e^{i\phi}$. Furthermore, since we have already values of the \mathbf{P} -functions computed at the Chebyshev nodes we can conveniently use the fast-Fourier transformation method. In a similar way we construct $\mathbf{P}^a \text{ Updated}$ and its Fourier modes $c^{a,n \text{ Updated}}$.

Finally, we have to impose

$$\vec{F}(\{c\}, \Delta) = \left\{ c_{a,n}^{\text{Updated}}(\{c\}, \Delta) - c_{a,n}, c^{a,n \text{ Updated}}(\{c\}, \Delta) - c^{a,n} \right\} = 0, \quad (4.17)$$

which we do with the Newton method. Notice, however, that the above equation is over-defined as $c_{a,n}$ are only non-zero for positive n and, furthermore, some of them are fixed to be zero for the gauge-fixing, as discussed around equation (4.4). At the same time we have an extra parameter Δ in addition to $\{c\}$. For the Newton method we have to equalise the number of equations and the number of parameters. To do that in practice we drop all negative n 's, we use some of $n = 0$ equations to solve for the parameters in the gluing matrix (as they are simply linear equations for α and β) while keeping one to match with Δ . We also remove the equations corresponding to the gauge fixing conditions. The exact details depends on the type of the state and can vary for a concrete implementation. Finally, one can use the discarded equations in order to estimate the accuracy of the gluing. Note that the Newton method, if convergent, finds zero in the multidimensional space of parameters with the precision which only depending on the number of iterations and is not suitable for precision control of the numerical approximation made at all other steps.

Let us note that for the Newton method we have to compute the derivative of the vector valued function \vec{F} , which we do by the simplest first order finite difference formula $\partial \vec{F} = \frac{1}{\epsilon} [\vec{F}(\dots + \epsilon) - \vec{F}]$. This is of course the slowest part of the algorithm as it requires approximately $8 \times \text{cutP}$ evaluations of the function \vec{F} . Furthermore, one should take into account the following subtlety in the technical implementation. The coefficients $c_{1,n}$ and $c_{3,n}$ are purely real, whereas $c_{2,n}$ and $c_{4,n}$ are purely imaginary. When computing numerical

Step 1: Parameters of the problem	Start with initial parameters $\Delta, c_{a,n} c^{a,n}, a = 1 \dots 4, n = 1 \dots \text{cutP}$, setting some $c_{a,n}$ to zero by the gauge choice.
Step 2: Finding $Q_{a i}$ at large u	Go to the large $\text{Im } u$ limit. Solve the linear system of coefficients of $Q_{a i} B_{a i,n}, a = 1 \dots 4, i = 1 \dots 4, n = 1 \dots \text{cutQai}$.
Step 3: Approaching the cut	Starting from large $\text{Im } u$ limit, shift $Q_{a i}$ down to the branch cut. Get $Q_{a i}$ just above the branch cut and calculate $\mathbf{Q}_i, \tilde{\mathbf{Q}}_i$ and $\tilde{\mathbf{Q}}^i$.
Newton-Fourier	<ul style="list-style-type: none"> • Use Steps 1–3 to find $c_{a,n}^{\text{Updated}} c^{a,n \text{ Updated}}$ as functions of the initial parameters by performing a Fourier transform on the unit circle in x. • Use Newton method to find the values of parameters such that $c_{a,n}^{\text{Updated}} = c_{a,n}$ and $c^{a,n \text{ Updated}} = c^{a,n}$. • Read-off the value of Δ among other parameters at the solution of the equation $c_{a,n}^{\text{Updated}} = c_{a,n}$ and $c^{a,n \text{ Updated}} = c^{a,n}$.

Table 5. The main steps of the numerical algorithm.

derivatives, these parameters need to be shifted by a small constant ϵ , as described above. To ensure the correct direction of the shifting, for real parameters $c_{1,n}$ and $c_{3,n}$ the real part of equations (4.17) is taken, and for imaginary parameters $c_{2,n}$ and $c_{4,n}$ the imaginary part. Furthermore, this restricts the gluing coefficients α and β in (3.34) to be real.

The main steps of the algorithm are summarised in table 5.

4.3 Details of the numerical procedure for different types of states

Based on the behaviour of the states w.r.t. the two discrete symmetries (left-right symmetry and parity symmetry) we split all operators into 4 types as explained in section 3.2. Accordingly we have 4 slightly different implementations of the QSC solver for each of these types and in this section we describe the specific differences.

4.3.1 Left-right and parity symmetric case (Type I)

This case is the most symmetric one and therefore the simplest. Here we will outline the simplifications in the algorithm which arise because of symmetries.

First of all, we have the least amount of independent parameters among all cases. Due to the left-right symmetry, at **Step 1** we introduce coefficients only for \mathbf{P}_a :

$$\mathbf{P}_a = (g x)^{\text{powP}_a} \left(\mathbb{A}_a + \sum_{n=1}^{\text{cutP}/2} \frac{c_{a,2n}}{x^{2n}} \right), \tag{4.18}$$

as \mathbf{P}^a can be obtained by raising the index $\mathbf{P}^a = \chi^{ab} \mathbf{P}_b$. Here let us note that we convert \mathbf{P}_a and \mathbf{P}^a available in the perturbative solver [10, 11] into the left-right symmetric form (3.35).

The details of this conversion are provided in the appendix B. The expansion (4.18) includes only even powers because of the parity symmetry. In addition, we impose the following gauge conditions:

$$c_{2,\text{pow}P_2-\text{pow}P_1} = 0, \quad c_{3,\text{pow}P_3-\text{pow}P_1} = 0, \quad c_{3,\text{pow}P_3-\text{pow}P_2} = 0, \quad c_{4,\text{pow}P_4-\text{pow}P_1} = 0. \quad (4.19)$$

In practice, three of the gauge conditions are already satisfied trivially, due to parity symmetry requiring that particular coefficients are zero. Because of this, we end up with only 2 cutP parameters (cf. table 4).

To start the algorithm, we need to find $Q_{a|i}$ at the large- u limit at **Step 2**. The linear system (4.7) for the coefficients $B_{a|i,2n}$ where $a = 1 \dots 4, i = 1 \dots 4, n = 1 \dots \text{cut}Q_{a|i}/2$ can be solved as a function of $c_{a,n}$ without complications, i.e. there are no zero-modes in this case.

The step **Step 3**, where we compute $Q_{a|i}$ does not require a modification.

The gluing conditions are simplified as they connect only \mathbf{Q}_i and $\tilde{\mathbf{Q}}_i$. The lists of \mathbf{Q}_i and $\tilde{\mathbf{Q}}_i$ can be obtained as

$$\mathbf{Q}_i = -Q_{a|i}^+ \chi^{ab} \mathbf{P}_b, \quad \tilde{\mathbf{Q}}_i = -Q_{a|i}^+ \chi^{ab} \tilde{\mathbf{P}}_b. \quad (4.20)$$

The gluing matrix (3.33) is simplified and involves the only one independent gluing constant

$$\tilde{\mathbf{Q}}_i = G^{(\text{LR})}{}^j{}_i \bar{\mathbf{Q}}_j, \quad G^{(\text{LR})}{}^j{}_i = \begin{pmatrix} 0 & 0 & \alpha & 0 \\ 0 & 0 & 0 & -\bar{\alpha} \\ \frac{1}{\bar{\alpha}} & 0 & 0 & 0 \\ 0 & -\frac{1}{\alpha} & 0 & 0 \end{pmatrix}_{ij}, \quad (4.21)$$

where $G^{(\text{LR})}{}^j{}_i = G_{ij} \chi^{jk} = \chi_{ik} G^{kj}$ is obtained by lowering the index $\mathbf{Q}^i = \chi^{ij} \mathbf{Q}_j$ of the general gluing conditions (3.32) and noticing that $\beta = \bar{\alpha}$. To close the system and set up a numerical search we follow the procedure of section 4.1. Regarding the Newton search at the last step, the main procedure is unchanged, and is the same as that described in section 4.2, albeit with only Δ and $c_{a,n}$ as parameters.

4.3.2 Left-right symmetric states with general parity (Type II)

For this case, the parity symmetry is relaxed but the left-right symmetry is preserved. Therefore, in **Step 1** the ansatz for \mathbf{P}_a should contain both even and odd powers in the expansion:

$$\mathbf{P}_a = (gx)^{\text{pow}P_a} \left(\mathbb{A}_a + \sum_{n=1}^{\text{cut}P} \frac{c_{a,n}}{x^n} \right), \quad (4.22)$$

which immediately gives twice more coefficients to define \mathbf{P}_a up to the same cutP. However, we still can use the left-right symmetry to define $\mathbf{P}^a = \chi^{ab} \mathbf{P}_b$. In addition, all 4 gauge conditions for the left-right symmetric case (4.19) are non-trivial. This gives us 4 cutP – 3 parameters (cf. table 4) to the numerics.

The main important difference here is due to the additional obstruction in the linear system for the asymptotic expansion of $Q_{a|i}$. In the absence of the parity symmetry we notice that \mathbf{Q}_1 and \mathbf{Q}_2 can mix, i.e. the large- u expansion of \mathbf{Q}_2 will be invariant under

$$\mathbf{Q}_2 \rightarrow \mathbf{Q}_2 + \eta \mathbf{Q}_1, \quad (4.23)$$

for some constant η , as well as the large- u expansion of \mathbf{Q}_4 will be invariant under

$$\mathbf{Q}_4 \rightarrow \mathbf{Q}_4 + \mu \mathbf{Q}_1, \tag{4.24}$$

for some constant μ . In the parity symmetric case one can avoid this mixing by requiring \mathbf{Q}_i to have definite parity, which then prevent the mixing as, for instance, \mathbf{Q}_1 and \mathbf{Q}_2 must have opposite parity due to the asymptotic. We notice that in the left-right symmetric case, due to the gluing condition (4.21), we must have $\mu = -\eta \frac{\alpha}{\alpha}$, where α is the gluing constant.

This freedom affects the **Step 2**, where we build a large- u expansion for $Q_{a|i}$. The ambiguity in the definition of \mathbf{Q}_i translates into existence of a zero mode in the linear system (4.7), responsible for the redefinition of $Q_{a|2} \rightarrow Q_{a|2} + \eta Q_{a|4}$ and $Q_{a|4} \rightarrow Q_{a|4} + \mu Q_{a|1}$ in accordance with (4.23) and (4.24). Thus the zero mode occurs at $n = n_\eta$ in (4.7), which, as follows from the asymptotics, should be equal to

$$n_\eta \equiv \text{pow}Q_2 - \text{pow}Q_1 = n_{a_1} - n_{a_2} + 1 = n_{b_2} - n_{b_1} + 1, \tag{4.25}$$

which is the first level in the linear system (4.7), where $Q_{a|1}$ and $Q_{a|2}$ can mix. Technically this implies that $T_{n_\eta}^{a|b|2}$ in (4.8) has a null vector. To be more specific, the four components of the right null vector $B_{a|2,n_\eta}^{\text{zero mode}}$ are

$$\begin{aligned} B_{1|2,n_\eta}^{\text{zero mode}} &= -\frac{i(2p - 2\Delta - 2\ell_1 + 3q_1 + q_2)}{(q_1 + 1)(p + q_1 + 2)(p + q_1 + q_2 + 3)(2p + 2\Delta + 2\ell_1 + q_1 + 3q_2 + 12)}, \\ B_{2|2,n_\eta}^{\text{zero mode}} &= \frac{2p - 2\Delta - 2\ell_1 - q_1 + q_2 - 4}{(p + 1)(p + q_2 + 2)(2p + 2\Delta + 2\ell_1 + q_1 + 3q_2 + 12)}, \\ B_{3|2,n_\eta}^{\text{zero mode}} &= \frac{i(-2p - 2\Delta - 2\ell_1 - q_1 + q_2 - 8)}{(q_2 + 1)(2p + 2\Delta + 2\ell_1 + q_1 + 3q_2 + 12)}, \\ B_{4|2,n_\eta}^{\text{zero mode}} &= 1. \end{aligned} \tag{4.26}$$

Note that we can always choose the 4th component to be 1, because the combination $2p + 2\Delta + 2\ell_1 + q_1 + 3q_2 + 12 > 0$. Since the $B_{4|2,n_\eta}^{\text{zero mode}}$ is always nonzero we can impose an additional constraint $B_{4|2,n_\eta} = 0$ and solve

$$T_{a|2,n_\eta}^b B_{b|2,n_\eta} = F_{a|2,n_\eta}, \tag{4.27}$$

for remaining $a = 1, \dots, 3$. However, in order for this reduction to be consistent, one should also impose that the r.h.s. of the linear system (4.7) shares the left null-vector with T . This is not guaranteed for arbitrary values of the parameters and imposes an additional constraint on the expansion coefficients $c_{a,n}$ of the \mathbf{P}_a , with $n = n_\eta$.

To give the simplest example for such a constraint, for the states ${}_4[0\ 0\ 4\ 3\ 2\ 1\ 0\ 0]_{\text{sol}1}$, with $\text{sol}1 = 1, 2$, the value $n_\eta = 1$ and the corresponding constraint is¹⁴

$$c_{1,1} = \frac{6(\Delta - 5)(\Delta + 7)(\Delta - 1)^2 c_{3,1} - 12(\Delta - 5)(\Delta + 3)^2 c_{2,1} + 5(\Delta - 5)(\Delta - 1)(\Delta + 3)c_{4,1}}{336(\Delta - 1)(\Delta + 3)(\Delta + 7)^2}. \tag{4.28}$$

¹⁴There is a freedom to choose which of the coefficients are considered to be the dependent ones. In our implementation we always treat c_{1,n_ν} as a dependent parameter for all type II states.

Conceptually, this constraint means that the power-like asymptotic for \mathbf{Q}_i is consistent with the ansatz for \mathbf{P}_a , the same way as for the general type of states the coefficients \mathbb{A}_a are partially fixed by the quantum numbers.

Once $Q_{a|i}$ at large u is defined, we can proceed with **Step 3**, i.e. shifting to the cut. Just above the cut we obtain \mathbf{Q}_i and $\tilde{\mathbf{Q}}_i$ the same way as it is done for the left-right and parity symmetric case in section 4.3.1.

During the Newton search, we need to treat the coefficient fixed by the constraint as a dependent parameter. Once the independent parameters are shifted by ϵ , we need to calculate the shift in the dependent variable using the constraint (cf. in the above example, where (4.28) which can be used to fix $c_{1,1}$).

4.3.3 General and parity symmetric states (Type III)

For this case we do not consider the left-right symmetry any more, though we keep parity symmetry. The ansatz for \mathbf{P}_a and \mathbf{P}^a in **Step 1** is as follows:

$$\mathbf{P}_a = (gx)^{\text{powP}_a} \left(\mathbb{A}_a + \sum_{n=1}^{\text{cutP}/2} \frac{c_{a,2n}}{x^{2n}} \right), \quad \mathbf{P}^a = (gx)^{-\text{powP}_a-1} \left(\mathbb{A}^a + \sum_{n=1}^{\text{cutP}/2} \frac{c^{a,2n}}{x^{2n}} \right), \quad (4.29)$$

which satisfy the identity (4.3). Due to this restriction, there are $7 \text{ cutP}/2$ parameters as one of the sets $\{c_a\}$ or $\{c^a\}$ is not independent.¹⁵ The gauge conditions are the most general (4.4) though some one them are trivially satisfied because of parity symmetry. This results in $7 \text{ cutP}/2 - 1$ parameters to start with (cf. table 4).

The rest of the algorithm is the same as outlined in the section 4.1. However, we will mention a technical subtlety in implementing the Newton's search: some coefficients $\{c\}$ are not independent due to the identity (4.3). Thus, we do not vary them in the Newton search and need to recalculate them after shifting the independent parameters.

4.3.4 General states (type IV)

As the main steps of the algorithm have been described on the basis of this case, we just highlight two points. Complications for this case, with least symmetry are essentially a combination of subtleties which we have seen separately for left-right symmetric and general (i.e. for type II states), and general and parity symmetric (i.e. for type III states) cases.

As mentioned in section 4.3.2, now there are two independent emergent ambiguity in the definition of \mathbf{Q}_i

$$\mathbf{Q}_2 \rightarrow \mathbf{Q}_2 + \eta \mathbf{Q}_1, \quad \mathbf{Q}_3 \rightarrow \mathbf{Q}_3 + \mu \mathbf{Q}_4, \quad (4.30)$$

for two independent constants η and μ . This implies an analogous ambiguity in $Q_{a|i}$:

$$Q_{a|i} \rightarrow Q_{a|i} + \eta \delta_{i2} Q_{a|1} + \mu \delta_{i4} Q_{a|3}. \quad (4.31)$$

Therefore, we have zero-modes at two levels now:

$$n_\eta \equiv \text{powQ}_2 - \text{powQ}_1 = n_{\mathbf{b}_2} - n_{\mathbf{b}_1} + 1, \quad n_\mu \equiv \text{powQ}_4 - \text{powQ}_3 = n_{\mathbf{a}_1} - n_{\mathbf{a}_2} + 1. \quad (4.32)$$

¹⁵There is a freedom to choose which coefficients are kept made dependent ones, in our implementation we always treat $c^{1,n}$ as dependent parameters.

There are two cases, $n_\eta = n_\mu$ and $n_\eta \neq n_\mu$. Both of the right null vectors $B_{a|2,n_\eta}^{\text{zero mode}}$ and $B_{a|4,n_\mu}^{\text{zero mode}}$ can be chosen to have a fourth component to be one, and this can be used to resolve the zero-modes at $n = n_\eta$ and $n = n_\mu$, analogously to how it was done in section 4.3.2. The left null vectors induce constraints on the coefficients c_{a,n_η} and c_{a,n_μ} .

When $n_\eta = n_\mu$ we need to impose two constraints at the same order. Let us provide the simplest example of the constraint for the oscillator numbers ${}_6[0\ 0\ 4\ 3\ 3\ 2\ 0\ 0]_{\text{so1}}$, with $\text{so1} = 4, \dots, 9$ ¹⁶ which has $n_\eta = n_\mu = 1$. In this case we get

$$c^{2,1} = \frac{(\Delta+2)\Delta(\Delta+6)^2 c_{1,1} + 60(\Delta+2)(\Delta^2+4\Delta-20)c_{2,1} + 8(\Delta+2)(\Delta-4)^2 c_{4,1}}{40(\Delta-4)\Delta^2(\Delta+6)} - \frac{5\Delta(\Delta+2)(\Delta-4)(\Delta+6)c_{3,1} - 600(\Delta+2)(\Delta+6)^2 c^{4,1} - 2880(\Delta+2)c_{2,1}}{40(\Delta-4)\Delta^2(\Delta+6)}, \quad (4.33)$$

$$c^{3,1} = \frac{180\Delta(\Delta+6)^2 c_{1,1} - 30\Delta(\Delta^2+4\Delta-20)c_{2,1} + 5\Delta^2(\Delta-4)(\Delta+2)(\Delta+6)c_{3,1}}{90(\Delta-4)(\Delta+2)(\Delta+6)} - \frac{16\Delta(\Delta-4)c_{4,1} + 900(\Delta+6)^2 \Delta c^{4,1} + 1440c_{2,1}}{90(\Delta-4)(\Delta+2)(\Delta+6)}. \quad (4.34)$$

When $n_\eta \neq n_\mu$, we need to impose constraints on different orders. Here one of the simplest examples is the constraints for ${}_{11/2}[0\ 0\ 4\ 3\ 1\ 1\ 1\ 0]_{\text{so1}}$ multiplets, with $\text{so1} = 1, 2$. In this case $n_\eta = 1$ and $n_\mu = 2$. The first constraint which looks the following:

$$c^{2,1} = -\frac{6(2\Delta+13)(2\Delta+21)c_{1,1}}{4(\Delta-7)\Delta+33} + \frac{3(2\Delta+5)(2\Delta+13)c_{2,1}}{(3-2\Delta)^2} - \frac{8(2\Delta-7)(2\Delta+1)c_{3,1}}{5(2\Delta-3)(2\Delta+9)} - \frac{11-2\Delta}{16}c_{4,1} - \frac{30(2\Delta+9)c^{3,1}}{2\Delta-3} + \frac{36(2\Delta+13)c^{4,1}}{2\Delta-3}, \quad (4.35)$$

and the second one is similar, but a more cumbersome expression for $c^{2,2}$. In general, the constraint for $n_\mu > 1$ becomes nonlinear in $c_{a,n}$ and $c^{a,n}$, however, it is linear in c^{a,n_μ} terms. Finally, let us note that there are poles in Δ in the constraints (4.33), (4.35). However, for states we have studied, the poles satisfy $\Delta \leq \Delta_0$ and as Δ is expected to grow monotonically with the coupling, they should not cause a problem at finite real g .

5 C++ implementation

This section is devoted to give the most necessary technical details for using the C++ implementation of the QSC solver algorithm described in the previous section. We give step by step instructions on the installation and usage.

The source-code is available at [GitHub](#) alongside with the **Mathematica** prototype and a database for the initial points and perturbative data.

5.1 Fast QSC solver: user manual

5.1.1 Installation

The numerical solution of the QSC equations requires higher than machine precision arithmetic. This implies, that the usual double arithmetic of C or C++ is not enough for our purposes.

¹⁶Our choice of independent parameters in the implementation is c^{2,n_η} and c^{3,n_μ} when $n_\eta = n_\mu$, c^{2,n_η} and c^{2,n_μ} when $n_\eta \neq n_\mu$.

This is why, we used the Class Library of Numbers (CLN), which is a special library for efficient computations with all kinds of numbers in arbitrary precision. All information about this free library can be found in the library's homepage: <https://www.ginac.de/CLN>. Nevertheless, for practical use of our C++ codes, knowing all subtle details is not necessary. The CLN package is available at Unix-like operating systems,¹⁷ but can also be used under Windows operating system, provided a Windows Subsystem for Linux (WSL) is installed.¹⁸ Then all linux programs can be executed from the Windows PowerShell. The only difference with respect to usual linux is that each command should be anticipated by typing `wsl` and a space to indicate that the WSL system is used.

The prerequisites to run the C++ codes is that, a C++ compiler and the CLN package should be installed on the computer. This requires the installation of three packages either using the package manager or from the terminal window. Namely, these are the `g++` compiler,¹⁹ and the `libcln` and `libcln-dev` packages for the usage of arbitrary precision arithmetic.²⁰ In Debian linux systems, they can be installed easily from terminal window by the following commands:

```
> sudo apt install g++
> sudo apt install libcln6
> sudo apt install libcln-dev21
```

Then if the C++ source file can be found in the current directory, the compilation can be done easily from terminal by typing:

```
> g++ source.cpp -lm -lcln -o executable.out
```

This command creates an executable output file named *executable.out* in the current directory out of the *source.cpp* C++ source file.

There are four C++ codes and four notebook files can be found in the [GitHub](#) repository under the names:

```
TypeI_core.cpp, and TypeI_example.nb,
TypeII_core.cpp, and TypeII_example.nb,
TypeIII_core.cpp, and TypeIII_example.nb,
TypeIV_core.cpp, and TypeIV_example.nb.
```

They correspond to the four special cases, namely left-right and parity symmetric, left-right symmetric and general parity, general and parity symmetric, and general states respectively, following the classification given in section 3.2. The `.cpp` codes are the C++ source codes and the `.nb` files serve as examples of how to run the C++ codes correctly with examples of an input, details of which we describe in the next section. The `.nb` files will work only if the names of executables in the four special cases are as follows:

```
TypeI_exec.out, TypeII_exec.out, TypeIII_exec.out and
TypeIV_exec.out. Thus compilation should be done such that the output files should have
```

¹⁷E.g. Linux and MAC.

¹⁸<https://learn.microsoft.com/en-us/windows/wsl/install>.

¹⁹Certainly, depending on taste other popular compilers (e.g. `clang`) can be used, as well.

²⁰The actual package names may change depending on the Linux distribution. For example in OpenSuse the `cln` and `cln-devel` packages should be installed.

²¹Just to show an example for windows users, the equivalent command from PowerShell using the WSL, is `> wsl sudo apt install libcln-dev`.

these names. For example:

> `g++ TypeI_core.cpp -lm -lcln -o TypeI_exec.out` etc. The source codes should be compiled only once.

5.1.2 Parameters and outputs

The parameters of an individual run are passed as arguments to the executable code. Here under the word parameters we mean all the data, which is necessary for a proper execution. For example: cutoff values, precision of internal computations, number of sampling points, quantum numbers of the states, initial values of Δ and $c_{a,n}$ etc. The simplified syntax for an execution from a terminal window is as follows:

> `executable.out` followed by numbers separated by space characters, such that each number corresponds to an argument of the executable code. The meaning of each argument can be read off from the example notebook files, where the string corresponding to the appropriate command for the execution is created and the C++ code is run from *Mathematica* as an external program.

Parameters. Here, we give the detailed list of arguments below, such that the numbers in front of the description of a given argument, indicates its position in the list of arguments.

1. **WorkingPrecision:** is an integer for specifying the precision of internal computations.
2. Integer cutoff: `cutP` or `cutP/2` in the general parity and parity symmetric cases respectively.
3. Integer cutoff: `cutQai` or `cutQai/2` in the general parity and parity symmetric cases respectively.
4. Integer cutoff: `QaiShift`.
5. An integer denoting the number of Chebyshev sampling points on the cut: `nPoints`.
6. **DH:** is an integer for giving the small shift $\epsilon = 10^{-DH}$ for computing the numerical derivatives by a first order formula.
7. **precSSF:** is an integer for specifying one of the quit conditions, as described below.
8. **precDelta:** is another integer for giving the 2nd condition for quitting the iteration cycle, as described below.
9. **maxiter:** is an integer giving the maximal number of iterations.

In terms of the previous three integers, one can give the condition at the fulfilment of which the program quits the iteration process and returns. This is as follows:

The program returns after the n^{th} iteration, if either $n \geq \text{maxiter}$ or if the following two conditions are simultaneously satisfied:

$$\sum_{a,n} \left\{ |c_{a,n} - c_{a,n}^{\text{Updated}}|^2 + |c^{a,n} - c^{a,n,\text{Updated}}|^2 \right\} < 10^{-\text{precSSF}},$$

$$|\Delta^{(n)} - \Delta^{(n-1)}| < 10^{-\text{precDelta}},$$

where $\Delta^{(n)}$ denotes the value of Δ after the n th iteration.

- 10. – 17. Integer oscillator quantum numbers: $n_{\mathbf{b}_1}, n_{\mathbf{b}_2}, n_{\mathbf{f}_1}, n_{\mathbf{f}_2}, n_{\mathbf{f}_3}, n_{\mathbf{f}_4}, n_{\mathbf{a}_1}, n_{\mathbf{a}_2}$,
- 18. An integer for giving the multiplicity label `sol` of the state,
- 19. A real number for the 't Hooft coupling g .
- 20. A real number for the initial value of the *anomalous* dimension $\gamma = \Delta - \Delta_0$.

Next come the initial values for $c_{a,n}$ and $c^{a,n}$ as real numbers:

- 21. $\text{Im}(c_{1,0}) \quad \text{Im}(c_{1,1}) \quad \dots \quad \text{Im}(c_{1,N^{(in)}})$
 $\text{Re}(c_{2,0}) \quad \text{Re}(c_{2,1}) \quad \dots \quad \text{Re}(c_{2,N^{(in)}})$
 $\text{Im}(c_{3,0}) \quad \text{Im}(c_{3,1}) \quad \dots \quad \text{Im}(c_{3,N^{(in)}})$
 $\text{Re}(c_{4,0}) \quad \text{Re}(c_{4,1}) \quad \dots \quad \text{Re}(c_{4,N^{(in)}})$
 $\text{Re}(c^{1,0}) \quad \text{Re}(c^{1,1}) \quad \dots \quad \text{Re}(c^{1,N^{(in)}})$
 $\text{Im}(c^{2,0}) \quad \text{Im}(c^{2,1}) \quad \dots \quad \text{Im}(c^{2,N^{(in)}})$
 $\text{Re}(c^{3,0}) \quad \text{Re}(c^{3,1}) \quad \dots \quad \text{Re}(c^{3,N^{(in)}})$
 $\text{Im}(c^{4,0}) \quad \text{Im}(c^{4,1}) \quad \dots \quad \text{Im}(c^{4,N^{(in)}}).$

A few important comments are in order. In the parity symmetric cases, only the $c_{a,2n}$ and $c^{a,2n}$ coefficients must be given in the list of arguments. In the left-right symmetric case, the initial values of $c^{a,n}$ must not be put in the list of arguments. All arguments must be positive integers or real floating point numbers. In the list of arguments an integer valued argument must be given as an exact integer. E.g. 5 and not 5.0. On the other hand giving the real floating point numbers might be also cumbersome. The code cannot interpret exact rational numbers. Thus e.g. 1/10 as a specification for g is uninterpretable for the code. Instead the value 1/10 should be given as 0.1000000...0000000000000000 with `WorkingPrecision` –1 zeroes followed by the digit 1. The initial value 0.1 for g would be interpreted as a machine precision number, but since in the code `WorkingPrecision` digit arithmetic is set, the code generates a `WorkingPrecision` precision number for g with a value deviating from 1/10 in the order of 10^{-16} . At that random generated value of g , the code will serve with precise `WorkingPrecision` precision computations and results. Though, this number representation seems to be a bit cumbersome it can be simply and safely treated e.g. in `Mathematica`. Because of such issues, the output of the C++ code also writes out the parameters of the actual calculation.

It is also very important to note, that the C++ implementation uses a bit different from (4.1) and (4.2) conventions for the \mathbf{P} -functions. Both in the input and the output, the coefficients $c_{a,n}$ and $c^{a,n}$ should be meant as coefficients of the series representation as follows:

$$\mathbf{P}_a = x^{\text{powP}_a} \sum_{n=0}^{\infty} \frac{c_{a,n}}{x^n}, \quad \mathbf{P}^a = x^{-\text{powP}_a - 1} \sum_{n=0}^{\infty} \frac{c^{a,n}}{x^n}. \tag{5.1}$$

Thus, the C++ code requires in the list of arguments, and in the output gives, the coefficients in the convention defined by (5.1). The relation between the coefficients of the two conventions can be given by simple formulas:

$$c_{a,n}^{(C++)} = g^{\text{powP}_a} c_{a,n}, \quad c^{a,n,(C++)} = g^{-\text{powP}_a - 1} c^{a,n}, \quad (5.2)$$

where c and $c^{(C++)}$ stands for the coefficients of (4.1)–(4.2) and (5.1), respectively. When listing the arguments, and the output of the C++ codes, for short we neglected to put the C++ label on the coefficients.

Output. The output contains numbers in a form immediately interpretable by `Mathematica`. If somebody would like to get the numbers in a different form, than it can be reached after appropriate string manipulations on the output string. The structure and content of the output is explained in the example notebook files, but for completeness we summarise them here, too.

The output is a huge `Mathematica` compatible table of numbers and vectors. Now, we describe the meaning of each element of this table one after the other.²²

1. The 1st element is a constant, which can take values 0 or 1. If it is equal to 0, then the program reached the desired convergence within less then `maxiter` iterations and the final result is within the desired precision given by the `precSSF` and `precDelta` input parameters. Otherwise, it takes the value 1, meaning that the program failed to converge in `maxiter` number of iterations to the desired precision.
2. The value of g .
3. Oscillator numbers and multiplicity label of the state in a vector of the form: $\{n_{\mathbf{b}_1}, n_{\mathbf{b}_2}, \{n_{\mathbf{f}_1}, n_{\mathbf{f}_2}, n_{\mathbf{f}_3}, n_{\mathbf{f}_4}\}, n_{\mathbf{a}_1}, n_{\mathbf{a}_2}\}, \text{sol}\}$.
4. The anomalous dimension of the state: $\gamma = \Delta - \Delta_0$.
5. A vector for $\{c_{1,n}\}_{n=0,\dots,\text{cutP}}$ in the general parity case or $\{c_{1,2n}\}_{n=0,\dots,\text{cutP}/2}$ in the parity symmetric case.
6. A vector for $\{c_{2,n}\}_{n=0,\dots,\text{cutP}}$ in the general parity case or $\{c_{2,2n}\}_{n=0,\dots,\text{cutP}/2}$ in the parity symmetric case.
7. A vector for $\{c_{3,n}\}_{n=0,\dots,\text{cutP}}$ in the general parity case or $\{c_{3,2n}\}_{n=0,\dots,\text{cutP}/2}$ in the parity symmetric case.
8. A vector for $\{c_{4,n}\}_{n=0,\dots,\text{cutP}}$ in the general parity case or $\{c_{4,2n}\}_{n=0,\dots,\text{cutP}/2}$ in the parity symmetric case.

The next four elements are present only in the non-LR symmetric cases:

9. A vector for $\{c^{1,n}\}_{n=0,\dots,\text{cutP}}$ in the general parity case or $\{c^{1,2n}\}_{n=0,\dots,\text{cutP}/2}$ in the parity symmetric case.

²²In the sequel, the number in front of a table element corresponds to its position within the table.

10. A vector for $\{c^{2,n}\}_{n=0,\dots,\text{cutP}}$ in the general parity case or $\{c^{2,2n}\}_{n=0,\dots,\text{cutP}/2}$ in the parity symmetric case.
11. A vector for $\{c^{3,n}\}_{n=0,\dots,\text{cutP}}$ in the general parity case or $\{c^{3,2n}\}_{n=0,\dots,\text{cutP}/2}$ in the parity symmetric case.
12. A vector for $\{c^{4,n}\}_{n=0,\dots,\text{cutP}}$ in the general parity case or $\{c^{4,2n}\}_{n=0,\dots,\text{cutP}/2}$ in the parity symmetric case.
13. (LR 9.)²³ The next element is a vector containing the parameters and some error estimates of the actual calculation. The meanings of its elements in order are as follows:

- (a) Number of iterations done
- (b) The value of the sum:

$$\sum_{a,n} \left\{ |c_{a,n} - c_{a,n}^{\text{Updated}}|^2 + |c^{a,n} - c^{a,n,\text{Updated}}|^2 \right\}$$

at the end of the last iteration.

- (c) The absolute value of the difference of the values of Δ obtained after the last and the penultimate iterations:

$$|\Delta^{(\text{last})} - \Delta^{(\text{last}-1)}|$$

- (d) The value used for `cutP` or `cutP/2` in the general parity and parity symmetric cases respectively.
- (e) The value used for `cutQai` or `cutQai/2` in the general parity and parity symmetric cases respectively.
- (f) The value used for `QaiShift`.
- (g) The number of Chebyshev sampling points `nPoints` used.
- (h) The value used for `DH` in the actual calculation. I.e. $\epsilon = 10^{-\text{DH}}$ was the small shift parameter for computing the numerical derivatives by a first order formula.
- (i) The actual value of `WorkingPrecision` used.
- (j) The actual value of `precDelta` used.
- (k) The actual value of `precSSF` set.
- (l) The value of `maxiter` for specifying the maximal number of iterations.
- (m) Another number measuring the “goodness” of the actual calculation: $\sum_a \left\{ |c_{a,-1}^{\text{Updated}}|^2 + |c_{-1}^{a,\text{Updated}}|^2 \right\}$ in the general parity or $\sum_a \left\{ |c_{a,-2}^{\text{Updated}}|^2 + |c_{-2}^{a,\text{Updated}}|^2 \right\}$ in the even cases²⁴. This should be as small as possible on the actual solution of QSC and is a good indicator of the overall precision.

²³Just to avoid confusion, with this notation we would like to indicate that this vector is the 9th element of the output table in the left-right symmetric case, since in that case the previous upper case *c*-vectors are not listed in the output.

²⁴In the left-right symmetric cases the superscripted terms are not involved.

14. (LR 10.) A number measuring the “goodness” of the cutoffs:

$$\sqrt{\sum_{i,n} \left\{ \left| \mathbf{Q}_i(u_n) \Big|_{\text{QaiShift}} - \mathbf{Q}_i(u_n) \Big|_{\text{QaiShift}-1} \right|^2 + \left| \mathbf{Q}_i(u_n) \Big|_{\text{QaiShift}} - \mathbf{Q}_i(u_n) \Big|_{\text{QaiShift}-1} \right|^2 \right\}},$$

where $\mathbf{Q}_i(u_n) \Big|_{\text{QaiShift}}$ denotes the numerical value of $\mathbf{Q}_i(u_n)$ computed with cutoff value QaiShift . This indicates how precise the solution of the QQ-system is within the given approximation.

15. (LR 11.) A quantity, which is proportional to the L^2 -norm of the deviations of the $\mathbf{Q}/\tilde{\mathbf{Q}}$ ratios from the gluing matrix elements:

$$\frac{1}{4 \text{ nPoints}} \sqrt{\sum_n \left\{ \left| \frac{\mathbf{Q}_1(u_n)}{\alpha_1 \tilde{\mathbf{Q}}^2(u_n)} - 1 \right|^2 + \left| \frac{\mathbf{Q}_2(u_n)}{\alpha_2 \tilde{\mathbf{Q}}^1(u_n)} - 1 \right|^2 + \left| \frac{\mathbf{Q}_3(u_n)}{\beta_1 \tilde{\mathbf{Q}}^4(u_n)} - 1 \right|^2 + \left| \frac{\mathbf{Q}_4(u_n)}{\beta_2 \tilde{\mathbf{Q}}^3(u_n)} - 1 \right|^2 \right\}}$$

This number is the indicator of the overall precision of the numerical solution, which is sensitive to both precision of the QQ-system and also measures the precision of the gluing condition fulfilment.

5.2 Management of the parameters, precision control and extrapolation

In this section we discuss our strategies for adjusting various parameters controlling precision of the solver and our adaptive strategy for selecting the step in the coupling g .

For managing and adjusting these parameters in the real time we provide a simple Python script, which is also available on [GitHub](#) .

5.2.1 Adjusting precision controlling parameters

There are quite a few parameters we have to adjust to ensure optimal performance within certain precision. Let us remind the main parameters:

- **cutP** - controls the number of parameters. Bigger **cutP** gives better approximation of **P**-functions but also slows the performance as $\sim \text{cutP}^3$.
- **QaiShift** - controls the number of jumps from the real axis to the domain where we use the asymptotic expansion. Increasing this parameter increases the precision of the **Q**-functions computed for given **P**-functions.
- **cutQai** - controls the number of terms in the asymptotic expansion of $Q_{a|i}$ to use. It also increases the precision of the **Q**-functions for given **P**-functions but due to the asymptotic nature of the large u expansion increase in this parameter has to be balanced with an increase in **QaiShift**.
- **nPoints** - number of the probe points to use. As roughly each probe point gives 8 gluing equations we can simply fix it to **cutP** + 2 for the general Type IV states, for Type I and III: **cutP** + 4 and **cutP** + 8 for the state of the Type II.

Step A. Optimizing QaiShift and cutQai. One has to ensure that at the given starting points for the parameters $\{c\}$ and Δ the QQ-relations are solved to a sufficiently good precision. To test this we rely on the output 14 with the goal to keep it below our targeted precision. If the output 14 is not small enough we have to increase either QaiShift or cutQai. In practice, to decide which of the parameters needs to be increased we run the C++ code with the input parameter 9 `maxiter = 0`, which then make the solver to stop before performing any Newton method iterations, and returns the output 14 very quickly. Then we run it multiple times, changing QaiShift and cutQai separately to check which parameter has the biggest impact on the precision and then adjusting them to reach the desired precision of the output 14.

Step B. Optimizing cutP. This parameter needs to be changed when we are confident that the Q-system is solved to a sufficiently high precision (Step A). Then the indicator that cutP needs an increment is 1) Newton method converges with a good enough precision, but at the same time 2) the output 15, measuring the “goodness” of the gluing condition is too large. In this situation we increase cutP by 1 or by 2, depending on the type of the state, and run again.

5.2.2 Extrapolation and step in g

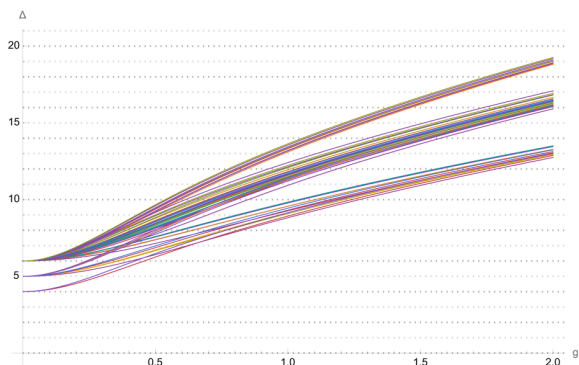
The convergence of the QSC Solver relies a lot on good set of initial points for c 's and Δ . At small g we use the perturbative QSC Solver of [10, 11]. The main advantage of the current algorithm is that it is very stable at very small values of g such as 10^{-5} , where the precision of the perturbative solution (which we provide for up to g^{10} order) is excellent and provides good starting points for our numerical QSC Solver. This way we managed to initialise all 219 states. Then having sufficiently many numerical points (say $n \times 10^{-5}$, $n = 1 \dots 10$) one can use polynomial extrapolation to create starting points for the next value of g . Here we explain the strategy we used to manage the step in g .

We start from the step $dg = 1/10/2^n$ where typically $n = 7$. Then if in 3 consecutive runs for different g 's the convergence was achieved with less than 4 iterations of the Newton method we increase dg by factor of 2 (making sure dg is below $1/10$). If the convergence failed within the limit of the iterations specified, this likely means that the starting point are too far from the true values, in this case we decrease the step by to $dg \rightarrow dg/2$ and step back, close to the previously computed point. Finally, when increasing g we make sure that the solver runs through all values of g for which $10g$ is an integer.

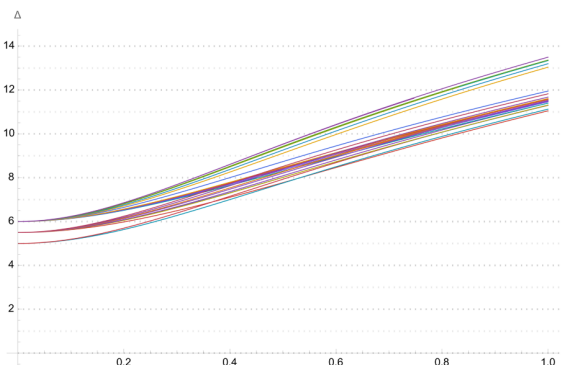
5.3 Examples of parameters and benchmarking

In this section we give the details on how fast our QSC solver is for various regimes in g and different types of states. We also compare the timings for the C++ code with our *Mathematica* implementation for a Type I state. We were using Mac Book Pro with 2.3 GHz Quad-Core Intel Core i7 and *Mathematica* version 12.3.1.0 for the benchmarking. We also give typical parameters and the corresponding precision estimate for the result for Δ for various types of states.

For St. No. 1 (Type I), which is in the Konishi multiplet we made a comparison between C++ and *Mathematica* performance in table 6. We see that when compared on single core C++ is about 8-times faster. Introducing 4 cores into *Mathematica* computation



(a) The scaling dimension of 92 states in $\mathcal{N} = 4$ SYM, with bare dimension $\Delta_0 \leq 6$, that are of type II (cf. section 4.3.2) and type III (cf. section 4.3.3). We provide their scaling dimensions in the range $g \in [0, 2] = \lambda \in [0, 64 \pi^2] \sim [0, 630]$.



(b) Here we have the of 82 states in $\mathcal{N} = 4$ SYM, with bare dimension $\Delta_0 \leq 6$, that have no additional symmetry (cf. type IV states, discussed in section 4.3.4). Their scaling dimensions are given in the range $g \in [0, 1] = \lambda \in [0, 16 \pi^2] \sim [0, 160]$.

only gives the factor of ~ 2.5 in efficiency of the *Mathematica* code, due to the overheads in the parallelisation procedure for this range of parameters. At the same time having the code running on one core allows computing several states simultaneously which gives proper multiplicative efficiency gain. Our computational code is open-source and readily available for usage, eliminating the necessity for costly licensing agreements associated with proprietary software such as *Mathematica*. We respectfully request that users of this code attribute its original source by citing the present paper.

States with bigger Δ_0 usually require higher values of parameters. For comparison we give the parameters and timings for another, more challenging, St. No. 78 (Type I) in table 7.

Finally in table 8 and table 9 the data for less symmetric states St. No. 9 (Type II) and St. No. 13 (Type III) is given. Let us emphasise once again that the C++ code require only one CPU core, so in practice we were running ~ 20 states simultaneously on an HPC.

6 Data analysis at strong coupling

In this section we present analysis of the numerical data obtained by the Fast QSC Solver for the first 219 states/operators — all the single trace operators with the bare dimension $\Delta_0 \leq 6$. Whereas at weak coupling, the perturbative expansion can be obtained analytico-numerically by using the Perturbative QSC solver [11], at the moment, the strong coupling behaviour of these states can only be obtained by fitting the high precision numerical data. The main content of this section thus dedicated to strong coupling analysis.

In section 6.1, we explain the fitting procedure which we use to obtain strong coupling predictions, and compare the predictions to those in the literature. In section 6.2, we analyse our database of states, to see the match to counting formulas available in the literature, and furthermore propose some predictions for strong coupling behaviour of a subset of the states we studied numerically, but also giving prediction for infinitely many states with large bare dimension. Finally, in section 6.3, we see how our spectral data can be used to initiate the bootstrability program for local operators of $\mathcal{N} = 4$ SYM at strong coupling.

g	Δ	cutP	cutQai	QaiShift	Iterations	Error	t_{C++}	$t_M^{4 \text{ cores}}$	$t_M^{1 \text{ core}}$
1/10	2.11551	22	24	60	1	10^{-37}	00:37	00:55	02:37
1/5	2.41886	22	36	60	1	10^{-25}	00:52	02:15	06:43
1/2	3.71272	36	36	60	2	10^{-23}	02:56	08:28	23:14
1	5.60407	50	36	60	2	10^{-21}	04:50	13:47	37:46
2	8.40482	72	44	60	2	10^{-21}	11:58	37:31	
5	14.0998	112	64	70	2	10^{-21}	54:36		

Table 6. Parameters we used for various states, and couplings, and comparison between C++ and *Mathematica* implementations for St. No. 1 (Type I).

g	Δ	cutP	cutQai	QaiShift	Iterations	Error	t_{C++}
1/10	6.04812	24	40	50	2	10^{-17}	01:59
1/5	6.19283	26	40	50	2	10^{-15}	02:05
1/2	7.19999	38	40	50	2	10^{-18}	03:23
1	10.1817	50	40	50	2	10^{-17}	04:39
2	15.37	78	48	60	2	10^{-21}	14:55
5	25.5	106	80	70	2	10^{-14}	01:17:18

Table 7. Parameters we used for various states, and couplings, and timings of the C++ implementation for St. No. 78 (Type I).

g	Δ	cutP	cutQai	QaiShift	Iterations	Error	t_{C++}
1/10	4.14474	17	26	100	1	10^{-25}	01:40
1/5	4.52873	23	26	100	1	10^{-27}	02:47
1/2	6.2573	33	26	100	1	10^{-24}	04:05
1	8.92989	45	30	100	2	10^{-22}	20:12

Table 8. Parameters we used for various states, and couplings, and timings of the C++ implementation for St. No. 9 (Type II).

g	Δ	cutP	cutQai	QaiShift	Iterations	Error	t_{C++}
1/10	5.06741	22	30	100	1	10^{-33}	00:56
2/10	5.26376	24	54	190	1	10^{-25}	03:40
1/5	6.41518	34	54	190	2	10^{-21}	12:29
1	8.82232	46	54	190	2	10^{-18}	24:22
2	12.7445	76	54	190	2	10^{-21}	01:03:42

Table 9. Parameters we used for various states, and couplings, and timings of the C++ implementation for St. No. 13 (Type III).

6.1 Strong coupling analysis of the numerical data

A convenient way to arrange the states at strong coupling was proposed in [92]. It was argued there that in the regime where the quantum numbers $[\ell_1 \ell_2 q_1 p q_2] \sim 1$, the states in $\mathcal{N} = 4$ SYM, should map to massive string states on $\text{AdS}_5 \times S^5$. In particular, in this regime, the spectrum should organise itself into “string mass levels”, parameterised by a positive integer δ , as

$$\Delta \simeq 2 \sqrt{\delta} \lambda^{1/4}. \tag{6.1}$$

Physically, in this regime the strings carry a lot of energy so that their wave-function is localised and can only explore a small part of the curved target space. Even though the 't Hooft coupling is large, this is a quantum regime, as opposed to classical strings, for which the quantum numbers scale as $[\ell_1 \ell_2 q_1 p q_2] \sim \sqrt{\lambda}$.

From (6.1) we see that the natural expansion parameter at strong coupling is the combination $\delta^2 \lambda$, which indeed simplifies the structure of the expansion coefficients as we show below. Even though there is no first principle derivation based on the string theory which would allow for a systematic large λ expansion, it is expected that the structure of the asymptotic strong coupling expansion should be of the following form [1, 3–5, 93–96]:

$$\Delta = \Delta_{\text{reg}} + \Delta_{\text{const}}, \tag{6.2}$$

$$\Delta_{\text{reg}} = (\delta \sqrt{\lambda})^{1/2} \left(2 + \sum_{n=1}^{\infty} \frac{d_n}{(\delta \sqrt{\lambda})^n} \right), \tag{6.3}$$

where Δ_{const} and d_n are undetermined coefficients. The subscript **reg** is used to remind that the expansion of $\Delta_{\text{reg}}/\lambda^{1/4}$ has an (asymptotic) expansion in integer powers of $1/\sqrt{\lambda}$.

6.1.1 Fixing Δ_{const}

In the absence of the general first principle derivation, in order to fix the constant term in the strong coupling expansion (6.3) we present a heuristic argument. Consider a state in $\mathcal{N} = 4$ SYM, with dimension Δ , and Dynkin labels $[\ell_1 \ell_2 q_1 p q_2]$. The quadratic Casimir of this representation is given by [78]

$$J^2 = \frac{1}{2}(\Delta + 2)^2 - 2 + \frac{1}{4}\ell_1(\ell_1 + 2) + \frac{1}{4}\ell_2(\ell_2 + 2) - \frac{1}{4}q_1(q_1 + 2) - \frac{1}{4}q_2(q_2 + 2) - \frac{1}{8}(2p + q_1 + q_2)^2 - (2p + q_1 + q_2). \tag{6.4}$$

It is reasonable to assume that the strong coupling expansion of this operator is regular in powers of $1/\sqrt{\lambda}$. If we substitute the form of the strong coupling expansion of Δ from equation (6.2) into (6.4), we see that the choice $\Delta_{\text{const}} = -2$ renders the strong coupling expansion of J^2 to be only in terms of Δ_{reg}^2 , thereby fulfilling this assumption. Based on this we conclude that

$$\Delta_{\text{const}} = -2, \tag{6.5}$$

for *all* states in planar $\mathcal{N} = 4$ SYM. In the next section, we give credence to this conjecture by performing some numerical fits. Of course for some states, such as Konishi [1, 3–5, 93–96], and those with quantum numbers $[\ell \ell 0 0 0]$ with even ℓ [53, 54], this is already well established, but here we argue that should be true in general.

6.1.2 Fitting procedure

For each of the 219 states in our database, our goal is to make numerical fits of our data, and obtain predictions for d_n in (6.3). To this end, we fit our numerical data against the truncated expansion (6.3). We also assume that $\Delta_{\text{const}} = -2$. Then for each state we proceed as follows:

Step 1: Determine δ . This is relatively easy to do, as for the range of 't Hooft coupling that we consider, we can clearly see how the states divide into bands with $2\sqrt{\delta}\lambda^{1/4}$ asymptotics, where $\delta = 1, 2, \dots$ (cf. figures 2, 3(a), and 3(b)). Thus, we can assign a positive integral value of δ , to each state in our database. Let δ_m be the value of δ associated with the state whose St. No. is m .

Step 2: Find the best hyperparameters. Let $\lambda_{\text{max};m}$ be the highest value of the 't Hooft coupling for which we have a data point for the state m . Consider the set of 't Hooft couplings for which we have data points for this state, in between some value of λ , denoted as λ_{min} and $\lambda_{\text{max};m}$. For a particular choice of λ_{min} , we choose a range of powers of $1/\sqrt{\lambda}$ up to $1/\lambda^{n_{\text{max}}/2}$. Thus, a choice of the tuple $\{\lambda_{\text{min}}, n_{\text{max}}\}$, defines the hyperparameters of our fit. We would like to fit our numerical data against the “model” (6.3). Let $d_{n;m}$ be the value of the coefficient d_n , associated with the state m . Thus, we need to determine the tuple $\{\lambda_{\text{min}}, n_{\text{max}}\}$, for which we get the best fit. For each choice of this tuple, we subtract the first two terms of (6.3), evaluated at each value of λ in between λ_{min} and $\lambda_{\text{max};m}$, where we have a data point. Then we fit this “refined” data with the following powers of λ : $\{\lambda^{1/4}, \dots, \lambda^{1/4-n_{\text{max}}/2}\}$, and measure the coefficient of $\lambda^{1/4}$, which should be zero, according to (6.3). We choose that tuple $\{\lambda_{\text{best}}, n_{\text{best}}\}$, for which this coefficient has the least magnitude. As an independent verification of the precision we also usually find the sub-leading coefficient d_1 to be some simple rational numbers.

Step 3: Make a prediction for d_1 . We fit the same refined data for λ between λ_{best} and $\lambda_{\text{max};m}$, with the following powers of λ : $\{\lambda^{-1/4}, \dots, \lambda^{1/4-n_{\text{best}}/2}\}$. The coefficient of $\delta_m^{-1/2}\lambda^{-1/4}$ gives us a prediction for $d_{1;m}$, the value of d_1 , associated with state m .

Step 4: Measure the precision of d_1 . We repeat **Step 3**, but use the powers: λ : $\{\lambda^{-1/4}, \dots, \lambda^{1/4-n_{\text{best}}/2-1/2}\}$. Then we check at which digit the coefficient of $\delta_m^{-1/2}\lambda^{-1/4}$, differs from our prediction for $d_{1;m}$. This gives us a measure of the precision of $d_{1;m}$.

In table 18, we provide the fitted values of d_1 , for every state in our database, up to the best precision, that we could obtain using this procedure.

6.1.3 Predictions from the literature.

Recall, from section 2, that $\mathfrak{sl}(2)$ operators are characterised by the number of derivatives S and length L . The State ID of such operators is of the form (2.10). Their quantum numbers are given by (2.11). As described in detail in appendix C, the scaling dimension of such operators, at one-loop at weak coupling, may be obtained by solving Bethe ansatz equations. As explained there, this procedure associates a set of integral mode numbers, which can be used as an alternative to the multiplicity label to distinguish between the states with the same quantum numbers. There are 27 $\mathfrak{sl}(2)$ states in our database.

St. No.	State ID	$[\ell_1 \ell_2 q_1 p q_2]$	$[S L n]$	Δ_0	$\Delta_0 + \# g^2$	δ	Discrepancy $2\sqrt{\delta}\lambda^{1/4} - 2$	Discrepancy d_1	Discrepancy d_2	Discrepancy d_3
1	$2[0 0 1 1 1 1 0 0]_1$	$[0 0 0 0 0]$	$[2 2 1]$	2	12	1	4.1×10^{-16}	2.4×10^{-16}	7.8×10^{-13}	1.4×10^{-10}
2	$3[0 0 2 2 1 1 0 0]_1$	$[0 0 0 1 0]$	$[2 3 1]$	3	8	1	8.5×10^{-12}	-1.9×10^{-10}	6.5×10^{-9}	-6.5×10^{-8}
7	$4[0 0 3 3 1 1 0 0]_2$	$[0 0 0 2 0]$	$[2 4 1]$	4	$10 - 2\sqrt{5}$	1	1.6×10^{-12}	-2.3×10^{-10}	7.8×10^{-10}	-2.2×10^{-7}
23	$5[0 0 4 4 1 1 0 0]_1$	$[0 0 0 3 0]$	$[2 5 1]$	5	4	1	1.8×10^{-12}	8.3×10^{-11}	-3.0×10^{-10}	5.0×10^{-11}
118	$6[0 0 5 5 1 1 0 0]_1$	$[0 0 0 4 0]$	$[2 6 1]$	6	3.012081585	1	-1.1×10^{-14}	1.4×10^{-13}	4.1×10^{-11}	-2.0×10^{-9}
12	$4[0 2 1 1 1 1 2 0]_1$	$[2 2 0 0 0]$	$[4 2 1]$	4	$\frac{50}{3}$	2	-1.6×10^{-9}	2.4×10^{-8}	5.2×10^{-6}	-5.5×10^{-6}
39	$5[0 2 2 2 1 1 2 0]_1$	$[2 2 0 1 0]$	$[4 3 1]$	5	12	2	-9.3×10^{-10}	1.6×10^{-7}	1.0×10^{-6}	-3.8×10^{-4}
206	$6[0 2 3 3 1 1 2 0]_3$	$[2 2 0 2 0]$	$[4 4 1]$	6	8.765533583	2	3.0×10^{-10}	2.4×10^{-8}	2.9×10^{-6}	-3.7×10^{-5}
219	$6[0 4 1 1 1 1 4 0]_1$	$[4 4 0 0 0]$	$[6 2 1]$	6	$\frac{98}{5}$	3	1.2×10^{-8}	-1.1×10^{-6}	8.9×10^{-5}	-3.4×10^{-3}

Table 10. Test of strong coupling predictions for $\mathfrak{sl}(2)$ states in our database with $n = 1$. The difference between the prediction for the various d_k from (6.6), and our fitted value for the same d_k is given in the last three columns. In all cases, the discrepancy occurs within the error of our fit.

St. No.	State ID	$[\ell_1 \ell_2 q_1 p q_2]$	$[S L n]$	Δ_0	$\Delta_0 + \# g^2$	δ	Best fit for d_4
1	$2[0 0 1 1 1 1 1 0 0]_1$	$[0 0 0 0 0]$	$[2 2 1]$	2	12	1	-91.97602351
2	$3[0 0 2 2 1 1 1 0 0]_1$	$[0 0 0 1 0]$	$[2 3 1]$	3	8	1	-68.2938
7	$4[0 0 3 3 1 1 1 0 0]_2$	$[0 0 0 2 0]$	$[2 4 1]$	4	$10 - 2\sqrt{5}$	1	-52.21062
23	$5[0 0 4 4 1 1 1 0 0]_1$	$[0 0 0 3 0]$	$[2 5 1]$	5	4	1	-89.959722
118	$6[0 0 5 5 1 1 1 0 0]_1$	$[0 0 0 4 0]$	$[2 6 1]$	6	3.012081585	1	-340.652525

Table 11. Best fit of d_4 for $\mathfrak{sl}(2)$ states in our database with $n = 1$.

For $\mathfrak{sl}(2)$ states, which are parity symmetric, and only have two distinct mode numbers n and $-n$, there are predictions in the literature [1–8, 93–96], for some of the coefficients d_k . Below, we will test them.

States with $n = 1$. This is the most studied case. In this case, there is a prediction for d_1 in [1–5, 93–96], a prediction for d_2 in [6], and finally a prediction for d_3 in [8], giving

$$\begin{aligned}
 \Delta_{S,L,n=1} &\simeq \sqrt{2S}\lambda^{1/4} - 2 + \frac{2L^2 + (3S-2)S}{4\sqrt{2S}} \frac{1}{\lambda^{1/4}} \\
 &+ \frac{1}{32(2S)^{3/2}} \left[-21S^4 + (24 - 96\zeta_3)S^3 + 4(5L^2 - 3)S^2 + 8L^2S - 4L^4 \right] \frac{1}{\lambda^{3/4}} \\
 &+ \frac{1}{128(2S)^{5/2}} \left[187S^6 + 6(208\zeta_3 + 160\zeta_5 - 43)S^5 + (-146L^2 - 4(336\zeta_3 - 41))S^4 \right. \\
 &\left. + (32(6\zeta_3 + 7)L^2 - 88)S^3 + (-28L^4 + 40L^2)S^2 - 24L^4S + 8L^6 \right] \frac{1}{\lambda^{5/4}}. \quad (6.6)
 \end{aligned}$$

In our database, we found 9 states with $n = 1$. In table 10 below, we test the predictions for the strong coupling expansion of the scaling dimension of these states and find perfect agreement within the numerical precision of our fit. The results are given in the table 10. We can also make a fit d_4 for some of these states, in table 11 below we display those, for which we have reliable precision.

Conjectures for states with $n > 1$. There are a number of conjectures about the strong coupling dimension of states with mode numbers $n > 1$ in the literature [2, 6–8]. In [6], the

St. No.	State ID	$[\ell_1 \ell_2 q_1 p q_2]$	$[S L n]$	Δ_0	$\Delta_0 + \# g^2$	δ	Discrepancy $2\sqrt{\delta} \lambda^{1/4} - 2$	Discrepancy d_1	Discrepancy d_2
6	$4[0 0 3 3 1 1 0 0]_1$	$[0 0 0 2 0]$	$[2 4 2]$	4	$10 + 2\sqrt{5}$	2	-4.6×10^{-10}	2.4×10^{-8}	2.0×10^{-2}
24	$5[0 0 4 4 1 1 0 0]_2$	$[0 0 0 3 0]$	$[2 5 2]$	5	12	2	1.8×10^{-11}	8.1×10^{-9}	-7.6×10^{-3}
119	$6[0 0 5 5 1 1 0 0]_2$	$[0 0 0 4 0]$	$[2 6 2]$	6	9.780167472	2	2.7×10^{-13}	-3.0×10^{-11}	-2.1×10^{-3}

Table 12. Test of strong coupling predictions for $\mathfrak{sl}(2)$ states in our database with $S = 2$ and $n = 2$. The difference between the prediction for the various d_k from (6.7), and our fitted value for the same d_k is given in the last two columns. In all cases, the discrepancy occurs within the error of our fit.

following expression is proposed for the dimension of a state with $n = 2$ or 3, though it must be noted that the authors of that article pointed out that this prediction is based on an assumption about the behaviour in S , which definitely breaks down for $n > 1$ state. So that is curious to see if this affects the prediction already at the low orders in $1/\sqrt{\lambda}$, which reads

$$\Delta_{S,L,n} \simeq \sqrt{2Sn} \lambda^{1/4} + \frac{2L^2 + 3S^2 - 2S}{4(2Sn)^{1/2} \lambda^{1/4}} + \frac{1}{32(2Sn)^{3/2}} \left[-21S^4 + (32B_2 + 12)S^3 + (20L^2 - 12)S^2 + 8L^2S - 4L^4 \right] \frac{1}{\lambda^{3/4}}. \tag{6.7}$$

Here B_2 depends on n , and we have

$$B_2 = \begin{cases} -3\zeta_3 + \frac{3}{8} & , \quad n = 1 \\ -24\zeta_3 - \frac{13}{8} & , \quad n = 2 \\ -81\zeta_3 - \frac{24}{8} & , \quad n = 3 \end{cases}. \tag{6.8}$$

In [7], the conjecture (6.7) was tested for $S = 2$, and various values of L and n . It was found that this conjecture holds water for $n = 2$, and deviations were observed at $n = 3$.

For the states with $n = 3$ studied in [7], apart from the leading contribution, the formula (6.7) doesn't predict either d_1 or d_2 correctly in this case. In [7], a prediction for d_1 is given for the case that $n = 3$ and $S = 2$. We have

$$\Delta_{2,L,3} \simeq 2\sqrt{3} \lambda^{1/4} + \frac{L^2}{4\sqrt{3}} \frac{1}{\lambda^{1/4}}. \tag{6.9}$$

We will now compare these results with our numerics.

States with $n = 2$. There are 4 states in our database with $n = 2$. First, let us consider states with $S = 2$. We display the 3 of them in table 12. For all these states our fit appear to agree within the numerical error with (6.7).

The **State Number 6**, with $[S L n] = [2 4 2]$ was studied in [6], and the states number **24** and **119**, with $[2 5 2]$ and $[2 6 2]$ respectively, were studied in [7] and we are able to corroborate the result, that (6.7) correctly predicts the scaling dimension at strong coupling for these states.

Next, consider the 1 state in our database with $S > 2$ as shown in table 13. Thus, for the **State Number 204**, with $S = 4$, we see that the formula (6.7) does not seem to work, even at sub-leading order at strong coupling. It would be interesting to understand the reason for this disagreement and find a general formula which works for all S .

St. No.	State ID	$[\ell_1 \ell_2 q_1 p q_2]$	$[S L n]$	Δ_0	$\Delta_0 + \# g^2$	δ	Discrepancy $2\sqrt{\delta}\lambda^{1/4} - 2$	Best fit for d_1	Prediction of [6]
204	${}_6[0\ 2\ 3\ 3\ 1\ 1\ 2\ 0]_1$	$[2\ 2\ 0\ 2\ 0]$	$[4\ 4\ 2]$	6	23.18267020	4	7.5×10^{-9}	12.00000	9

Table 13. Test of strong coupling predictions for the $\mathfrak{sl}(2)$ state in our database with $S > 2$ and $n = 2$. We find a disagreement with the prediction (6.7).

St. No.	State ID	$[\ell_1 \ell_2 q_1 p q_2]$	$[S L n]$	Δ_0	$\Delta_0 + \# g^2$	δ	Discrepancy $2\sqrt{\delta}\lambda^{1/4} - 2$	Discrepancy d_1
120	${}_6[0\ 0\ 5\ 5\ 1\ 1\ 0\ 0]_3$	$[0\ 0\ 0\ 4\ 0]$	$[2\ 6\ 3]$	6	15.20775094	3	4.1×10^{-12}	-2.0×10^{-10}

Table 14. Test of strong coupling predictions for the $\mathfrak{sl}(2)$ state in our database with $S > 2$ and $n = 2$. The difference between the prediction for d_1 from (6.9), and our fitted value is given in the last column. The discrepancy occurs within the error of our fit.

States with $n = 3$. There is 1 state in our database with $n = 3$, which is displayed in table 14.

This state, number 120, is the same state as was studied in [7]. Therefore we are only able to obtain a consistency check, rather than a confirmation of the prediction (6.9).

In general we conclude that even in the simplest $\mathfrak{sl}(2)$ sector we still do not know an analytic way of computing even the leading non-trivial strong coupling coefficient d_1 , which would work for all states.

6.2 Counting of states and Kaluza-Klein towers

The authors of [97] perform a counting of states of $\mathcal{N} = 4$ SYM, that scale as $\sim \lambda^{1/4}$ at strong coupling. In order to do this, they take the flat-space limit of $\text{AdS}_5 \times S^5$, and perform a counting of representations of $\text{SO}(9)$, the massive little group of $\mathbb{R}^{1,9}$. In particular, they count representations of $\text{SO}(4) \times \text{SO}(5)$, corresponding to the split into AdS_5 and S^5 . Compactifying five directions to S^5 , implies that each representation $[m\ n]$ of $\text{SO}(5)$ gets replaced by a Kaluza-Klein (KK-) tower [98] of $\text{SO}(6)$ representations. Introduce the following notation for the KK-tower of states with Lorentz spin labels $(\ell_1\ \ell_2)$, and $\text{SO}(5)$ labels $[m\ n]$: [98]

$$\begin{aligned}
 [\ell_1\ \ell_2; m\ n] &= \sum_{r=0}^m \sum_{s=0}^n \sum_{p=m-r}^{\infty} [\ell_1, \ell_2, r+n-s, p, r+s] \\
 &+ \sum_{r=0}^{m-1} \sum_{s=0}^{n-1} \sum_{p=m-r-1}^{\infty} [\ell_1, \ell_2, r+n-s, p, r+s+1]. \quad (6.10)
 \end{aligned}$$

This counting is useful at infinite coupling, where states are split according to the string level δ . States within a KK-tower will share the same δ but their Δ will in general split already at $1/\lambda^{1/4}$ order. There are infinitely many states in each KK-tower, which then implies that there should be infinitely many states for a given string level δ . However, the number of KK-towers at each δ is finite and we will give some examples below.

Thus, for each δ , one can introduce a counting function count_δ , following [97], which

St. No.	State ID	$[\ell_1 \ell_2 q_1 p q_2]$	Δ_0	$\Delta_0 + \# g^2$	δ	d_1	j_1	$[S L n]$	Type
1	${}_2[0 0 1 1 1 1 0 0]_1$	$[0 0 0 0 0]$	2	12	1	2	2	$[2 2 1]$	I
2	${}_3[0 0 2 2 1 1 0 0]_1$	$[0 0 0 1 0]$	3	8	1	$\frac{13}{4}$	2	$[2 3 1]$	I
7	${}_4[0 0 3 3 1 1 0 0]_2$	$[0 0 0 2 0]$	4	$10 - 2\sqrt{5}$	1	5	2	$[2 4 1]$	I
23	${}_5[0 0 4 4 1 1 0 0]_1$	$[0 0 0 3 0]$	5	4	1	$\frac{29}{4}$	2	$[2 5 1]$	I
118	${}_6[0 0 5 5 1 1 0 0]_1$	$[0 0 0 4 0]$	6	3.012081585	1	10	2	$[2 6 1]$	I

Table 15. All states in our database with $\delta = 1$.

contains the KK-towers with that value of δ . For example

$$\text{count}_1 = [00; 00], \quad (6.11)$$

$$\text{count}_2 = 2[00; 00] + [00; 20] + [00; 02] + 2[11; 10] + [22; 00] + [20; 00] + [02; 00]. \quad (6.12)$$

The count_3 is also known explicitly [99], and is given in appendix D.2. Below we identify states belonging to different KK-towers and check the counting (6.11) and (6.12).

The process of assigning a specific state to a given Kaluza-Klein tower solely based on quantum numbers can generally be ambiguous. This is due to the degeneracies in the spectrum and the absence of additional input from the wave functions. As we mentioned already, the states within the same tower could have different sub-leading coefficients d_1 . However, we noticed that when computing the expansion of the quadratic Casimir instead of Δ , the states within the same tower have the same sub-leading coefficient, which can in turn be used to assign states to different KK-towers. Furthermore, if this observation is correct, it implies a non-trivial set relations on the d_1 coefficients in the expansion of Δ among infinite set of states within one KK-tower. More precisely one gets the following identity:

$$d_1 = \frac{p^2}{4} + \frac{p}{4}(q_1 + q_2 + 4) + \frac{1}{16} \left[16 - 2\ell_1(\ell_1 + 2) - 2\ell_2(\ell_2 + 2) + 3q_1(q_1 + 4) + 3q_2(q_2 + 4) + 2q_1q_2 \right] + \frac{j_1}{2}, \quad (6.13)$$

where j_1 is the sub-leading coefficient in the strong coupling expansion for $J^2 \simeq 2\delta\sqrt{\lambda} + j_1$, which we conjecture to be the same for all states in one tower, based on the data we have. We also checked that the next coefficient j_2 is already different for states in a KK-tower.

Below we analyse the $\delta = 1, 2, 3$ cases, confirming our conjecture and also confirming the counting of [97, 99].

States with $\delta = 1$. There are 5 such states in our database. All of them have Lorentz spin labels $(0 0)$. We present them in table 15.

Clearly, all these states are members of the KK-tower $[0 0; 0 0]$, in exact agreement with (6.11), and thus the results of [97]. Furthermore we see that for all these states $j_1 = 2$. All the states are $\mathfrak{sl}(2)$ states of the form $[S, L, n] = [2, p + 2, 1]$, as can be seen by comparing with section 6.1.3. The strong coupling dimensions of these states, at first three sub-leading orders is given by equation (6.6).

All the other states in the tower should have bigger bare dimension due to the unitarity bounds (see e.g. [100]):

$$\Delta > 2 + \max \left\{ \ell_1 + \frac{1}{2}(3q_1 + 2p + q_2), \ell_2 + \frac{1}{2}(q_1 + 2p + 3q_2) \right\}, \quad (6.14)$$

which for the current set of states would imply

$$\Delta > p + 2. \quad (6.15)$$

Thus, we see that a state with quantum numbers [0 0 0 5 0], must have $\Delta > 7$, and thus are not present in the current data set.

States with higher δ . At $\delta > 1$ we can face an ambiguity when assigning the states from our database to various KK-towers (given in (6.12) for $\delta = 2$ and in (D.1) for $\delta = 3$). We see that there are many states, whose quantum numbers are consistent with being a member of more than one KK-tower. But this ambiguity is lifted if we look at the j_1 coefficient. Or in other words we verified the conjecture (6.13) which relates the sub-leading coefficients in Δ between various members of the KK-tower.

We have a total of 38 states in our database, with $\delta = 2$. We have classified them into the 9 KK-towers given in (6.12). The assignment is described in appendix D.1, specifically in tables 20–23. We have a total of 128 states in our database, with $\delta = 3$. We have classified them into KK-towers given in (D.1). The assignment is described in appendix D.2, specifically in tables 24–35. It is also shown there that j_1 is indeed a good classifier of states, into KK-towers.

In other words, where we have sufficient precision, our fits confirm the formula (6.13). It is important to notice that, by using the formula (6.13), it is possible to obtain the d_1 coefficients for every state in the KK tower, even ones which are not practically accessible by numerical methods.²⁵

In the next section, we will see how this new spectral information, can be injected into the conformal bootstrap constraints obtained in [53, 54].

6.3 Bootstrability

Following the philosophy of [12–14], the results for the spectrum, joined with the constraints from the conformal crossing relations for some correlators could give narrow bounds, or even analytic results for some structure constants. In the current set-up of the local operators our predictions at strong coupling can be fed into the conformal constraints obtained in [53, 54].

One of the complications of the consideration based purely on conformal constraints is typically related to the mixing problem — when there are several states with the same quantum numbers and same δ . As we know how the degeneracy is lifted from our data, we should be able to inject this information and improve the results based on conformal bootstrap (with some input from localisation).

²⁵Such as states with very high bare dimension Δ_0 , where current methods are not able to obtain perturbative data.

Below, we describe the setup of [53, 54]. They consider a four point function of four $\mathbf{20}'$ 1/2-BPS operators in $\mathcal{N} = 4$ SYM. These are operators which transform under the rank-2 symmetric traceless representation of the $SO(6)$ R -symmetry group. They are defined as

$$\mathcal{O}_2(\vec{x}, Y) \equiv \text{Tr } \Phi_I(\vec{x}) \Phi_J(\vec{x}) Y^I Y^J, \quad (6.16)$$

where Φ_I is a fundamental real scalar field of $\mathcal{N} = 4$ SYM, and Y^I is a polarisation null vector. After extracting the kinematic factors, the four-point function of four such operators can be written in terms of a function of the conformal and R -symmetry cross ratios. We have

$$\langle \mathcal{O}_2(\vec{x}_1, Y_1) \mathcal{O}_2(\vec{x}_2, Y_2) \mathcal{O}_2(\vec{x}_3, Y_3) \mathcal{O}_2(\vec{x}_4, Y_4) \rangle = \frac{Y_{12}^2 Y_{34}^2}{x_{12}^4 x_{34}^4} \mathcal{S}(U, V; \sigma, \tau), \quad (6.17)$$

where $Y_{IJ} \equiv Y_I \cdot Y_J$, $x_{ij} \equiv x_i - x_j$, U and V are the conformal cross-ratios, and σ and τ are R -symmetry cross ratios. These are defined as

$$U \equiv \frac{x_{12}^2 x_{34}^2}{x_{13}^2 x_{24}^2} \equiv z \bar{z}, \quad V \equiv \frac{x_{14}^2 x_{23}^2}{x_{13}^2 x_{24}^2} \equiv (1-z)(1-\bar{z}), \quad \sigma \equiv \frac{Y_{13} \cdot Y_{24}}{Y_{12} \cdot Y_{34}}, \quad \tau \equiv \frac{Y_{14} \cdot Y_{23}}{Y_{12} \cdot Y_{34}}. \quad (6.18)$$

Using superconformal symmetry, \mathcal{S} can be written as [101]

$$\mathcal{S}(U, V; \sigma, \tau) = \mathcal{S}_{\text{free}}(U, V; \sigma, \tau) + \Theta(U, V; \sigma, \tau) \mathcal{T}(U, V), \quad (6.19)$$

$$\Theta(U, V; \sigma, \tau) \equiv \tau + [1 - \sigma - \tau]V + \tau[\tau - 1 - \sigma]U + \sigma[\sigma - 1 - \tau]UV + \sigma V^2 + \sigma \tau U^2, \quad (6.20)$$

$$\mathcal{S}_{\text{free}}(U, V; \sigma, \tau) = 1 + U^2 \sigma^2 + \frac{U^2}{V^2} \tau^2 + \frac{1}{c} \left(U \sigma + \frac{U}{V} \tau + \frac{U^2}{V} \sigma \tau \right). \quad (6.21)$$

Here $\mathcal{S}_{\text{free}}$ denotes the free theory correlator, $\mathcal{T}(U, V)$ is called the reduced correlator, and c is the central charge, which is given by $c = \frac{N^2-1}{4}$. The reduced correlator satisfies a crossing equation $\mathcal{T}(U, V) = \mathcal{T}(1/U, V/U) = 1/V^2 \mathcal{T}(U/V, 1/V)$, and can be expanded using the operator product expansion (OPE). We have

$$\mathcal{T}(U, V) = U^{-2} \sum_{T, \ell} C_{T, \ell}^2 G_{T+4, \ell}(U, V). \quad (6.22)$$

Here, the four-dimensional conformal block G is given by [102]

$$G_{T, \ell}(U, V) = \frac{z \bar{z}}{z - \bar{z}} (k_{T+2, \ell}(z) k_{T-2, \ell}(\bar{z}) - k_{T+2, \ell}(\bar{z}) k_{T-2, \ell}(z)), \quad (6.23)$$

where k_h is

$$k_h(z) \equiv z^{\frac{h}{2}} {}_2F_1(h/2, h/2, h, z). \quad (6.24)$$

In the planar limit, the superprimaries exchanged in the OPE (6.22) include single- and double-trace operators, and belong to both short and long multiplets. In [53, 54] it was shown that it is possible to rewrite the crossing equation in a way that focuses on the long multiplets

$\delta \backslash \ell$	0	2	4	6	8
1	1				
2	3, 4	12			
3	76, 78, 81, 83, 84, 85	196, 197, 198, 199	219		
4	77, 79, 80, 86, ? (22)	195, 200, 201, ? (24)	? (6)	? (1)	
5	80, ? (99)	? (157)	? (40)	? (6)	? (1)

Table 16. States in our database with quantum numbers $[\ell \ell 0 0 0]$ with even ℓ , i.e. those which are exchanged in the OPE (6.22). Each entry contains the *St. No.* of the state(s) with the corresponding δ and ℓ . The cells where we have all the exchanged states in our database are shaded. In the cases we have some or none of the exchanged states in our database, we write the *St. Nos.* of the states that are there, followed by a “?” with the total number of states with that δ and ℓ in parenthesis. The counting of states in this table is from [97].

corresponding to the “stringy” operators exchanged in the OPE (6.22) i.e. those operators that we studied in this paper with $\Delta \sim \lambda^{1/4}$ scaling. The stringy operators exchanged in the OPE (6.22) have quantum numbers $[\ell \ell 0 0 0]$ with $\ell = 0, 2, 4, \dots$

In order to make a comparison we introduce further notations from [53, 54]. For twists $T \equiv \Delta - \ell$ we have

$$T(\lambda) \simeq 2\sqrt{\delta} \lambda^{\frac{1}{4}} - 2 - \ell + \frac{T_1}{\lambda^{1/4}}, \quad T_1 \equiv \frac{d_1}{\sqrt{\delta}}. \tag{6.25}$$

Then, for the OPE coefficients, we have [53, 54]

$$C^2(\lambda) = \frac{\pi^3}{2^{12}} \frac{2^{-2T(\lambda)} T(\lambda)^6}{\sin^2\left(\frac{\pi T(\lambda)}{2}\right)} \frac{1}{2^{2\ell(\ell+1)}} f(\lambda). \tag{6.26}$$

The prefactor of C^2 in (6.26) is highly oscillating when $\lambda \rightarrow \infty$ and becomes infinite each time the twist T crosses an even integer. At the same time the function $f(\lambda)$ has a regular asymptotic expansion:

$$f(\lambda) \simeq f_0 + \frac{f_1}{\lambda^{1/4}} + \frac{f_2}{\lambda^{1/2}}. \tag{6.27}$$

The result of [53, 54] includes formulas for the CFT-data of the exchanged operators at strong coupling. In order to compare we introduce an integer “Regge trajectory number” [103] $t \equiv \delta - \ell/2$.

In table 16, we present all the 23 states in our database, that can be exchanged in the OPE (6.22) for given δ and ℓ .

Thus, for each value of t , we have a set of states, with particular values of δ and ℓ , associated with it. These states are said to be “on the Regge trajectory t .” In the papers [53, 54] the mixing problem appeared to be an obstacle to disentangle various exchanged operators with the same values of δ and ℓ , only “average” formulas were obtained that compute a sum over such operators, which they denote by $\langle \dots \rangle$. Namely, they compute $\langle f_0 \rangle$ [53], $\langle f_1 \rangle$, $\langle T_1 f_0 \rangle$ and $\langle f_2 \rangle$ [54], for the states on various Regge trajectories.

Regge trajectory 1. On the leading Regge trajectory, i.e. for the states with $t = 1$, the degeneracy of states is trivial, up to $\delta = 7$ [97], and therefore, the average formulas give immediately results for the coefficients in the strong coupling expansion of the CFT-data. Correspondingly, the first 3 coefficients f_0 , f_1 and f_2 are already known analytically for these states (see [53, 54] for explicit results).

Predictions on Regge trajectory 2. States on this Regge trajectory have $\ell = 2(\delta - 2)$. The average of the OPE coefficients is given by [53]

$$\langle f_0 \rangle = \frac{r_1(\delta)}{3} (2\delta^2 + 3\delta - 8), \tag{6.28}$$

where

$$r_n(\delta) = \frac{4^{2-2\delta} \delta^{2\delta-2n-1} (2\delta - 2n - 1)}{\Gamma(\delta) \Gamma(\delta - \lfloor \frac{n}{2} \rfloor)}. \tag{6.29}$$

The average of the leading OPE coefficients, weighted by the twist is [54]

$$\langle f_0 T_1 \rangle = \frac{r_1(\delta)}{18\sqrt{\delta}} (18\delta^4 + 25\delta^3 - 57\delta^2 + 50\delta - 72). \tag{6.30}$$

Note that the number of states with a given spin contributing to (6.33) depends on the spin. For this trajectory we only have two cells in ℓ, δ table 16 with complete number of states: $\ell = 0, \delta = 2$ (two states) and $\ell = 2, \delta = 3$ (four states) according to [97] and the counting in section 6.2.

Consider first $\ell = 0$ case. The two states are **St. No. 3** and **4** (as defined in table 18). For those state we have

$$T_{1;3} = \sqrt{2}, \quad T_{1;4} = 4\sqrt{2}, \tag{6.31}$$

where the second index corresponds to the **State Number**. Then from (6.28) and (6.30) we get

$$\langle f_0 \rangle = f_{0;3} + f_{0;4} = \frac{1}{4}, \tag{6.32}$$

$$\langle f_0 T_1 \rangle = f_{0;3} T_{1;3} + f_{0;4} T_{1;4} = \sqrt{2}, \tag{6.33}$$

resulting in

$$\boxed{f_{0;3} = 0, \quad f_{0;4} = \frac{1}{4}}. \tag{6.34}$$

Curiously only one of the two OPE coefficients is nonzero, which may indicate some additional simplification at strong coupling.

For $\ell = 2$ there are four states with **St. Nos. 196, 197, 198** and **199**. Furthermore, **198**, and **199**, which are Type II states, form a parity doublet, and thus their dimensions are exactly degenerate, as discussed in section 3.2. Since the external BPS operators are parity invariant, their OPE coefficients should be equal as well, which reduces the system to 3 unknowns. Using that

$$T_{1;196} = \frac{8}{\sqrt{3}}, \quad T_{1;197} = \frac{17}{\sqrt{3}}, \quad T_{1;198} = \frac{13}{\sqrt{3}}, \tag{6.35}$$

St. No.	d_1 numeric	d_1 prediction	d_2 numeric	d_2 guess	discrepancy
3	1.9999999	2	-24.34936	$\frac{9}{2} - 24\zeta_3$	-5.4×10^{-7}
4	8.00000	8	-66.34945	$-\frac{75}{2} - 24\zeta_3$	8.7×10^{-6}
196	8.00000	8	-140.366		
197	16.99999	17	-293.365		
198, 199	12.999	13	-179.3		

Table 17. sub-leading and sub-sub-leading dimension at strong coupling for states on Regge trajectory 2.

from (6.28) and (6.30) we get

$$\langle f_0 \rangle = f_{0;196} + f_{0;197} + 2 f_{0;198} = \frac{513}{1024}, \tag{6.36}$$

$$\langle f_0 T_1 \rangle = f_{0;196} T_{1;196} + f_{0;197} T_{1;197} + 2 f_{0;198} T_{1;198} = \frac{2547 \sqrt{3}}{1024}, \tag{6.37}$$

which allows to express everything in terms of $f_{0;196}$:

$$f_{0;197} = \frac{5}{4} f_{0;196} + \frac{243}{1024}, \quad f_{0;198} = -\frac{9}{8} f_{0;196} + \frac{135}{1024}. \tag{6.38}$$

Furthermore, as the OPE coefficients have to be non-negative, we have three further inequalities which impose:

$$f_{0;196} \geq 0, \quad f_{0;197} \geq 0, \quad f_{0;198} \geq 0. \tag{6.39}$$

Subjecting the solution (6.38) to the inequalities (6.39), we get the allowed regions

$$f_{0;196} \in \left[0, \frac{15}{128} \right], \quad f_{0;198} \in \left[0, \frac{135}{1024} \right], \quad f_{0;197} \in \left[\frac{243}{1024}, \frac{393}{1024} \right] \simeq [0.237305, 0.383789]. \tag{6.40}$$

Optimistically one could hope that only one of the OPE coefficients is non-zero, however, clearly $f_{0;196}$ and $f_{0;197}$ cannot vanish simultaneously due to (6.38).

Next order on Regge trajectory 2. At the next order, we are able to obtain some predictions for the d_2 coefficient of states 3, 4, 196 and 197. They are presented below.

Note added. While this paper was at the final stage of preparation for publication we received a communication confirming that in an upcoming paper [104], analytical expressions for T_1 , T_2 and f_0 for the state numbers 3 and 4, are obtained using the analytical conformal bootstrap, and they confirm our predictions for these quantities.

Predictions on Regge trajectory 3. For states with $\ell = 2(\delta - 3)$ the average of the OPE coefficients for this trajectory is given by the following expression [53]

$$\langle f_0 \rangle = \frac{r_2(\delta)}{45} \left(10 \delta^4 + 43 \delta^3 + 8 \delta^2 - 352 \delta - 192 \right), \tag{6.41}$$

$$\langle f_0 T_1 \rangle = \frac{r_2(\delta)}{1350 \sqrt{\delta}} \left(450 \delta^6 + 1985 \delta^5 + 1043 \delta^4 - 12782 \delta^3 - 2552 \delta^2 - 35712 \delta - 11520 \right),$$

where r_2 is defined in (6.29).

For this trajectory only for $\ell = 0$ and $\delta = 3$ we have complete set of 6 states in the database: St. Nos. 76, 78, 81, 83, 84 and 85. Again states 76 and 85 are exactly degenerate due to the LR-symmetry, which is also the symmetry of the external operators, implying that $f_{0;76} = f_{0;85}$. From table 18 we know the sub-leading coefficients in their dimensions to be (within the numerical accuracy of our data)

$$T_{1;76} = \frac{31}{4\sqrt{3}}, \quad T_{1;78} = \frac{1}{\sqrt{3}}, \quad T_{1;81} = \frac{10}{\sqrt{3}}, \quad T_{1;83} = \frac{11}{\sqrt{3}}, \quad T_{1;84} = \frac{19}{\sqrt{3}}. \quad (6.42)$$

From (6.41), we get

$$\begin{aligned} f_{0;83} &= -\frac{45}{16} f_{0;76} - \frac{9}{4} f_{0;78} - \frac{9}{8} f_{0;81} + \frac{25}{1024}, \\ f_{0;84} &= \frac{13}{16} f_{0;76} + \frac{5}{4} f_{0;78} + \frac{1}{8} f_{0;81} + \frac{81}{1024}. \end{aligned} \quad (6.43)$$

Furthermore, we have the inequalities

$$f_{0;76} \geq 0, \quad f_{0;78} \geq 0, \quad f_{0;81} \geq 0, \quad f_{0;83} \geq 0, \quad f_{0;84} \geq 0. \quad (6.44)$$

We can subject the solution (6.43) to the inequalities (6.44), to get the following allowed regions:

$$\begin{aligned} f_{0;76} &\in \left[0, \frac{5}{576}\right], \quad f_{0;78} \in \left[0, \frac{25}{2304}\right], \quad f_{0;81} \in \left[0, \frac{25}{1152}\right], \\ f_{0;83} &\in \left[0, \frac{25}{1024}\right], \quad f_{0;84} \in \left[\frac{81}{1152}, \frac{427}{4608}\right]. \end{aligned} \quad (6.45)$$

To further constrain the OPE coefficients one may consider correlators with non-BPS external legs and/or additional input from localisation [105, 106]. Having external non-BPS operators is at the moment technically challenging, since the super-conformal blocks for these representations are not yet known.

7 Conclusion

We present a highly efficient numerical method and its C++ implementation for studying the spectrum of non-protected observables in planar $\mathcal{N} = 4$ supersymmetric Yang-Mills theory (SYM) using the Quantum Spectral Curve (QSC) method. This work addresses the need for a more comprehensive study of a larger set of states, due to its relevance in the conformal Bootstrap approach.

Our new method facilitates efficient initialisation of numerical iterations benefiting from already available perturbative solvers at small g , overcoming a key challenge in previous computations. Furthermore, our C++ implementation delivers a 8-fold performance improvement over the most efficient existing *Mathematica* implementation.

We used our developed algorithm to compute all states with a bare dimension ≤ 6 . The data generated and the codes used have been made publicly available on [GitHub](#) for the wider scientific community. We provide our code as open-source and kindly request that users cite this paper when using the code or any of its original components.

By combining the strong coupling analysis of our data with the recent results from conformal bootstrap we managed to resolve the degeneracy issue in some cases and give a prediction for strong coupling expansion coefficient of a structure constant of two BPS one non-BPS operator (with bare dimension $\Delta_0 = 4$).

Possible future applications and directions for our approach include:

- Combining our results with the constraints from conformal symmetry and numerical conformal bootstrap to establish narrow bounds on the structure constants or other observables beyond the spectrum.
- Studying other non-local observables, including light-ray operators and Regge trajectories.
- Adapting the method for use in different theories, such as ABJM.
- Modifying the approach for use in AdS_3 cases.
- Using the method to calculate the Hagedorn temperature non-perturbatively.

By making our code and data publicly accessible, we aim to aid and inspire further research in these and related systems.

Acknowledgments

We are very grateful to Luis Fernando Alday, Tobias Hansen and Joao Silva for stimulating discussions, and for sharing some of their unpublished work with us. We thank Dionysios Anninos, Andrea Cavaglià, Jeremy Mann, Sameer Murthy, Michelangelo Preti and Dmytro Volin for discussions related to some parts of this work. We thank Andrea Cavaglià for beta testing the GitHub repository. The work of Á.H. was supported by the NKFIH grant K134946. The work of N.G., J.J. and N.S. was supported by the European Research Council (ERC) under the European Union’s Horizon 2020 research and innovation programme (grant agreement No. 865075) EXACTC. The work of N.G. was also partially supported by the STFC grant (ST/P000258/1).

A Spectral data for all states in planar $\mathcal{N} = 4$ SYM with $\Delta_0 \leq 6$

In this appendix we give the list of all the states which we studied, i.e. all states with bare dimension ≤ 6 . In order to help with the identification of the states we provide in the table below their oscillator numbers, quantum numbers, one loop anomalous dimension and the first two strong coupling orders: string level δ and the one loop analytic guess for the correction d_1 . The states of the types II, III and IV, which breaks some of the discrete symmetries are paired with the states with exactly the same $\Delta(g)$ in the last column. The numerical values of the Δ can be found on [GitHub](#) repository.

St. No.	State ID	$[\ell_1 \ell_2 q_1 p q_2]$	Δ_0	$\Delta_0 + \# g^2$	δ	$2\sqrt{\delta}\lambda^{1/4} - 2 + \frac{\#}{\sqrt{\delta}}\lambda^{1/4}$	d_1	j_1	Type	Degs.
1	$_2[0 0 1 1 1 1 0 0]_1$	[0 0 0 0 0]	2	12	1	2.00000000000000	2	2	I	
2	$_3[0 0 2 2 1 1 0 0]_1$	[0 0 0 1 0]	3	8	1	3.250000001	$\frac{13}{4}$	2	I	
3	$_4[0 0 2 2 2 2 0 0]_1$	[0 0 0 0 0]	4	$13 - \sqrt{41}$	2	1.9999999	2	2	I	
4	$_4[0 0 2 2 2 2 0 0]_2$	[0 0 0 0 0]	4	$13 + \sqrt{41}$	2	8.00000	8	14	I	
5	$_4[0 0 3 2 2 1 0 0]_1$	[0 0 1 0 1]	4	12	2	4.000000	4	2	I	
6	$_4[0 0 3 3 1 1 0 0]_1$	[0 0 0 2 0]	4	$10 + 2\sqrt{5}$	2	4.9999998	5	2	I	
7	$_4[0 0 3 3 1 1 0 0]_2$	[0 0 0 2 0]	4	$10 - 2\sqrt{5}$	1	4.9999999998	5	2	I	
8	$_4[0 0 1 1 1 1 2 0]_1$	[0 2 0 0 0]	4	18	2	6.9997	7	14	III	11
9	$_4[0 1 2 2 1 1 1 0]_1$	[1 1 0 1 0]	4	15	2	5.4991	$\frac{11}{2}$	8	II	10
10	$_4[0 1 2 2 1 1 1 0]_2$	[1 1 0 1 0]	4	15	2	5.4999	$\frac{11}{2}$	8	II	9
11	$_4[0 2 2 2 2 2 0 0]_1$	[2 0 0 0 0]	4	18	2	6.9997	7	14	III	8
12	$_4[0 2 1 1 1 1 2 0]_1$	[2 2 0 0 0]	4	$\frac{50}{3}$	2	6.0000001	6	14	I	
13	$_5[0 0 3 3 3 1 0 0]_1$	[0 0 0 0 2]	5	6.788897449	2	4.2493		1.9986	III	15
14	$_5[0 0 3 3 3 1 0 0]_2$	[0 0 0 0 2]	5	21.21110255	3	9.871		13.2420	III	16
15	$_5[0 0 4 2 2 2 0 0]_1$	[0 0 2 0 0]	5	6.788897449	2	4.2493		1.9986	III	13
16	$_5[0 0 4 2 2 2 0 0]_2$	[0 0 2 0 0]	5	21.21110255	3	9.871		13.2420	III	14
17	$_5[0 0 3 3 2 2 0 0]_1$	[0 0 0 1 0]	5	5.527864045	2	3.2500000	$\frac{13}{4}$	2	I	
18	$_5[0 0 3 3 2 2 0 0]_2$	[0 0 0 1 0]	5	14.47213595	2	9.2499989	$\frac{37}{4}$	14	I	
19	$_5[0 0 3 3 2 2 0 0]_3$	[0 0 0 1 0]	5	20	3	8.89		13.26	III	20
20	$_5[0 0 3 3 2 2 0 0]_4$	[0 0 0 1 0]	5	20	3	8.904		13.309	III	19
21	$_5[0 0 4 3 2 1 0 0]_1$	[0 0 1 1 1]	5	10	2	5.7501		2.0001	II	22
22	$_5[0 0 4 3 2 1 0 0]_2$	[0 0 1 1 1]	5	10	2	5.7501		2.0002	II	21
23	$_5[0 0 4 4 1 1 0 0]_1$	[0 0 0 3 0]	5	4	1	7.250000000	$\frac{29}{4}$	2	I	
24	$_5[0 0 4 4 1 1 0 0]_2$	[0 0 0 3 0]	5	12	2	7.249999957	$\frac{29}{4}$	2	I	
25	$_5[0 0 3 1 1 1 2 0]_1$	[0 2 2 0 0]	5	3	3	8.86		13.22	III	36
26	$_5[0 0 2 2 1 1 2 0]_1$	[0 2 0 1 0]	5	$16 + 2\sqrt{2}$	3	7.88	7.88	13.3	III	37
27	$_5[0 0 2 2 1 1 2 0]_2$	[0 2 0 1 0]	5	$16 - 2\sqrt{2}$	2	8.2499	$\frac{33}{4}$	14	III	38
28	$_5[0 1 2 2 2 2 1 0]_1$	[1 1 0 0 0]	5	18	3	7.0		13.5	IV	29
29	$_5[0 1 2 2 2 2 1 0]_2$	[1 1 0 0 0]	5	18	3	6.92		13.3	IV	28
30	$_5[0 1 3 2 2 1 1 0]_1$	[1 1 1 0 1]	5	10	2	6.249981	$\frac{25}{4}$	8	II	31
31	$_5[0 1 3 2 2 1 1 0]_2$	[1 1 1 0 1]	5	10	2	6.249981	$\frac{25}{4}$	8	II	30
32	$_5[0 1 3 2 2 1 1 0]_3$	[1 1 1 0 1]	5	20	3	0.4		9.0	IV	33
33	$_5[0 1 3 2 2 1 1 0]_4$	[1 1 1 0 1]	5	20	3	0.4		9.0	IV	32
34	$_5[0 1 3 3 1 1 1 0]_1$	[1 1 0 2 0]	5	12	2	7.249984	$\frac{29}{4}$	8	II	35
35	$_5[0 1 3 3 1 1 1 0]_2$	[1 1 0 2 0]	5	12	2	7.24998	$\frac{29}{4}$	8	II	34
36	$_5[0 2 3 3 3 1 0 0]_1$	[2 0 0 0 2]	5	3	3	8.86		13.22	III	25
37	$_5[0 2 3 3 2 2 0 0]_1$	[2 0 0 1 0]	5	$16 + 2\sqrt{2}$	3	7.88		13.26	III	26
38	$_5[0 2 3 3 2 2 0 0]_2$	[2 0 0 1 0]	5	$16 - 2\sqrt{2}$	2	8.2499	$\frac{33}{4}$	14	III	27
39	$_5[0 2 2 2 1 1 2 0]_1$	[2 2 0 1 0]	5	12	2	7.250000	$\frac{29}{4}$	14	I	
40	$\frac{11}{2}[0 0 3 2 2 2 1 0]_1$	[0 1 1 0 0]	$\frac{11}{2}$	18.61803399	3	9.4		15.5	IV	41, 50, 51

Table 18. Spectral data for all states in planar $\mathcal{N} = 4$ SYM. This table has the following columns. The first two columns contain the **St. No.** and **State ID**, both of which uniquely identify a state. The third column gives the quantum numbers of the state. The fourth column is the bare dimension Δ_0 and the fifth column gives the one-loop dimension, from [11]. The sixth column gives the string mass level δ . The seventh column gives our best fit for the sub-leading dimension at strong coupling, more precisely the d_1 coefficient and where possible, the eighth column gives our prediction for this coefficient. The ninth column gives the sub-leading value of the Casimir at strong coupling: j_1 . The tenth column gives the state type, and consequently the eleventh column gives the **St. Nos.** of other states degenerate to the state, if applicable. (*continues ...*)

St. No.	State ID	$[\ell_1 \ell_2 q_1 p q_2]$	Δ_0	$\Delta_0 + \# g^2$	δ	$2\sqrt{\delta}\lambda^{1/4} - 2 + \frac{\#}{\sqrt{\delta}}\frac{1}{\lambda^{1/4}}$	d_1	j_1	Type	Degs.
41	$\frac{11}{2}[00322210]_2$	[01100]	$\frac{11}{2}$	18.61803399	3	9.4		15.5	IV	40, 50, 51
42	$\frac{11}{2}[00322210]_3$	[01100]	$\frac{11}{2}$	16.38196601	3	0.4		0.7	IV	43, 52, 53
43	$\frac{11}{2}[00322210]_4$	[01100]	$\frac{11}{2}$	16.38196601	3	0.4		0.7	IV	42, 52, 53
44	$\frac{11}{2}[00332110]_1$	[01011]	$\frac{11}{2}$	18.82842712	3	12.0		0.7	IV	45, 54, 55
45	$\frac{11}{2}[00332110]_2$	[01011]	$\frac{11}{2}$	18.82842712	3	12.0		0.7	IV	44, 54, 55
46	$\frac{11}{2}[00332110]_3$	[01011]	$\frac{11}{2}$	13.17157288	3	0.3		0.2	IV	47, 56, 57
47	$\frac{11}{2}[00332110]_4$	[01011]	$\frac{11}{2}$	13.17157288	3	0.3		0.2	IV	46, 56, 57
48	$\frac{11}{2}[00431110]_1$	[01120]	$\frac{11}{2}$	16	3	0.4		0.2	IV	49, 58, 59
49	$\frac{11}{2}[00431110]_2$	[01120]	$\frac{11}{2}$	16	3	0.4		0.2	IV	48, 58, 59
50	$\frac{11}{2}[01333200]_1$	[10001]	$\frac{11}{2}$	18.61803399	3	9.4		15.5	IV	40, 41, 51
51	$\frac{11}{2}[01333200]_2$	[10001]	$\frac{11}{2}$	18.61803399	3	9.4		15.5	IV	40, 41, 50
52	$\frac{11}{2}[01333200]_3$	[10001]	$\frac{11}{2}$	16.38196601	3	0.4		0.7	IV	42, 43, 53
53	$\frac{11}{2}[01333200]_4$	[10001]	$\frac{11}{2}$	16.38196601	3	0.4		0.7	IV	42, 43, 52
54	$\frac{11}{2}[01432200]_1$	[10110]	$\frac{11}{2}$	18.82842712	3	12.0		0.7	IV	44, 45, 55
55	$\frac{11}{2}[01432200]_2$	[10110]	$\frac{11}{2}$	18.82842712	3	12.0		0.7	IV	44, 45, 54
56	$\frac{11}{2}[01432200]_3$	[10110]	$\frac{11}{2}$	13.17157288	3	0.3		0.2	IV	46, 47, 57
57	$\frac{11}{2}[01432200]_4$	[10110]	$\frac{11}{2}$	13.17157288	3	0.3		0.2	IV	46, 47, 56
58	$\frac{11}{2}[01442100]_1$	[10021]	$\frac{11}{2}$	16	3	0.4		0.2	IV	48, 49, 59
59	$\frac{11}{2}[01442100]_2$	[10021]	$\frac{11}{2}$	16	3	0.4		0.2	IV	48, 49, 58
60	$\frac{11}{2}[01222120]_1$	[12001]	$\frac{11}{2}$	15.45861873	3	0.4		0.8	IV	61, 66, 67
61	$\frac{11}{2}[01222120]_2$	[12001]	$\frac{11}{2}$	15.45861873	3	0.4		0.8	IV	60, 66, 67
62	$\frac{11}{2}[01222120]_3$	[12001]	$\frac{11}{2}$	21.54138127	3	14.9		1.2	IV	63, 68, 69
63	$\frac{11}{2}[01222120]_4$	[12001]	$\frac{11}{2}$	21.54138127	3	14.9		1.2	IV	62, 68, 69
64	$\frac{11}{2}[01321120]_1$	[12110]	$\frac{11}{2}$	18	3	10.9		17.9	IV	65, 70, 71
65	$\frac{11}{2}[01321120]_2$	[12110]	$\frac{11}{2}$	18	3	10.9		17.9	IV	64, 70, 71
66	$\frac{11}{2}[02322210]_1$	[21100]	$\frac{11}{2}$	15.45861873	3	0.4		0.8	IV	60, 61, 67
67	$\frac{11}{2}[02322210]_2$	[21100]	$\frac{11}{2}$	15.45861873	3	0.4		0.8	IV	60, 61, 66
68	$\frac{11}{2}[02322210]_3$	[21100]	$\frac{11}{2}$	21.54138127	3	14.9		1.2	IV	62, 63, 69
69	$\frac{11}{2}[02322210]_4$	[21100]	$\frac{11}{2}$	21.54138127	3	14.9		1.2	IV	62, 63, 68
70	$\frac{11}{2}[02332110]_1$	[21011]	$\frac{11}{2}$	18	3	10.9		17.9	IV	64, 65, 71
71	$\frac{11}{2}[02332110]_2$	[21011]	$\frac{11}{2}$	18	3	10.9		17.9	IV	64, 65, 70
72	$\frac{11}{2}[02211130]_1$	[23100]	$\frac{11}{2}$	20	3	12.9		28.2	IV	73, 74, 75
73	$\frac{11}{2}[02211130]_2$	[23100]	$\frac{11}{2}$	20	3	12.9		28.2	IV	72, 74, 75
74	$\frac{11}{2}[03222120]_1$	[32001]	$\frac{11}{2}$	20	3	12.9		28.2	IV	72, 73, 75
75	$\frac{11}{2}[03222120]_2$	[32001]	$\frac{11}{2}$	20	3	12.9		28.2	IV	72, 73, 74
76	$\frac{11}{2}[00222211]_1$	[00000]	6	13.67544468	3	7.7491	$\frac{31}{4}$	$\frac{27}{2}$	III	85

Table 18. Spectral data for all states in planar $\mathcal{N} = 4$ SYM. This table has the following columns. The first two columns contain the **St. No.** and **State ID**, both of which uniquely identify a state. The third column gives the quantum numbers of the state. The fourth column is the bare dimension Δ_0 and the fifth column gives the one-loop dimension, from [11]. The sixth column gives the string mass level δ . The seventh column gives our best fit for the sub-leading dimension at strong coupling, more precisely the d_1 coefficient and where possible, the eighth column gives our prediction for this coefficient. The ninth column gives the sub-leading value of the Casimir at strong coupling: j_1 . The tenth column gives the state type, and consequently the eleventh column gives the **St. Nos.** of other states degenerate to the state, if applicable. (*continues ...*)

St. No.	State ID	$[\ell_1 \ell_2 q_1 p q_2]$	Δ_0	$\Delta_0 + \# g^2$	δ	$2\sqrt{\delta}\lambda^{1/4} - 2 + \frac{\#}{\sqrt{\delta}} \frac{1}{\lambda^{1/4}}$	d_1	j_1	Type	Degs.
77	$6[0 0 2 2 2 2 1]_2$	$[0 0 0 0 0]$	6	26.32455532	4	14.9996	15	28	III	86
78	$6[0 0 3 3 3 3 0]_1$	$[0 0 0 0 0]$	6	4.808186901	3	0.999997	1	0	I	
79	$6[0 0 3 3 3 3 0]_2$	$[0 0 0 0 0]$	6	18.89861433	4	6.9999997	7	12	I	
80	$6[0 0 3 3 3 3 0]_3$	$[0 0 0 0 0]$	6	21.35059644	4	11.00000	11	20	I	
81	$6[0 0 3 3 3 3 0]_4$	$[0 0 0 0 0]$	6	12.93049869	3	10.0000	10	18	I	
82	$6[0 0 3 3 3 3 0]_5$	$[0 0 0 0 0]$	6	28.01210364	5	10.8167		19.63356	I	
83	$6[1 1 2 2 2 2 1]_1$	$[0 0 0 0 0]$	6	15.52786405	3	10.999999	11	20	I	
84	$6[1 1 2 2 2 2 1]_2$	$[0 0 0 0 0]$	6	24.47213595	3	19.00000	19	36	I	
85	$6[1 1 3 3 3 3 0]_1$	$[0 0 0 0 0]$	6	13.67544468	3	7.7491	$\frac{31}{4}$	$\frac{27}{2}$	III	76
86	$6[1 1 3 3 3 3 0]_2$	$[0 0 0 0 0]$	6	26.32455532	4	14.9996	15	28	III	77
87	$6[0 0 4 3 3 2 0]_1$	$[0 0 1 0 1]$	6	6.658879771	3	3.0000	3	0	I	
88	$6[0 0 4 3 3 2 0]_2$	$[0 0 1 0 1]$	6	23.78136598	4	12.999995	13	20	I	
89	$6[0 0 4 3 3 2 0]_3$	$[0 0 1 0 1]$	6	15.55975425	3	12.00000	12	18	I	
90	$6[0 0 4 3 3 2 0]_4$	$[0 0 1 0 1]$	6	20	4	1.4		1.6	IV	91
91	$6[0 0 4 3 3 2 0]_5$	$[0 0 1 0 1]$	6	20	4	0.4		0.4	IV	90
92	$6[0 0 4 3 3 2 0]_6$	$[0 0 1 0 1]$	6	16	3			9.5	IV	93, 94, 95
93	$6[0 0 4 3 3 2 0]_7$	$[0 0 1 0 1]$	6	16	3			9.5	IV	92, 94, 95
94	$6[0 0 4 3 3 2 0]_8$	$[0 0 1 0 1]$	6	16	3			9.5	IV	92, 93, 95
95	$6[0 0 4 3 3 2 0]_9$	$[0 0 1 0 1]$	6	16	3			9.5	IV	92, 93, 94
96	$6[0 0 5 3 3 1 0]_1$	$[0 0 2 0 2]$	6	22.60437364	4	11.999	12	12	I	
97	$6[0 0 5 3 3 1 0]_2$	$[0 0 2 0 2]$	6	6.491188584	2	6.9999997	7	2	I	
98	$6[0 0 5 3 3 1 0]_3$	$[0 0 2 0 2]$	6	10.90443778	3	5.999999	6	0	I	
99	$6[0 0 4 4 3 1 0]_1$	$[0 0 0 1 2]$	6	5.395626364	2	6.00017	6	2	III	102
100	$6[0 0 4 4 3 1 0]_2$	$[0 0 0 1 2]$	6	21.50881142	4	10.9996	11	12	III	103
101	$6[0 0 4 4 3 1 0]_3$	$[0 0 0 1 2]$	6	17.09556222	3	11.57		13.15	III	104
102	$6[0 0 5 3 2 2 0]_1$	$[0 0 2 1 0]$	6	5.395626364	2	6.00017	6	2	III	99
103	$6[0 0 5 3 2 2 0]_2$	$[0 0 2 1 0]$	6	21.50881142	4	10.9996	11	12	III	100
104	$6[0 0 5 3 2 2 0]_3$	$[0 0 2 1 0]$	6	17.09556222	3	11.57		13.15	III	101
105	$6[0 0 4 4 2 2 0]_1$	$[0 0 0 2 0]$	6	16	3	10.60		13.15	III	106
106	$6[0 0 4 4 2 2 0]_2$	$[0 0 0 2 0]$	6	16	3	10.60		13.15	III	105
107	$6[0 0 4 4 2 2 0]_3$	$[0 0 0 2 0]$	6	10.67351551	2	11.000000	11	14	I	
108	$6[0 0 4 4 2 2 0]_4$	$[0 0 0 2 0]$	6	17.89750309	3	13.0000	13	18	I	
109	$6[0 0 4 4 2 2 0]_5$	$[0 0 0 2 0]$	6	4.524563121	2	5.000000	5	2	I	
110	$6[0 0 4 4 2 2 0]_6$	$[0 0 0 2 0]$	6	20.39072479	4	9.9998	10	12	I	
111	$6[0 0 4 4 2 2 0]_7$	$[0 0 0 2 0]$	6	24.88621488	4	13.99999	14	20	I	
112	$6[0 0 4 4 2 2 0]_8$	$[0 0 0 2 0]$	6	7.627478610	3	4.00000	4	0	I	
113	$6[0 0 4 4 2 2 0]_9$	$[0 0 0 2 0]$	6	14	3	9.004	9	10	II	114
114	$6[0 0 4 4 2 2 0]_{10}$	$[0 0 0 2 0]$	6	14	3	9.000	9	10	II	113
115	$6[0 0 5 4 2 1 0]_1$	$[0 0 1 2 1]$	6	12	3	7.00000	7	0	I	
116	$6[0 0 5 4 2 1 0]_2$	$[0 0 1 2 1]$	6	8	2	8.0000	8	2	II	117
117	$6[0 0 5 4 2 1 0]_3$	$[0 0 1 2 1]$	6	8	2	8.0000	8	2	II	116

Table 18. Spectral data for all states in planar $\mathcal{N} = 4$ SYM. This table has the following columns. The first two columns contain the **St. No.** and **State ID**, both of which uniquely identify a state. The third column gives the quantum numbers of the state. The fourth column is the bare dimension Δ_0 and the fifth column gives the one-loop dimension, from [11]. The sixth column gives the string mass level δ . The seventh column gives our best fit for the sub-leading dimension at strong coupling, more precisely the d_1 coefficient and where possible, the eighth column gives our prediction for this coefficient. The ninth column gives the sub-leading value of the Casimir at strong coupling: j_1 . The tenth column gives the state type, and consequently the eleventh column gives the **St. Nos.** of other states degenerate to the state, if applicable. (*continues ...*)

St. No.	State ID	$[\ell_1 \ell_2 q_1 p q_2]$	Δ_0	$\Delta_0 + \# g^2$	δ	$2\sqrt{\delta}\lambda^{1/4} - 2 + \frac{\#}{\sqrt{\delta}} \frac{1}{\lambda^{1/4}}$	d_1	j_1	Type	Degs.
118	$6[0 0 5 5 1 1 0 0]_1$	$[0 0 0 4 0]$	6	3.012081585	1	10.0000000000	10	2	I	
119	$6[0 0 5 5 1 1 0 0]_2$	$[0 0 0 4 0]$	6	9.780167472	2	10.00000000	10	2	I	
120	$6[0 0 5 5 1 1 0 0]_3$	$[0 0 0 4 0]$	6	15.20775094	3	9.000000000	9	0	I	
121	$6[0 0 2 2 2 2 2 0]_1$	$[0 2 0 0 0]$	6	20.97783214	4	9.9988	10	20	III	181
122	$6[0 0 2 2 2 2 2 0]_2$	$[0 2 0 0 0]$	6	11.34832950	3	9.00	9	18	III	182
123	$6[0 0 2 2 2 2 2 0]_3$	$[0 2 0 0 0]$	6	25.67383837	4	13.9997	14	28	III	183
124	$6[1 1 2 2 2 2 2 0]_1$	$[0 2 0 0 0]$	6	11.54748008	3	6.7499	$\frac{27}{4}$	$\frac{27}{2}$	III	179
125	$6[1 1 2 2 2 2 2 0]_2$	$[0 2 0 0 0]$	6	23.78585325	3	17.999	18	36	III	180
126	$6[0 0 3 2 2 1 2 0]_1$	$[0 2 1 0 1]$	6	23.12310563	4	12.000	12	20	III	184
127	$6[0 0 3 2 2 1 2 0]_2$	$[0 2 1 0 1]$	6	14.87689437	3	11.0008	11	18	III	185
128	$6[0 0 3 2 2 1 2 0]_3$	$[0 2 1 0 1]$	6	14.87689437	3	7.21			IV	129, 186, 187
129	$6[0 0 3 2 2 1 2 0]_4$	$[0 2 1 0 1]$	6	14.87689437	3	7.2			IV	128, 186, 187
130	$6[0 0 3 2 2 1 2 0]_5$	$[0 2 1 0 1]$	6	23.12310563	4	17.5		32.0	IV	131, 188, 189
131	$6[0 0 3 2 2 1 2 0]_6$	$[0 2 1 0 1]$	6	23.12310563	4	17.5		32.0	IV	130, 188, 189
132	$6[0 0 4 2 1 1 2 0]_1$	$[0 2 2 1 0]$	6	16	3	10.57		13.15	III	190
133	$6[0 0 3 3 1 1 2 0]_1$	$[0 2 0 2 0]$	6	24.07364133	4	13.000	13	20	III	191
134	$6[0 0 3 3 1 1 2 0]_2$	$[0 2 0 2 0]$	6	17.26106778	3	11.999	12	18	III	192
135	$6[0 0 3 3 1 1 2 0]_3$	$[0 2 0 2 0]$	6	9.656169691	2	9.99999	10	14	III	193
136	$6[0 0 3 3 1 1 2 0]_4$	$[0 2 0 2 0]$	6	15.00912120	3	9.57		13.15	III	194
137	$6[0 0 1 1 1 1 4 0]_1$	$[0 4 0 0 0]$	6	24	4	12.002	12	28	III	217
138	$6[1 1 1 1 1 1 4 0]_1$	$[0 4 0 0 0]$	6	22	3	16.0000	16	36	III	216
139	$6[0 1 3 3 3 1 1 0]_1$	$[1 1 0 0 2]$	6	15.45861873	3	9.8		14.7	IV	140, 143, 144
140	$6[0 1 3 3 3 1 1 0]_2$	$[1 1 0 0 2]$	6	15.45861873	3	9.8		14.7	IV	139, 143, 144
141	$6[0 1 3 3 3 1 1 0]_3$	$[1 1 0 0 2]$	6	21.54138127	4	0.5		0.6	IV	142, 145, 146
142	$6[0 1 3 3 3 1 1 0]_4$	$[1 1 0 0 2]$	6	21.54138127	4	0.5		0.6	IV	141, 145, 146
143	$6[0 1 4 2 2 2 1 0]_1$	$[1 1 2 0 0]$	6	15.45861873	3	9.8		14.7	IV	139, 140, 144
144	$6[0 1 4 2 2 2 1 0]_2$	$[1 1 2 0 0]$	6	15.45861873	3	9.8		14.7	IV	139, 140, 143
145	$6[0 1 4 2 2 2 1 0]_3$	$[1 1 2 0 0]$	6	21.54138127	4	0.5		0.6	IV	141, 142, 146
146	$6[0 1 4 2 2 2 1 0]_4$	$[1 1 2 0 0]$	6	21.54138127	4	0.5		0.6	IV	141, 142, 145
147	$6[0 1 3 3 2 2 1 0]_1$	$[1 1 0 1 0]$	6	19.61100719	3	14.9997	15	27	II	148
148	$6[0 1 3 3 2 2 1 0]_2$	$[1 1 0 1 0]$	6	19.61100719	3	14.9997	15	27	II	147
149	$6[0 1 3 3 2 2 1 0]_3$	$[1 1 0 1 0]$	6	20.51664428	4	9.499	$\frac{19}{2}$	16	II	150
150	$6[0 1 3 3 2 2 1 0]_4$	$[1 1 0 1 0]$	6	20.51664428	4	9.500	$\frac{19}{2}$	16	II	149
151	$6[0 1 3 3 2 2 1 0]_5$	$[1 1 0 1 0]$	6	16.40430841	3	10.997	11	19	II	152
152	$6[0 1 3 3 2 2 1 0]_6$	$[1 1 0 1 0]$	6	16.40430841	3	10.997	11	19	II	151
153	$6[0 1 3 3 2 2 1 0]_7$	$[1 1 0 1 0]$	6	8.468040123	3	5.8		9.03	II	154
154	$6[0 1 3 3 2 2 1 0]_8$	$[1 1 0 1 0]$	6	8.468040123	3	5.8		9.01	II	153
155	$6[0 1 3 3 2 2 1 0]_9$	$[1 1 0 1 0]$	6	14.27984675	3	7.5		0.7	IV	156, 157, 158
156	$6[0 1 3 3 2 2 1 0]_{10}$	$[1 1 0 1 0]$	6	14.27984675	3	7.5		0.7	IV	155, 157, 158
157	$6[0 1 3 3 2 2 1 0]_{11}$	$[1 1 0 1 0]$	6	14.27984675	3	7.5		0.7	IV	155, 156, 158
158	$6[0 1 3 3 2 2 1 0]_{12}$	$[1 1 0 1 0]$	6	14.27984675	3	7.5		0.7	IV	155, 156, 157

Table 18. Spectral data for all states in planar $\mathcal{N} = 4$ SYM. This table has the following columns. The first two columns contain the **St. No.** and **State ID**, both of which uniquely identify a state. The third column gives the quantum numbers of the state. The fourth column is the bare dimension Δ_0 and the fifth column gives the one-loop dimension, from [11]. The sixth column gives the string mass level δ . The seventh column gives our best fit for the sub-leading dimension at strong coupling, more precisely the d_1 coefficient and where possible, the eighth column gives our prediction for this coefficient. The ninth column gives the sub-leading value of the Casimir at strong coupling: j_1 . The tenth column gives the state type, and consequently the eleventh column gives the **St. Nos.** of other states degenerate to the state, if applicable. (*continues ...*)

St. No.	State ID	$[\ell_1 \ell_2 q_1 p q_2]$	Δ_0	$\Delta_0 + \# g^2$	δ	$2\sqrt{\delta}\lambda^{1/4} - 2 + \frac{\#}{\sqrt{\delta}} \frac{1}{\lambda^{1/4}}$	d_1	j_1	Type	Degs.
159	$6[0 1 3 3 2 2 1 0]_{13}$	[1 1 0 1 0]	6	24.72015325	4	0.6		1.0	IV	160, 161, 162
160	$6[0 1 3 3 2 2 1 0]_{14}$	[1 1 0 1 0]	6	24.72015325	4	0.6		1.0	IV	159, 161, 162
161	$6[0 1 3 3 2 2 1 0]_{15}$	[1 1 0 1 0]	6	24.72015325	4	0.6		1.0	IV	159, 160, 162
162	$6[0 1 3 3 2 2 1 0]_{16}$	[1 1 0 1 0]	6	24.72015325	4	0.6		1.0	IV	159, 160, 161
163	$6[0 1 4 3 2 1 1 0]_1$	[1 1 1 1 1]	6	16	3	10.9		14.0	IV	164
164	$6[0 1 4 3 2 1 1 0]_2$	[1 1 1 1 1]	6	16	3	10.9		14.0	IV	163
165	$6[0 1 4 3 2 1 1 0]_3$	[1 1 1 1 1]	6	22.84371184	4	11.998	12	16	II	166
166	$6[0 1 4 3 2 1 1 0]_4$	[1 1 1 1 1]	6	22.84371184	4	11.998	12	16	II	165
167	$6[0 1 4 3 2 1 1 0]_5$	[1 1 1 1 1]	6	7.429856598	2	7.9994	8	8	II	168
168	$6[0 1 4 3 2 1 1 0]_6$	[1 1 1 1 1]	6	7.429856598	2	7.9994	8	8	II	167
169	$6[0 1 4 3 2 1 1 0]_7$	[1 1 1 1 1]	6	12.72643156	3	8.500	$\frac{17}{2}$	9	II	170
170	$6[0 1 4 3 2 1 1 0]_8$	[1 1 1 1 1]	6	12.72643156	3	8.500	$\frac{17}{2}$	9	II	169
171	$6[0 1 4 4 1 1 1 0]_1$	[1 1 0 3 0]	6	$\frac{25}{2} + \frac{\sqrt{37}}{2}$	3	10.000	10	9	II	172
172	$6[0 1 4 4 1 1 1 0]_2$	[1 1 0 3 0]	6	$\frac{25}{2} + \frac{\sqrt{37}}{2}$	3	10.000	10	9	II	171
173	$6[0 1 4 4 1 1 1 0]_3$	[1 1 0 3 0]	6	$\frac{25}{2} - \frac{\sqrt{37}}{2}$	2	9.5000	$\frac{19}{2}$	8	II	174
174	$6[0 1 4 4 1 1 1 0]_4$	[1 1 0 3 0]	6	$\frac{25}{2} - \frac{\sqrt{37}}{2}$	2	9.5000	$\frac{19}{2}$	8	II	173
175	$6[0 1 2 2 1 1 3 0]_1$	[1 3 0 1 0]	6	18.48338852	3	12.0		23.5	IV	176, 210, 211
176	$6[0 1 2 2 1 1 3 0]_2$	[1 3 0 1 0]	6	18.48338852	3	12.0		23.5	IV	175, 210, 211
177	$6[0 1 2 2 1 1 3 0]_3$	[1 3 0 1 0]	6	23.51661148	4	0.5		1.1	IV	178, 212, 213
178	$6[0 1 2 2 1 1 3 0]_4$	[1 3 0 1 0]	6	23.51661148	4	0.5		1.1	IV	177, 212, 213
179	$6[0 2 2 2 2 2 1 1]_1$	[2 0 0 0 0]	6	11.54748008	3	6.7499	$\frac{27}{4}$	$\frac{27}{2}$	III	124
180	$6[0 2 2 2 2 2 1 1]_2$	[2 0 0 0 0]	6	23.78585325	3	17.999	18	36	III	125
181	$6[0 2 3 3 3 3 0 0]_1$	[2 0 0 0 0]	6	20.97783214	4	9.9988	10	20	III	121
182	$6[0 2 3 3 3 3 0 0]_2$	[2 0 0 0 0]	6	11.34832950	3	9.00	9	18	III	122
183	$6[0 2 3 3 3 3 0 0]_3$	[2 0 0 0 0]	6	25.67383837	4	13.9997	14	28	III	123
184	$6[0 2 4 3 3 2 0 0]_1$	[2 0 1 0 1]	6	23.12310563	4	12.000	12	20	III	126
185	$6[0 2 4 3 3 2 0 0]_2$	[2 0 1 0 1]	6	14.87689437	3	11.0008	11	18	III	127
186	$6[0 2 4 3 3 2 0 0]_3$	[2 0 1 0 1]	6	14.87689437	3	7.21			IV	128, 129, 187
187	$6[0 2 4 3 3 2 0 0]_4$	[2 0 1 0 1]	6	14.87689437	3	7.2			IV	128, 129, 186
188	$6[0 2 4 3 3 2 0 0]_5$	[2 0 1 0 1]	6	23.12310563	4	17.5		32.0	IV	130, 131, 189
189	$6[0 2 4 3 3 2 0 0]_6$	[2 0 1 0 1]	6	23.12310563	4	17.5		32.0	IV	130, 131, 188
190	$6[0 2 4 4 3 1 0 0]_1$	[2 0 0 1 2]	6	16	3	10.57		13.15	III	132
191	$6[0 2 4 4 2 2 0 0]_1$	[2 0 0 2 0]	6	24.07364133	4	13.000	13	20	III	133
192	$6[0 2 4 4 2 2 0 0]_2$	[2 0 0 2 0]	6	17.26106778	3	11.999	12	18	III	134
193	$6[0 2 4 4 2 2 0 0]_3$	[2 0 0 2 0]	6	9.656169691	2	9.99999	10	14	III	135
194	$6[0 2 4 4 2 2 0 0]_4$	[2 0 0 2 0]	6	15.00912120	3	9.57		13.15	III	136
195	$6[0 2 2 2 2 2 2 0]_1$	[2 2 0 0 0]	6	20.42082091	4	8.99999	9	20	I	
196	$6[0 2 2 2 2 2 2 0]_2$	[2 2 0 0 0]	6	9.804773390	3	8.00000	8	18	I	
197	$6[0 2 2 2 2 2 2 0]_3$	[2 2 0 0 0]	6	23.10773903	3	16.99999	17	36	I	
198	$6[0 2 2 2 2 2 2 0]_4$	[2 2 0 0 0]	6	$\frac{58}{3}$	3	12.999	13	28	II	199
199	$6[0 2 2 2 2 2 2 0]_5$	[2 2 0 0 0]	6	$\frac{58}{3}$	3	12.999	13	28	II	198

Table 18. Spectral data for all states in planar $\mathcal{N} = 4$ SYM. This table has the following columns. The first two columns contain the **St. No.** and **State ID**, both of which uniquely identify a state. The third column gives the quantum numbers of the state. The fourth column is the bare dimension Δ_0 and the fifth column gives the one-loop dimension, from [11]. The sixth column gives the string mass level δ . The seventh column gives our best fit for the sub-leading dimension at strong coupling, more precisely the d_1 coefficient and where possible, the eighth column gives our prediction for this coefficient. The ninth column gives the sub-leading value of the Casimir at strong coupling: j_1 . The tenth column gives the state type, and consequently the eleventh column gives the **St. Nos.** of other states degenerate to the state, if applicable. (*continues ...*)

St. No.	State ID	$[\ell_1 \ell_2 q_1 p q_2]$	Δ_0	$\Delta_0 + \# g^2$	δ	$2\sqrt{\delta}\lambda^{1/4} - 2 + \frac{\#}{\sqrt{\delta}} \frac{1}{\lambda^{1/4}}$	d_1	j_1	Type	Degs.
200	$6[0\ 2\ 2\ 2\ 2\ 2\ 2\ 0]_6$	$[2\ 2\ 0\ 0\ 0]$	6	$\frac{74}{3}$	4	14.5		111.5	IV	201
201	$6[0\ 2\ 2\ 2\ 2\ 2\ 2\ 0]_7$	$[2\ 2\ 0\ 0\ 0]$	6	$\frac{74}{3}$	4	14.5		111.5	IV	200
202	$6[0\ 2\ 3\ 2\ 2\ 1\ 2\ 0]_1$	$[2\ 2\ 1\ 0\ 1]$	6	$\frac{55}{3} + \frac{\sqrt{145}}{3}$	4	10.999997	11	20	I	
203	$6[0\ 2\ 3\ 2\ 2\ 1\ 2\ 0]_2$	$[2\ 2\ 1\ 0\ 1]$	6	$\frac{55}{3} - \frac{\sqrt{145}}{3}$	3	10.0000	10	18	I	
204	$6[0\ 2\ 3\ 3\ 1\ 1\ 2\ 0]_1$	$[2\ 2\ 0\ 2\ 0]$	6	23.18267020	4	12.00000	12	20	I	
205	$6[0\ 2\ 3\ 3\ 1\ 1\ 2\ 0]_2$	$[2\ 2\ 0\ 2\ 0]$	6	16.71846288	3	11.00000	11	18	I	
206	$6[0\ 2\ 3\ 3\ 1\ 1\ 2\ 0]_3$	$[2\ 2\ 0\ 2\ 0]$	6	8.765533583	2	8.99999981	9	14	I	
207	$6[0\ 2\ 3\ 3\ 1\ 1\ 2\ 0]_4$	$[2\ 2\ 0\ 2\ 0]$	6	$\frac{46}{3}$	3	11.000	11	18	II	208
208	$6[0\ 2\ 3\ 3\ 1\ 1\ 2\ 0]_5$	$[2\ 2\ 0\ 2\ 0]$	6	$\frac{46}{3}$	3	10.9995	11	18	II	207
209	$6[0\ 2\ 1\ 1\ 1\ 1\ 4\ 0]_1$	$[2\ 4\ 0\ 0\ 0]$	6	$\frac{64}{3}$	3	15.000	15	36	III	218
210	$6[0\ 3\ 3\ 3\ 2\ 2\ 1\ 0]_1$	$[3\ 1\ 0\ 1\ 0]$	6	18.48338852	3	12.0		23.5	IV	175, 176, 211
211	$6[0\ 3\ 3\ 3\ 2\ 2\ 1\ 0]_2$	$[3\ 1\ 0\ 1\ 0]$	6	18.48338852	3	12.0		23.5	IV	175, 176, 210
212	$6[0\ 3\ 3\ 3\ 2\ 2\ 1\ 0]_3$	$[3\ 1\ 0\ 1\ 0]$	6	23.51661148	4	0.5		1.1	IV	177, 178, 213
213	$6[0\ 3\ 3\ 3\ 2\ 2\ 1\ 0]_4$	$[3\ 1\ 0\ 1\ 0]$	6	23.51661148	4	0.5		1.1	IV	177, 178, 212
214	$6[0\ 3\ 2\ 2\ 1\ 1\ 3\ 0]_1$	$[3\ 3\ 0\ 1\ 0]$	6	$\frac{35}{2}$	3	12.0000	12	27	II	215
215	$6[0\ 3\ 2\ 2\ 1\ 1\ 3\ 0]_2$	$[3\ 3\ 0\ 1\ 0]$	6	$\frac{35}{2}$	3	12.0000	12	27	II	214
216	$6[0\ 4\ 2\ 2\ 2\ 2\ 1\ 1]_1$	$[4\ 0\ 0\ 0\ 0]$	6	22	3	16.0000	16	36	III	138
217	$6[0\ 4\ 3\ 3\ 3\ 3\ 0\ 0]_1$	$[4\ 0\ 0\ 0\ 0]$	6	24	4	12.002	12	28	III	137
218	$6[0\ 4\ 2\ 2\ 2\ 2\ 2\ 0]_1$	$[4\ 2\ 0\ 0\ 0]$	6	$\frac{64}{3}$	3	15.000	15	36	III	209
219	$6[0\ 4\ 1\ 1\ 1\ 1\ 4\ 0]_1$	$[4\ 4\ 0\ 0\ 0]$	6	$\frac{98}{5}$	3	13.00000	13	36	I	

Table 18. Spectral data for all states in planar $\mathcal{N} = 4$ SYM. This table has the following columns. The first two columns contain the **St. No.** and **State ID**, both of which uniquely identify a state. The third column gives the quantum numbers of the state. The fourth column is the bare dimension Δ_0 and the fifth column gives the one-loop dimension, from [11]. The sixth column gives the string mass level δ . The seventh column gives our best fit for the sub-leading dimension at strong coupling, more precisely the d_1 coefficient and where possible, the eighth column gives our prediction for this coefficient. The ninth column gives the sub-leading value of the Casimir at strong coupling: j_1 . The tenth column gives the state type, and consequently the eleventh column gives the **St. Nos.** of other states degenerate to the state, if applicable.

B Conversion to the left-right symmetric form

This appendix contains technical details on how to convert the perturbative results of [10, 11] into our conventions in order to be used as starting points for the numerical procedure.

The perturbative solver [10, 11] does not present \mathbf{P}_a and \mathbf{P}^a in the left-right symmetric form for states which have this symmetry. In order to use the perturbative data from the solver, we need to convert it to the left-right symmetric form, i.e. so that $\mathbf{P}^a = \chi^{ab}\mathbf{P}_b$, by a composition of Λ - and H -transformations (cf. equations (3.17)–(3.20)).

Let \mathbf{P}_a^{MV} and $\mathbf{P}^{a,MV}$ be the \mathbf{P} -functions obtained from the perturbative QSC solver of [10, 11]. Then, the Ansatz looks as follows in their conventions

$$\mathbf{P}_a^{MV} = x^{\text{pow}\mathbf{P}_a^{MV}} \left(\mathbb{A}_a + \sum_{n=1}^{\infty} \frac{c_{a,n}^{MV}}{x^n} \right), \quad (\text{B.1})$$

$$\mathbf{P}^{a,MV} = x^{-\text{pow}\mathbf{P}_a^{MV}-1} \left(\mathbb{A}^a + \sum_{n=1}^{\infty} \frac{c^{a,n,MV}}{x^n} \right). \quad (\text{B.2})$$

We use the Λ -symmetry ($\text{powP}_a^{\text{MV}} \rightarrow \text{powP}_a^{\text{MV}} - \Lambda = \text{powP}_a$) in order to ensure the asymptotics of the \mathbf{P}_a and \mathbf{P}^a satisfy the left-right symmetric condition (3.35). Since for LR symmetric states we have

$$\begin{aligned} \text{powP}_1 &= -\text{powP}_4 - 1, & \text{powP}_2 &= -\text{powP}_3 - 1, \\ \text{powP}_3 &= -\text{powP}_2 - 1, & \text{powP}_4 &= -\text{powP}_1 - 1, \end{aligned} \tag{B.3}$$

we need to solve equations of the form

$$\text{powP}_1^{\text{MV}} - \Lambda = -(\text{powP}_4^{\text{MV}} - \Lambda) - 1 \tag{B.4}$$

and similarly for other \mathbf{P}_a to get

$$\Lambda = \frac{1 + \text{powP}_1^{\text{MV}} + \text{powP}_4^{\text{MV}}}{2} = \frac{1 + \text{powP}_2^{\text{MV}} + \text{powP}_3^{\text{MV}}}{2}. \tag{B.5}$$

Such a Λ can only be found if

$$\text{powP}_1^{\text{MV}} + \text{powP}_4^{\text{MV}} = \text{powP}_2^{\text{MV}} + \text{powP}_3^{\text{MV}}, \tag{B.6}$$

or in terms of oscillator numbers

$$n_{\mathbf{f}_1} + n_{\mathbf{f}_4} = n_{\mathbf{f}_2} + n_{\mathbf{f}_3}. \tag{B.7}$$

It must be noted, however, that this is a necessary and not sufficient condition for left-right symmetry. Indeed, we can have non left-right symmetric states, whose oscillator numbers satisfy the equation (B.7).

Let us denote the \mathbf{P} -functions obtained after performing the Λ -transformation (B.5) by $\mathbf{P}_a^{\text{Lambda}}$ and $\mathbf{P}^{a \text{ Lambda}}$. Now that the asymptotic have been fixed, we are looking for an H -transformation (3.19), (3.20)

$$\begin{aligned} \mathbf{P}_a^{\text{LR}} &= H_a^b \mathbf{P}_b^{\text{Lambda}} \\ \mathbf{P}^{a \text{ LR}} &= \mathbf{P}^{c \text{ Lambda}} (H^{-1})_c^a \end{aligned} \tag{B.8}$$

which brings $\mathbf{P}_a^{\text{Lambda}}$ and $\mathbf{P}^{a, \text{Lambda}}$ to the form that manifests left-right symmetry, i.e.

$$\mathbf{P}^{\text{LR}, a} = \chi^{ab} \mathbf{P}_b^{\text{LR}}. \tag{B.9}$$

In order to ensure that the H -transformation does not change the asymptotic of $\mathbf{P}_a^{\text{Lambda}}$ and $\mathbf{P}^{a \text{ Lambda}}$, it must be lower triangular. Thus, we need to find 10 lower triangular matrix elements H_a^b . Plugging (B.8) into (B.9), we get

$$\mathbf{P}^{a \text{ Lambda}} = (H^T \cdot \chi \cdot H)^{ab} \mathbf{P}_b^{\text{Lambda}}, \tag{B.10}$$

where due to H being lower triangular and the anti-symmetry of χ , $H^T \cdot \chi \cdot H$ can be parameterised only by 4 independent elements:

$$H^T \cdot \chi \cdot H = \begin{pmatrix} 0 & h_1 & h_2 & h_3 \\ -h_1 & 0 & h_4 & 0 \\ -h_2 & -h_4 & 0 & 0 \\ -h_3 & 0 & 0 & 0 \end{pmatrix}, \tag{B.11}$$

where h_i can be determined from (B.10) in terms of the coefficients of the \mathbf{P}^{MV} -functions:

$$\begin{aligned}
 h_1 &= \frac{c^{1, \text{powP}_4 - \text{powP}_2 \text{ MV}}}{\mathbb{A}_2} = -\frac{c^{2, \text{powP}_3 - \text{powP}_1 \text{ MV}}}{\mathbb{A}_1}, & h_2 &= \frac{c^{1, \text{powP}_4 - \text{powP}_3 \text{ MV}}}{\mathbb{A}_3} = -\frac{c^{3, \text{powP}_2 - \text{powP}_1 \text{ MV}}}{\mathbb{A}_1}, \\
 h_3 &= \frac{\mathbb{A}^1}{\mathbb{A}_4} = -\frac{\mathbb{A}^4}{\mathbb{A}_1}, & h_4 &= \frac{\mathbb{A}^2}{\mathbb{A}_3} = -\frac{\mathbb{A}^3}{\mathbb{A}_2}.
 \end{aligned}
 \tag{B.12}$$

From (B.10) the relation of h_i to the matrix elements H_a^b can be read off, as well:

$$h_1 = -H_2^2 H_3^1 + H_2^1 H_3^2 - H_1^1 H_4^2, \quad h_2 = H_2^1 H_3^3 - H_1^1 H_4^3, \tag{B.13}$$

$$h_3 = -H_1^1 H_4^4, \quad h_4 = H_2^2 H_3^3. \tag{B.14}$$

Thus, we have 4 conditions on the 10 elements of the lower triangular matrix H . We have the freedom to fix the other 6 conditions. We have chosen to fix 4 gauge conditions by imposing (4.19), from where it follows that $H_{2,1} = 0, H_{3,1} = 0, H_{3,2} = 0, H_{4,1} = 0$. The remaining two conditions are fixed by imposing $H_1^1 = H_2^2 = 1$, so that H takes the final form as follows:

$$H = \begin{pmatrix} 1 & 0 & 0 & 0 \\ 0 & 1 & 0 & 0 \\ 0 & 0 & h_4 & 0 \\ 0 & -h_1 & -h_2 & h_3 \end{pmatrix}. \tag{B.15}$$

In the repository we have added a *Mathematica* notebook which performs the conversion as described in this appendix.

C One-loop spectrum of $\mathfrak{sl}(2)$ sector and mode numbers

The one-loop anomalous dimension of $\mathfrak{sl}(2)$ operators at weak coupling may be obtained by solving the $\mathfrak{sl}(2)$ Bethe ansatz equations (BAE) [78, 107]. A multiplet is characterised by a number of derivatives S and a length L , via (2.10). To obtain the one-loop dimension, we need solve the following set of equations: the $\mathfrak{sl}(2)$ BAE

$$\left(\frac{v_k + i/2}{v_k - i/2} \right)^L = \prod_{l=1, l \neq k}^S \frac{v_k - v_l - i}{v_k - v_l + i}. \tag{C.1}$$

These equations are solved by a set of Bethe roots $\{v_1, \dots, v_S\}$. The number of different Bethe root sets corresponds to the multiplicity of the multiplet described by S and L , via (2.10). Thus, we can associate each set of Bethe roots with a particular value of the multiplicity label sol . Denote such a set as $\{v_1, \dots, v_S\}_{\text{sol}}$.

Given a set of Bethe roots, the one-loop anomalous dimension of the state can be obtained from [107]

$$\Delta \simeq L + S - 2 + \sum_{v_k \in \{v_1, \dots, v_S\}_{\text{sol}}} \frac{2g^2}{v_k^2 + 1/4}. \tag{C.2}$$

Another way of classifying solutions to the BAE is by using “mode numbers”. We explain how in the sequel. Consider the logarithm of the equations (C.1). We need to specify the branch of the logarithm, and this introduces an integer constant n_k , associated with the logarithm of the k^{th} Bethe equation. We have

$$L \log \left(\frac{v_k + i/2}{v_k - i/2} \right) = \sum_{l=1, l \neq k}^S \log \left[\frac{v_k - v_l - i}{v_k - v_l + i} \right] + 2\pi i n_k. \quad (\text{C.3})$$

Thus, to the solution $\{v_1, \dots, v_S\}_{\text{sol}}$, we can associate a set $\{n_1, \dots, n_S\}_{\text{sol}}$, which we call the mode numbers of this solution of the BAE, and consequently the state described by them. The mode numbers can be used as an alternative multiplicity label, in lieu of **sol**, for $\mathfrak{sl}(2)$ multiplets.

Below, in table 19, we present a table of mode numbers, for all the 27 $\mathfrak{sl}(2)$ states in our database.

St. No.	State ID	$[\ell_1 \ell_2 q_1 p q_2]$	Δ_0	$\Delta_0 + \# g^2$	δ	d_1	$[S L n]$	Mode numbers	Type	Degs.
1	${}_2[0 0 1 1 1 1 0 0]_1$	$[0 0 0 0 0]$	2	12	1	2	$[2 2 1]$	$\{1, -1\}$	I	
2	${}_3[0 0 2 2 1 1 0 0]_1$	$[0 0 0 1 0]$	3	8	1	$\frac{13}{4}$	$[2 3 1]$	$\{1, -1\}$	I	
7	${}_4[0 0 3 3 1 1 0 0]_2$	$[0 0 0 2 0]$	4	$10 - 2\sqrt{5}$	1	5	$[2 4 1]$	$\{1, -1\}$	I	
6	${}_4[0 0 3 3 1 1 0 0]_1$	$[0 0 0 2 0]$	4	$10 + 2\sqrt{5}$	2	5	$[2 4 2]$	$\{2, -2\}$	I	
23	${}_5[0 0 4 4 1 1 0 0]_1$	$[0 0 0 3 0]$	5	4	1	$\frac{29}{4}$	$[2 5 1]$	$\{1, -1\}$	I	
24	${}_5[0 0 4 4 1 1 0 0]_2$	$[0 0 0 3 0]$	5	12	2	$\frac{29}{4}$	$[2 5 2]$	$\{2, -2\}$	I	
118	${}_6[0 0 5 5 1 1 0 0]_1$	$[0 0 0 4 0]$	6	3.012081585	1	10	$[2 6 1]$	$\{1, -1\}$	I	
119	${}_6[0 0 5 5 1 1 0 0]_2$	$[0 0 0 4 0]$	6	9.780167472	2	10	$[2 6 2]$	$\{2, -2\}$	I	
120	${}_6[0 0 5 5 1 1 0 0]_3$	$[0 0 0 4 0]$	6	15.20775094	3	9	$[2 6 3]$	$\{3, -3\}$	I	
9	${}_4[0 1 2 2 1 1 1 0]_1$	$[1 1 0 1 0]$	4	15	2	$\frac{11}{2}$	$[3 3 1]$	$\{-1, -1, 2\}$	II	10
10	${}_4[0 1 2 2 1 1 1 0]_2$	$[1 1 0 1 0]$	4	15	2	$\frac{11}{2}$	$[3 3 1]$	$\{1, 1, -2\}$	II	9
34	${}_5[0 1 3 3 1 1 1 0]_1$	$[1 1 0 2 0]$	5	12	2	$\frac{29}{4}$	$[3 4 1]$	$\{-1, -1, 2\}$	II	35
35	${}_5[0 1 3 3 1 1 1 0]_2$	$[1 1 0 2 0]$	5	12	2	$\frac{29}{4}$	$[3 4 1]$	$\{1, 1, -2\}$	II	34
173	${}_6[0 1 4 4 1 1 1 0]_3$	$[1 1 0 3 0]$	6	$\frac{25}{2} - \frac{\sqrt{37}}{2}$	2	$\frac{19}{2}$	$[3 5 1]$	$\{3, -2, -1\}$	II	174
174	${}_6[0 1 4 4 1 1 1 0]_4$	$[1 1 0 3 0]$	6	$\frac{25}{2} - \frac{\sqrt{37}}{2}$	2	$\frac{19}{2}$	$[3 5 1]$	$\{1, 1, -2\}$	II	173
171	${}_6[0 1 4 4 1 1 1 0]_1$	$[1 1 0 3 0]$	6	$\frac{25}{2} + \frac{\sqrt{37}}{2}$	3	10	$[3 5 2]$	$\{3, -2, -1\}$	II	172
172	${}_6[0 1 4 4 1 1 1 0]_2$	$[1 1 0 3 0]$	6	$\frac{25}{2} + \frac{\sqrt{37}}{2}$	3	10	$[3 5 2]$	$\{1, 2, -3\}$	II	171
12	${}_4[0 2 1 1 1 1 2 0]_1$	$[2 2 0 0 0]$	4	$\frac{50}{3}$	2	6	$[4 2 1]$	$\{1, 1, -1, -1\}$	I	
39	${}_5[0 2 2 2 1 1 2 0]_1$	$[2 2 0 1 0]$	5	12	2	$\frac{29}{4}$	$[4 3 1]$	$\{1, 1, -1, -1\}$	I	
206	${}_6[0 2 3 3 1 1 2 0]_3$	$[2 2 0 2 0]$	6	8.765533583	2	9	$[4 4 1]$	$\{1, 1, -1, -1\}$	I	
205	${}_6[0 2 3 3 1 1 2 0]_2$	$[2 2 0 2 0]$	6	16.71846288	3	11	$[4 4 2]$	$\{1, 2, -2, -1\}$	I	
207	${}_6[0 2 3 3 1 1 2 0]_4$	$[2 2 0 2 0]$	6	$\frac{46}{3}$	3	11	$[4 4 2]$	$\{1, 1, 1, 1\}$	II	208
208	${}_6[0 2 3 3 1 1 2 0]_5$	$[2 2 0 2 0]$	6	$\frac{46}{3}$	3	11	$[4 4 2]$	$\{-1, -1, -1, -1\}$	II	207
204	${}_6[0 2 3 3 1 1 2 0]_1$	$[2 2 0 2 0]$	6	23.18267020	4	12	$[4 4 3]$	$\{2, 2, -2, -2\}$	I	
214	${}_6[0 3 2 2 1 1 3 0]_1$	$[3 3 0 1 0]$	6	$\frac{35}{2}$	3	12	$[5 3 1]$	$\{1, 1, 1, -2, -1\}$	II	215
215	${}_6[0 3 2 2 1 1 3 0]_2$	$[3 3 0 1 0]$	6	$\frac{35}{2}$	3	12	$[5 3 1]$	$\{1, 2, -1, -1, -1\}$	II	214
219	${}_6[0 4 1 1 1 1 4 0]_1$	$[4 4 0 0 0]$	6	$\frac{98}{5}$	3	13	$[6 2 1]$	$\{1, 1, 1, -1, -1, -1\}$	I	

Table 19. Mode numbers for $\mathfrak{sl}(2)$ states in our database.

In table 19 above, consider the states in shaded rows. Entries shaded with

- have mode numbers ± 1 ,
- have mode numbers ± 2 ,
- have mode numbers ± 3 .

D Counting of states at higher δ

Here we present details of the counting of the states at strong coupling as discussed in section 6.2. In particular, we assign states in our database, with $\delta = 2$ and $\delta = 3$, to KK-towers available from formulas in the literature [97, 99]. In some cases, where there is an ambiguity, we use the conjecture (6.13), to break this ambiguity. Therefore, we show that the subleading Casimir j_1 , is a good classifier of KK-towers.

D.1 States with $\delta = 2$

As we mentioned in 6.2 there are 9 KK-towers expected at the level $\delta = 2$. For the convenience of the reader, we display the counting from [97], i.e. equation (6.12) below:

$$\text{count}_2 = 2[0\ 0; 0\ 0] + [0\ 0; 2\ 0] + [0\ 0; 0\ 2] + 2[1\ 1; 1\ 0] + [2\ 2; 0\ 0] + [2\ 0; 0\ 0] + [0\ 2; 0\ 0].$$

First consider the case of zero spin. For the Lorentz spin labels $(\ell_1\ \ell_2) = (0\ 0)$, we have the following states, presented in table 20:

St. No.	State ID	$[\ell_1\ \ell_2\ q_1\ p\ q_2]$	Δ_0	$\Delta_0 + \# g^2$	δ	$2\sqrt{\delta}\lambda^{1/4} - 2 + \frac{\#}{\sqrt{\delta}}\frac{1}{\lambda^{1/4}}$	d_1	j_1	Type	Degs.
3	${}_4[0\ 0\ 2\ 2\ 2\ 2\ 0\ 0]_1$	$[0\ 0\ 0\ 0\ 0]$	4	$13 - \sqrt{41}$	2	1.9999999	2	2	I	
4	${}_4[0\ 0\ 2\ 2\ 2\ 2\ 0\ 0]_2$	$[0\ 0\ 0\ 0\ 0]$	4	$13 + \sqrt{41}$	2	8.0000	8	14	I	
5	${}_4[0\ 0\ 3\ 2\ 2\ 1\ 0\ 0]_1$	$[0\ 0\ 1\ 0\ 1]$	4	12	2	4.000000	4	2	I	
6	${}_4[0\ 0\ 3\ 3\ 1\ 1\ 0\ 0]_1$	$[0\ 0\ 0\ 2\ 0]$	4	$10 + 2\sqrt{5}$	2	4.9999998	5	2	I	
13	${}_5[0\ 0\ 3\ 3\ 3\ 1\ 0\ 0]_1$	$[0\ 0\ 0\ 0\ 2]$	5	6.788897449	2	4.25		2.00	III	15
15	${}_5[0\ 0\ 4\ 2\ 2\ 2\ 0\ 0]_1$	$[0\ 0\ 2\ 0\ 0]$	5	6.788897449	2	4.25		2.00	III	13
17	${}_5[0\ 0\ 3\ 3\ 2\ 2\ 0\ 0]_1$	$[0\ 0\ 0\ 1\ 0]$	5	5.527864045	2	3.2500000	$\frac{13}{4}$	2	I	
18	${}_5[0\ 0\ 3\ 3\ 2\ 2\ 0\ 0]_2$	$[0\ 0\ 0\ 1\ 0]$	5	14.47213595	2	9.2499999	$\frac{31}{4}$	14	I	
21	${}_5[0\ 0\ 4\ 3\ 2\ 1\ 0\ 0]_1$	$[0\ 0\ 1\ 1\ 1]$	5	10	2	5.75007	$\frac{23}{4}$	2	II	22
22	${}_5[0\ 0\ 4\ 3\ 2\ 1\ 0\ 0]_2$	$[0\ 0\ 1\ 1\ 1]$	5	10	2	5.750	$\frac{23}{4}$	2	II	21
24	${}_5[0\ 0\ 4\ 4\ 1\ 1\ 0\ 0]_2$	$[0\ 0\ 0\ 3\ 0]$	5	12	2	7.24999996	$\frac{29}{4}$	2	I	
97	${}_6[0\ 0\ 5\ 3\ 3\ 1\ 0\ 0]_2$	$[0\ 0\ 2\ 0\ 2]$	6	6.491188584	2	7.00000	7	2	I	
99	${}_6[0\ 0\ 4\ 4\ 3\ 1\ 0\ 0]_1$	$[0\ 0\ 0\ 1\ 2]$	6	5.395626364	2	6.000	6	2	III	102
102	${}_6[0\ 0\ 4\ 4\ 3\ 1\ 0\ 0]_1$	$[0\ 0\ 2\ 1\ 0]$	6	5.395626364	2	6.000	6	2	III	99
107	${}_6[0\ 0\ 4\ 4\ 2\ 2\ 0\ 0]_3$	$[0\ 0\ 0\ 2\ 0]$	6	10.67351551	2	11.000000	11	14	I	
109	${}_6[0\ 0\ 4\ 4\ 2\ 2\ 0\ 0]_5$	$[0\ 0\ 0\ 2\ 0]$	6	4.524563121	2	5.00000	5	2	I	
116	${}_6[0\ 0\ 5\ 4\ 2\ 1\ 0\ 0]_2$	$[0\ 0\ 1\ 2\ 1]$	6	8	2	8.000	8	2	II	117
117	${}_6[0\ 0\ 5\ 4\ 2\ 1\ 0\ 0]_3$	$[0\ 0\ 1\ 2\ 1]$	6	8	2	8.000	8	2	II	116
119	${}_6[0\ 0\ 5\ 5\ 1\ 1\ 0\ 0]_2$	$[0\ 0\ 0\ 4\ 0]$	6	9.780167472	2	10.00000000	10	2	I	

Table 20. States in our database with $\delta = 2$ and $(\ell_1\ \ell_2) = (0\ 0)$. We predict that the states in rows with the same colour belong to the same KK-tower.

We claim that in table 20, the entries shaded with

- belong to one of the 2 $[0\ 0; 0\ 0]$, with the value of j_1 breaking the ambiguity,
- belong to $[0\ 0; 0\ 2]$, belong to $[0\ 0; 2\ 0]$,
- belong to either $[0\ 0; 2\ 0]$, $[0\ 0; 0\ 2]$ but it can't be identified uniquely.

In order to assign some of the $[0\ 0\ 0\ p\ 0]$, with $p \geq 2$ states to the $[0\ 0; 2\ 0]$, we also used the fact that they are all $\mathfrak{sl}(2)$ states of the form $[2, p + 2, 2]$, and assumed that these are in the same KK-tower.

Next, let us consider states with Lorentz spin labels $(1\ 1)$. There are 10 such states, presented in table 21. We have

St. No.	State ID	$[\ell_1 \ell_2 q_1 p q_2]$	Δ_0	$\Delta_0 + \# g^2$	δ	$2\sqrt{\delta}\lambda^{1/4} - 2 + \frac{\#}{\sqrt{\delta}} \frac{1}{\lambda^{1/4}}$	d_1	j_1	Type	Degs.
9	$4[0 1 2 2 1 1 1 0]_1$	$[1 1 0 1 0]$	4	15	2	5.50	$\frac{11}{2}$	8	II	10
10	$4[0 1 2 2 1 1 1 0]_2$	$[1 1 0 1 0]$	4	15	2	5.4999	$\frac{11}{2}$	8	II	9
30	$5[0 1 3 2 2 1 1 0]_1$	$[1 1 1 0 1]$	5	10	2	6.2500	$\frac{25}{4}$	8	II	31
31	$5[0 1 3 2 2 1 1 0]_2$	$[1 1 1 0 1]$	5	10	2	6.2500	$\frac{25}{4}$	8	II	30
34	$5[0 1 3 3 1 1 1 0]_1$	$[1 1 0 2 0]$	5	12	2	7.24998	$\frac{29}{4}$	8	II	35
35	$5[0 1 3 3 1 1 1 0]_2$	$[1 1 0 2 0]$	5	12	2	7.24998	$\frac{29}{4}$	8	II	34
167	$6[0 1 4 3 2 1 1 0]_5$	$[1 1 1 1 1]$	6	7.429856598	2	7.999	8	8	II	168
168	$6[0 1 4 3 2 1 1 0]_6$	$[1 1 1 1 1]$	6	7.429856598	2	7.999	8	8	II	167
173	$6[0 1 4 4 1 1 1 0]_3$	$[1 1 0 3 0]$	6	$\frac{25}{2} - \frac{\sqrt{37}}{2}$	2	9.5000	$\frac{19}{2}$	8	II	174
174	$6[0 1 4 4 1 1 1 0]_4$	$[1 1 0 3 0]$	6	$\frac{25}{2} - \frac{\sqrt{37}}{2}$	2	9.5000	$\frac{19}{2}$	8	II	173

Table 21. States in our database with $\delta = 2$ and $(\ell_1 \ell_2) = (1 1)$.

In table 21, the entries shaded with belong to one of the 2 $[1 1; 1 0]$.

Next, we consider states with Lorentz spin labels $(0 2)$ and $(2 0)$. There are 6 such states, presented in table 22. We have

St. No.	State ID	$[\ell_1 \ell_2 q_1 p q_2]$	Δ_0	$\Delta_0 + \# g^2$	δ	$2\sqrt{\delta}\lambda^{1/4} - 2 + \frac{\#}{\sqrt{\delta}} \frac{1}{\lambda^{1/4}}$	d_1	j_1	Type	Degs.
8	$4[0 0 1 1 1 1 2 0]_1$	$[0 2 0 0 0]$	4	18	2	7.000	7	14	III	11
27	$5[0 0 2 2 1 1 2 0]_2$	$[0 2 0 1 0]$	5	$16 - 2\sqrt{2}$	2	8.250	$\frac{33}{4}$	14	III	38
135	$6[0 0 3 3 1 1 2 0]_3$	$[0 2 0 2 0]$	6	9.656169691	2	10.0	10	14	III	193
11	$4[0 2 2 2 2 2 0 0]_1$	$[2 0 0 0 0]$	4	18	2	7.000	7	14	III	8
38	$5[0 2 3 3 2 2 0 0]_2$	$[2 0 0 1 0]$	5	$16 - 2\sqrt{2}$	2	8.250	$\frac{33}{4}$	14	III	27
193	$6[0 2 4 4 2 2 0 0]_3$	$[2 0 0 2 0]$	6	9.656169691	2	10.0	10	14	III	135

Table 22. States in our database with $\delta = 2$ and $(\ell_1 \ell_2) = (0 2)$ or $(\ell_1 \ell_2) = (2 0)$.

In table 22, the entries shaded with belong to $[0 2; 0 0]$, belong to $[2 0; 0 0]$.

Finally, let us consider states with Lorentz spin labels $(2 2)$. There are 3 such states in our database, and are displayed in table 23. We have

St. No.	State ID	$[\ell_1 \ell_2 q_1 p q_2]$	Δ_0	$\Delta_0 + \# g^2$	δ	$2\sqrt{\delta}\lambda^{1/4} - 2 + \frac{\#}{\sqrt{\delta}} \frac{1}{\lambda^{1/4}}$	d_1	j_1	Type	Degs.
12	$4[0 2 1 1 1 1 2 0]_1$	$[2 2 0 0 0]$	4	$\frac{50}{3}$	2	6.000000	6	14	I	
39	$5[0 2 2 2 1 1 2 0]_1$	$[2 2 0 1 0]$	5	12	2	7.2499996	$\frac{29}{4}$	14	I	
206	$6[0 2 3 3 1 1 2 0]_3$	$[2 2 0 2 0]$	6	8.765533583	2	9.000000	9	14	I	

Table 23. States in our database with $\delta = 2$ and $(\ell_1 \ell_2) = (2 2)$.

In table 23, the entries shaded with belong to $[2 2; 0 0]$.

They are all $\mathfrak{sl}(2)$ states of the form $[4 p + 2 1]$, as can be seen by comparing with section 6.1.3. Their strong coupling dimensions, at first three sub-leading orders is given by equation (6.6).

D.2 States with $\delta = 3$

The KK-towers at $\delta = 3$ are given by [99]. We have

$$\begin{aligned}
 \text{count}_3 = & 6[00;00] + 2[00;10] + 4[00;02] + 4[00;20] + [00;22] + [00;04] + [00;40] \\
 & + 4[01;01] + 4[01;11] + 2[01;21] + 4[10;01] + 4[10;11] + 2[10;21] \\
 & + 2[11;00] + 8[11;10] + 2[11;02] + 2[11;12] + 2[11;30]
 \end{aligned}$$

$$\begin{aligned}
 &+3[02;00]+[02;10]+2[02;02]+[02;20]+3[20;00]+[20;10]+2[20;02]+[20;20] \\
 &+4[12;01]+2[12;11]+4[21;01]+2[21;11]+4[22;00]+[22;02]+3[22;20] \\
 &+2[13;10]+2[31;10]+2[23;01]+2[32;01]+2[33;10] \\
 &+[04;00]+[40;00]+[24;00]+[42;00]+[44;00].
 \end{aligned} \tag{D.1}$$

There are 118 states in our database with $\delta = 3$. Out of them, 27 have Lorentz spin (0 0). They are

St. No.	State ID	$[\ell_1 \ell_2 q_1 p q_2]$	Δ_0	$\Delta_0 + \# g^2$	δ	$2\sqrt{\delta}\lambda^{1/4} - 2 + \frac{\#}{\sqrt{\delta}} \frac{1}{\lambda^{1/4}}$	d_1	j_1	Type	Degs.
14	${}_5[00333100]_2$	[00002]	5	21.21110255	3	9.9		13.2	III	16
16	${}_5[00422200]_2$	[00200]	5	21.21110255	3	9.9		13.2	III	14
19	${}_5[00332200]_3$	[00010]	5	20	3	8.9		13.3	III	20
20	${}_5[00332200]_4$	[00010]	5	20	3	8.9		13.3	III	19
76	${}_6[00222211]_1$	[00000]	6	13.67544468	3	7.749	$\frac{31}{4}$	$\frac{27}{2}$	III	85
78	${}_6[00333300]_1$	[00000]	6	4.808186901	3	1.0000	1	0	I	
81	${}_6[00333300]_4$	[00000]	6	12.93049869	3	10.0000	10	18	I	
83	${}_6[11222211]_1$	[00000]	6	15.52786405	3	10.999999	11	20	I	
84	${}_6[11222211]_2$	[00000]	6	24.47213595	3	19.00000	19	36	I	
85	${}_6[11333300]_1$	[00000]	6	13.67544468	3	7.749	$\frac{31}{4}$	$\frac{27}{2}$	III	76
87	${}_6[00433200]_1$	[00101]	6	6.658879771	3	3.00	3	0	I	
89	${}_6[00433200]_3$	[00101]	6	15.55975425	3	12.0000	12	18	I	
92	${}_6[0433200]_6$	[00101]	6	16	3			9.5	IV	93, 94, 95
93	${}_6[00433200]_7$	[00101]	6	16	3			9.5	IV	92, 94, 95
94	${}_6[00433200]_8$	[00101]	6	16	3			9.5	IV	92, 93, 95
95	${}_6[00433200]_9$	[00101]	6	16	3			9.5	IV	92, 93, 94
98	${}_6[00533100]_3$	[00202]	6	10.90443778	3	5.999999	6	0	I	
101	${}_6[00443100]_3$	[00012]	6	17.09556222	3	11.57		13.1	III	104
104	${}_6[00532200]_3$	[00210]	6	17.09556222	3	11.57		13.1	III	101
105	${}_6[00442200]_1$	[00020]	6	16	3	10.60		13.2	III	106
106	${}_6[00442200]_2$	[00020]	6	16	3	10.60		13.2	III	105
108	${}_6[00442200]_4$	[00020]	6	17.89750309	3	13.0000	13	18	I	
112	${}_6[00442200]_8$	[00020]	6	7.627478610	3	4.00000	4	0	I	
113	${}_6[00442200]_9$	[00020]	6	14	3	9.00	9	10	II	114
114	${}_6[00442200]_{10}$	[00020]	6	14	3	9.00	9	10	II	113
116	${}_6[00542100]_2$	[00121]	6	8	3	7.0000	7	0	I	
120	${}_6[00551100]_3$	[00040]	6	15.20775094	3	9.00	9	0	III	

Table 24. States in our database with $\delta = 3$ and $(\ell_1 \ell_2) = (00)$.

In table 24, the entries shaded with

	belong to one of the 6 $[00; 00]$,		belong to one of the 2 $[00; 10]$,
	belong to one of the 4 $[00; 02]$,		belong to one of the 4 $[00; 20]$,
	belong to $[00; 22]$,		belong to $[00; 04]$,
	belong to $[00; 40]$		

The 10 states with Lorentz spin labels (0 1) and 10 states with Lorentz spin labels (1 0) are given below, in table 25:

St. No.	State ID	$[\ell_1 \ell_2 q_1 p q_2]$	Δ_0	$\Delta_0 + \# g^2$	δ	$2\sqrt{\delta}\lambda^{1/4} - 2 + \frac{\#}{\sqrt{\delta}} \frac{1}{\lambda^{1/4}}$	d_1	j_1	Type	Degs.
40	$\frac{11}{2}[00322210]_1$	[01100]	$\frac{11}{2}$	18.61803399	3	9.4		15.5	IV	41, 50, 51
41	$\frac{11}{2}[00322210]_2$	[01100]	$\frac{11}{2}$	18.61803399	3	9.4		15.5	IV	40, 50, 51
42	$\frac{11}{2}[00322210]_3$	[01100]	$\frac{11}{2}$	16.38196601	3	0.4		0.7	IV	43, 52, 53

43	$\frac{11}{2}[0\ 0\ 3\ 2\ 2\ 2\ 1\ 0]_4$	$[0\ 1\ 1\ 0\ 0]$	$\frac{11}{2}$	16.38196601	3	0.4		0.7	IV	42, 52, 53
44	$\frac{11}{2}[0\ 0\ 3\ 3\ 2\ 1\ 1\ 0]_1$	$[0\ 1\ 0\ 1\ 1]$	$\frac{11}{2}$	18.82842712	3	12.0		0.7	IV	45, 54, 55
45	$\frac{11}{2}[0\ 0\ 3\ 3\ 2\ 1\ 1\ 0]_2$	$[0\ 1\ 0\ 1\ 1]$	$\frac{11}{2}$	18.82842712	3	12.0		0.7	IV	44, 54, 55
46	$\frac{11}{2}[0\ 0\ 3\ 3\ 2\ 1\ 1\ 0]_3$	$[0\ 1\ 0\ 1\ 1]$	$\frac{11}{2}$	13.17157288	3	0.3		0.2	IV	47, 56, 57
47	$\frac{11}{2}[0\ 0\ 3\ 3\ 2\ 1\ 1\ 0]_4$	$[0\ 1\ 0\ 1\ 1]$	$\frac{11}{2}$	13.17157288	3	0.3		0.2	IV	46, 56, 57
48	$\frac{11}{2}[0\ 0\ 4\ 3\ 1\ 1\ 1\ 0]_1$	$[0\ 1\ 1\ 2\ 0]$	$\frac{11}{2}$	16	3	0.4		0.2	IV	49, 58, 59
49	$\frac{11}{2}[0\ 0\ 4\ 3\ 1\ 1\ 1\ 0]_2$	$[0\ 1\ 1\ 2\ 0]$	$\frac{11}{2}$	16	3	0.4		0.2	IV	48, 58, 59
50	$\frac{11}{2}[0\ 1\ 3\ 3\ 3\ 2\ 0\ 0]_1$	$[1\ 0\ 0\ 0\ 1]$	$\frac{11}{2}$	18.61803399	3	9.4		15.5	IV	40, 41, 51
51	$\frac{11}{2}[0\ 1\ 3\ 3\ 3\ 2\ 0\ 0]_2$	$[1\ 0\ 0\ 0\ 1]$	$\frac{11}{2}$	18.61803399	3	9.4		15.5	IV	40, 41, 50
52	$\frac{11}{2}[0\ 1\ 3\ 3\ 3\ 2\ 0\ 0]_3$	$[1\ 0\ 0\ 0\ 1]$	$\frac{11}{2}$	16.38196601	3	0.4		0.7	IV	42, 43, 53
53	$\frac{11}{2}[0\ 1\ 3\ 3\ 3\ 2\ 0\ 0]_4$	$[1\ 0\ 0\ 0\ 1]$	$\frac{11}{2}$	16.38196601	3	0.4		0.7	IV	42, 43, 52
54	$\frac{11}{2}[0\ 1\ 4\ 3\ 2\ 2\ 0\ 0]_1$	$[1\ 0\ 1\ 1\ 0]$	$\frac{11}{2}$	18.82842712	3	12.0		0.7	IV	44, 45, 55
55	$\frac{11}{2}[0\ 1\ 4\ 3\ 2\ 2\ 0\ 0]_2$	$[1\ 0\ 1\ 1\ 0]$	$\frac{11}{2}$	18.82842712	3	12.0		0.7	IV	44, 45, 54
56	$\frac{11}{2}[0\ 1\ 4\ 3\ 2\ 2\ 0\ 0]_3$	$[1\ 0\ 1\ 1\ 0]$	$\frac{11}{2}$	13.17157288	3	0.3		0.2	IV	46, 47, 57
57	$\frac{11}{2}[0\ 1\ 4\ 3\ 2\ 2\ 0\ 0]_4$	$[1\ 0\ 1\ 1\ 0]$	$\frac{11}{2}$	13.17157288	3	0.3		0.2	IV	46, 47, 56
58	$\frac{11}{2}[0\ 1\ 4\ 4\ 2\ 1\ 0\ 0]_1$	$[1\ 0\ 0\ 2\ 1]$	$\frac{11}{2}$	16	3	0.4		0.2	IV	48, 49, 59
59	$\frac{11}{2}[0\ 1\ 4\ 4\ 2\ 1\ 0\ 0]_2$	$[1\ 0\ 0\ 2\ 1]$	$\frac{11}{2}$	16	3	0.4		0.2	IV	48, 49, 58

Table 25. States in our database with $\delta = 3$ and $(\ell_1\ \ell_2) = (0\ 1)$ or $(\ell_1\ \ell_2) = (1\ 0)$.

In table 25, the entries shaded with

	belong to one of the 4 $[1\ 0; 0\ 1]$,		belong to one of the 4 $[1\ 0; 1\ 1]$,
	belong to one of the 2 $[1\ 0; 2\ 1]$,		belong to one of the 4 $[0\ 1; 0\ 1]$,
	belong to one of the 4 $[0\ 1; 1\ 1]$,		belong to one of the 4 $[0\ 1; 2\ 1]$.

The 20 states with Lorentz spin labels $(1\ 1)$ are given below in table 26, they are

St. No.	State ID	$[\ell_1\ \ell_2\ q_1\ p\ q_2]$	Δ_0	$\Delta_0 + \# g^2$	δ	$2\sqrt{\delta}\lambda^{1/4} - 2 + \frac{\#}{\sqrt{\delta}}\frac{1}{\lambda^{1/4}}$	d_1	j_1	Type	Degs.
28	$5[0\ 1\ 2\ 2\ 2\ 2\ 1\ 0]_1$	$[1\ 1\ 0\ 0\ 0]$	5	18	3	7.0		13.5	IV	29
29	$5[0\ 1\ 2\ 2\ 2\ 2\ 1\ 0]_2$	$[1\ 1\ 0\ 0\ 0]$	5	18	3	6.9		13.3	IV	28
32	$5[0\ 1\ 3\ 2\ 2\ 1\ 1\ 0]_3$	$[1\ 1\ 1\ 0\ 1]$	5	20	3	0.4		9.0	IV	33
33	$5[0\ 1\ 3\ 2\ 2\ 1\ 1\ 0]_4$	$[1\ 1\ 1\ 0\ 1]$	5	20	3	0.4		9.0	IV	32
147	$6[0\ 1\ 3\ 3\ 2\ 2\ 1\ 0]_1$	$[1\ 1\ 0\ 1\ 0]$	6	19.61100719	3	15.0	15	27	II	148
148	$6[0\ 1\ 3\ 3\ 2\ 2\ 1\ 0]_2$	$[1\ 1\ 0\ 1\ 0]$	6	19.61100719	3	15.0	15	27	II	147
151	$6[0\ 1\ 3\ 3\ 2\ 2\ 1\ 0]_5$	$[1\ 1\ 0\ 1\ 0]$	6	16.40430841	3	11.00	11	19	II	152
152	$6[0\ 1\ 3\ 3\ 2\ 2\ 1\ 0]_6$	$[1\ 1\ 0\ 1\ 0]$	6	16.40430841	3	11.00	11	19	II	151
153	$6[0\ 1\ 3\ 3\ 2\ 2\ 1\ 0]_7$	$[1\ 1\ 0\ 1\ 0]$	6	8.468040123	3	5.8		9.0	II	154
154	$6[0\ 1\ 3\ 3\ 2\ 2\ 1\ 0]_8$	$[1\ 1\ 0\ 1\ 0]$	6	8.468040123	3	5.8		9.0	II	153
155	$6[0\ 1\ 3\ 3\ 2\ 2\ 1\ 0]_9$	$[1\ 1\ 0\ 1\ 0]$	6	14.27984675	3	7.5		0.7	IV	156, 157, 158
156	$6[0\ 1\ 3\ 3\ 2\ 2\ 1\ 0]_{10}$	$[1\ 1\ 0\ 1\ 0]$	6	14.27984675	3	7.5		0.7	IV	155, 157, 158
157	$6[0\ 1\ 3\ 3\ 2\ 2\ 1\ 0]_{11}$	$[1\ 1\ 0\ 1\ 0]$	6	14.27984675	3	6.5		9.6	IV	155, 156, 158
158	$6[0\ 1\ 3\ 3\ 2\ 2\ 1\ 0]_{12}$	$[1\ 1\ 0\ 1\ 0]$	6	14.27984675	3	7.5		0.7	IV	155, 156, 157
163	$6[0\ 1\ 4\ 3\ 2\ 1\ 1\ 0]_1$	$[1\ 1\ 1\ 1\ 1]$	6	16	3	10.9		14.0	IV	164
164	$6[0\ 1\ 4\ 3\ 2\ 1\ 1\ 0]_2$	$[1\ 1\ 1\ 1\ 1]$	6	16	3	10.9		14.0	IV	163
169	$6[0\ 1\ 4\ 3\ 2\ 1\ 1\ 0]_7$	$[1\ 1\ 1\ 1\ 1]$	6	12.72643156	3	8.50	$\frac{17}{2}$	9	II	170
170	$6[0\ 1\ 4\ 3\ 2\ 1\ 1\ 0]_8$	$[1\ 1\ 1\ 1\ 1]$	6	12.72643156	3	8.50	$\frac{17}{2}$	9	II	169
171	$6[0\ 1\ 4\ 4\ 1\ 1\ 1\ 0]_1$	$[1\ 1\ 0\ 3\ 0]$	6	$\frac{25}{2} + \frac{\sqrt{37}}{2}$	3	10.0	10	9	II	172
172	$6[0\ 1\ 4\ 4\ 1\ 1\ 1\ 0]_2$	$[1\ 1\ 0\ 3\ 0]$	6	$\frac{25}{2} + \frac{\sqrt{37}}{2}$	3	10.0	10	9	II	171

Table 26. States in our database with $\delta = 3$ and $(\ell_1\ \ell_2) = (1\ 1)$.

In table 26, the entries shaded with

	belong to one of the 2 $[1\ 1; 0\ 0]$,		belong to one of the 8 $[1\ 1; 1\ 0]$,
	belong to one of the 2 $[1\ 1; 1\ 2]$,		belong to one of the 2 $[1\ 1; 3\ 0]$,
	belong either to $[1\ 1; 1\ 0]$ or $[1\ 1; 0\ 2]$.		

The 11 states with Lorentz spin labels $(0\ 2)$ and 11 states with Lorentz spin labels $(2\ 0)$, are displayed in table 27.

St. No.	State ID	$[\ell_1\ \ell_2\ q_1\ p\ q_2]$	Δ_0	$\Delta_0 + \# g^2$	δ	$2\sqrt{\delta}\lambda^{1/4} - 2 + \frac{\#}{\sqrt{\delta}}\frac{1}{\lambda^{1/4}}$	d_1	j_1	Type	Degs.
25	${}_5[0\ 0\ 3\ 1\ 1\ 1\ 2\ 0]_1$	$[0\ 2\ 2\ 0\ 0]$	5	3	3	8.86		13.22	III	36
26	${}_5[0\ 0\ 2\ 2\ 1\ 1\ 2\ 0]_1$	$[0\ 2\ 0\ 1\ 0]$	5	$16 + 2\sqrt{2}$	3	7.9		13.3	III	37
122	${}_6[0\ 0\ 2\ 2\ 2\ 2\ 2\ 0]_2$	$[0\ 2\ 0\ 0\ 0]$	6	11.34832950	3	9.00	9	18	III	182
124	${}_6[1\ 1\ 1\ 1\ 1\ 1\ 2\ 0]_1$	$[0\ 2\ 0\ 0\ 0]$	6	11.54748008	3	6.750	$\frac{27}{4}$	$\frac{27}{2}$	III	179
125	${}_6[1\ 1\ 1\ 1\ 1\ 1\ 2\ 0]_2$	$[0\ 2\ 0\ 0\ 0]$	6	23.78585325	3	17.999	18	36	III	180
127	${}_6[0\ 0\ 3\ 2\ 2\ 1\ 2\ 0]_2$	$[0\ 2\ 1\ 0\ 1]$	6	14.87689437	3	11.00	11	18	III	185
128	${}_6[0\ 0\ 3\ 2\ 2\ 1\ 2\ 0]_3$	$[0\ 2\ 1\ 0\ 1]$	6	14.87689437	3	7.2		14.8	IV	129, 186, 187
129	${}_6[0\ 0\ 3\ 2\ 2\ 1\ 2\ 0]_4$	$[0\ 2\ 1\ 0\ 1]$	6	14.87689437	3	7.2		10.1	IV	128, 186, 187
132	${}_6[0\ 0\ 4\ 2\ 1\ 1\ 2\ 0]_1$	$[0\ 2\ 2\ 1\ 0]$	6	16	3	10.57		13.1	III	190
134	${}_6[0\ 0\ 3\ 3\ 1\ 1\ 2\ 0]_2$	$[0\ 2\ 0\ 2\ 0]$	6	17.26106778	3	11.999	12	18	III	192
136	${}_6[0\ 0\ 3\ 3\ 1\ 1\ 2\ 0]_4$	$[0\ 2\ 0\ 2\ 0]$	6	15.00912120	3	9.57		13.2	III	194
36	${}_5[0\ 2\ 3\ 3\ 3\ 1\ 0\ 0]_1$	$[2\ 0\ 0\ 0\ 2]$	5	3	3	8.86		13.22	III	25
37	${}_5[0\ 2\ 3\ 3\ 2\ 2\ 0\ 0]_1$	$[2\ 0\ 0\ 1\ 0]$	5	$16 + 2\sqrt{2}$	3	7.9		13.3	III	26
179	${}_6[0\ 2\ 2\ 2\ 2\ 2\ 1\ 1]_1$	$[2\ 0\ 0\ 0\ 0]$	6	11.54748008	3	6.750	$\frac{27}{4}$	$\frac{27}{2}$	III	124
180	${}_6[0\ 2\ 2\ 2\ 2\ 2\ 1\ 1]_2$	$[2\ 0\ 0\ 0\ 0]$	6	23.78585325	3	17.999	18	36	III	125
182	${}_6[0\ 2\ 3\ 3\ 3\ 3\ 0\ 0]_2$	$[2\ 0\ 0\ 0\ 0]$	6	11.34832950	3	9.00	9	18	III	122
185	${}_6[0\ 2\ 4\ 3\ 3\ 2\ 0\ 0]_2$	$[2\ 0\ 1\ 0\ 1]$	6	14.87689437	3	11.00	11	18	III	127
186	${}_6[0\ 2\ 4\ 3\ 3\ 2\ 0\ 0]_3$	$[2\ 0\ 1\ 0\ 1]$	6	14.87689437	3	7.2			IV	128, 129, 187
187	${}_6[0\ 2\ 4\ 3\ 3\ 2\ 0\ 0]_4$	$[2\ 0\ 1\ 0\ 1]$	6	14.87689437	3	7.2			IV	128, 129, 186
190	${}_6[0\ 2\ 4\ 4\ 3\ 1\ 0\ 0]_1$	$[2\ 0\ 0\ 1\ 2]$	6	16	3	10.57		13.1	III	132
192	${}_6[0\ 2\ 4\ 4\ 2\ 2\ 0\ 0]_2$	$[2\ 0\ 0\ 2\ 0]$	6	17.26106778	3	11.999	12	18	III	134
194	${}_6[0\ 2\ 4\ 4\ 2\ 2\ 0\ 0]_4$	$[2\ 0\ 0\ 2\ 0]$	6	15.00912120	3	9.57		13.2	III	136

Table 27. States in our database with $\delta = 3$ and $(\ell_1\ \ell_2) = (0\ 2)$ or $(\ell_1\ \ell_2) = (2\ 0)$.

In table 27, the entries shaded with

	belong to one of the 3 $[0\ 2; 0\ 0]$,		belong $[0\ 2; 0\ 2]$,
	belong to one of the 2 $[0\ 2; 0\ 2]$,		belong to $[0\ 2; 2\ 0]$
	belong to one of the 3 $[2\ 0; 0\ 2]$,		belong to $[2\ 0; 0\ 2]$
	belong to one of the 2 $[2\ 0; 0\ 2]$,		belong to $[2\ 0; 2\ 0]$

The 6 states with Lorentz spin labels $(1\ 2)$ and 6 states with Lorentz spin labels $(2\ 1)$, are given in table 28. They are

St. No.	State ID	$[\ell_1\ \ell_2\ q_1\ p\ q_2]$	Δ_0	$\Delta_0 + \# g^2$	δ	$2\sqrt{\delta}\lambda^{1/4} - 2 + \frac{\#}{\sqrt{\delta}}\frac{1}{\lambda^{1/4}}$	d_1	j_1	Type	Degs.
60	$\frac{11}{2}[0\ 1\ 2\ 2\ 2\ 1\ 2\ 0]_1$	$[1\ 2\ 0\ 0\ 1]$	$\frac{11}{2}$	15.45861873	3	0.4		0.8	IV	61, 66, 67
61	$\frac{11}{2}[0\ 1\ 2\ 2\ 2\ 1\ 2\ 0]_2$	$[1\ 2\ 0\ 0\ 1]$	$\frac{11}{2}$	15.45861873	3	0.4		0.8	IV	60, 66, 67
62	$\frac{11}{2}[0\ 1\ 2\ 2\ 2\ 1\ 2\ 0]_3$	$[1\ 2\ 0\ 0\ 1]$	$\frac{11}{2}$	21.54138127	3	14.9		1.2	IV	63, 68, 69
63	$\frac{11}{2}[0\ 1\ 2\ 2\ 2\ 1\ 2\ 0]_4$	$[1\ 2\ 0\ 0\ 1]$	$\frac{11}{2}$	21.54138127	3	14.9		1.2	IV	62, 68, 69
64	$\frac{11}{2}[0\ 1\ 3\ 2\ 1\ 1\ 2\ 0]_1$	$[1\ 2\ 1\ 1\ 0]$	$\frac{11}{2}$	18	3	10.9		17.9	IV	65, 70, 71
65	$\frac{11}{2}[0\ 1\ 3\ 2\ 1\ 1\ 2\ 0]_2$	$[1\ 2\ 1\ 1\ 0]$	$\frac{11}{2}$	18	3	10.9		17.9	IV	64, 70, 71

66	$\frac{11}{2}[0\ 2\ 3\ 2\ 2\ 2\ 1\ 0]_1$	$[2\ 1\ 1\ 0\ 0]$	$\frac{11}{2}$	15.45861873	3	0.4		0.8	IV	60, 61, 67
67	$\frac{11}{2}[0\ 2\ 3\ 2\ 2\ 2\ 1\ 0]_2$	$[2\ 1\ 1\ 0\ 0]$	$\frac{11}{2}$	15.45861873	3	0.4		0.8	IV	60, 61, 66
68	$\frac{11}{2}[0\ 2\ 3\ 2\ 2\ 2\ 1\ 0]_3$	$[2\ 1\ 1\ 0\ 0]$	$\frac{11}{2}$	21.54138127	3	14.9		1.2	IV	62, 63, 69
69	$\frac{11}{2}[0\ 2\ 3\ 2\ 2\ 2\ 1\ 0]_4$	$[2\ 1\ 1\ 0\ 0]$	$\frac{11}{2}$	21.54138127	3	14.9		1.2	IV	62, 63, 68
70	$\frac{11}{2}[0\ 2\ 3\ 3\ 2\ 1\ 1\ 0]_1$	$[2\ 1\ 0\ 1\ 1]$	$\frac{11}{2}$	18	3	10.9		17.9	IV	64, 65, 71
71	$\frac{11}{2}[0\ 2\ 3\ 3\ 2\ 1\ 1\ 0]_2$	$[2\ 1\ 0\ 1\ 1]$	$\frac{11}{2}$	18	3	10.9		17.9	IV	64, 65, 70

Table 28. States in our database with $\delta = 3$ and $(\ell_1\ \ell_2) = (1\ 2)$ or $(\ell_1\ \ell_2) = (2\ 1)$.

In table 28, the entries shaded with

- belong to one of the 4 $[1\ 2; 0\ 1]$,
- belong to one of the 2 $[1\ 2; 1\ 1]$,
- belong to one of the 4 $[2\ 1; 0\ 1]$,
- belong to one of the 2 $[2\ 1; 1\ 1]$.

The 8 states with Lorentz spin labels $(2\ 2)$, are given in table 29. They are

St. No.	State ID	$[\ell_1\ \ell_2\ q_1\ p\ q_2]$	Δ_0	$\Delta_0 + \# g^2$	δ	$2\sqrt{\delta}\lambda^{1/4} - 2 + \frac{\#}{\sqrt{\delta}}\frac{1}{\lambda^{1/4}}$	d_1	j_1	Type	Degs.
196	${}_6[0\ 2\ 2\ 2\ 2\ 2\ 2\ 0]_2$	$[2\ 2\ 0\ 0\ 0]$	6	9.804773390	3	8.0000	8	18	I	
197	${}_6[0\ 2\ 2\ 2\ 2\ 2\ 2\ 0]_3$	$[2\ 2\ 0\ 0\ 0]$	6	23.10773903	3	17.0000	17	36	I	
198	${}_6[0\ 2\ 2\ 2\ 2\ 2\ 2\ 0]_4$	$[2\ 2\ 0\ 0\ 0]$	6	$\frac{58}{3}$	3	12.999	13	28	II	199
199	${}_6[0\ 2\ 2\ 2\ 2\ 2\ 2\ 0]_5$	$[2\ 2\ 0\ 0\ 0]$	6	$\frac{58}{3}$	3	12.999	13	28	II	198
203	${}_6[0\ 2\ 3\ 2\ 2\ 1\ 2\ 0]_2$	$[2\ 2\ 1\ 0\ 1]$	6	$\frac{55}{3} - \frac{\sqrt{145}}{3}$	3	10.0000	10	18	I	
205	${}_6[0\ 2\ 3\ 3\ 1\ 1\ 2\ 0]_2$	$[2\ 2\ 0\ 2\ 0]$	6	16.71846288	3	11.0000	11	18	I	
207	${}_6[0\ 2\ 3\ 3\ 1\ 1\ 2\ 0]_4$	$[2\ 2\ 0\ 2\ 0]$	6	$\frac{46}{3}$	3	11.000	11	18	II	208
208	${}_6[0\ 2\ 3\ 3\ 1\ 1\ 2\ 0]_5$	$[2\ 2\ 0\ 2\ 0]$	6	$\frac{46}{3}$	3	11.000	11	18	II	207

Table 29. States in our database with $\delta = 3$ and $(\ell_1\ \ell_2) = (2\ 2)$.

In table 29, the entries shaded with

- belong to one of the 4 $[2\ 2; 0\ 0]$,
- belong to $[2\ 2; 0\ 2]$,
- belong to one of the 3 $[2\ 2; 2\ 0]$.

We didn't find any states with Lorentz spin labels $(0\ 3)$ and $(3\ 0)$, exactly as expected by [99] through (D.1). The 2 states with Lorentz spin labels $(1\ 3)$ and 2 states with Lorentz spin labels $(3\ 1)$, are given in table 30:

St. No.	State ID	$[\ell_1\ \ell_2\ q_1\ p\ q_2]$	Δ_0	$\Delta_0 + \# g^2$	δ	$2\sqrt{\delta}\lambda^{1/4} - 2 + \frac{\#}{\sqrt{\delta}}\frac{1}{\lambda^{1/4}}$	d_1	j_1	Type	Degs.
175	${}_6[0\ 1\ 2\ 2\ 1\ 1\ 3\ 0]_1$	$[1\ 3\ 0\ 1\ 0]$	6	18.48338852	3	12.0		23.5	IV	176, 210, 211
176	${}_6[0\ 1\ 2\ 2\ 1\ 1\ 3\ 0]_2$	$[1\ 3\ 0\ 1\ 0]$	6	18.48338852	3	12.0		23.5	IV	175, 210, 211
210	${}_6[0\ 3\ 3\ 3\ 2\ 2\ 1\ 0]_1$	$[3\ 1\ 0\ 1\ 0]$	6	18.48338852	3	12.0		23.5	IV	175, 176, 211
211	${}_6[0\ 3\ 3\ 3\ 2\ 2\ 1\ 0]_2$	$[3\ 1\ 0\ 1\ 0]$	6	18.48338852	3	12.0		23.5	IV	175, 176, 210

Table 30. States in our database with $\delta = 3$ and $(\ell_1\ \ell_2) = (1\ 3)$ or $(\ell_1\ \ell_2) = (3\ 1)$.

In table 30, the entries shaded with

- belong to one of the 2 $[1\ 3; 1\ 0]$,
- belong to one of the 2 $[3\ 1; 1\ 0]$.

The 2 states with Lorentz spin labels (2 3) and 2 states with Lorentz spin labels (3 2), are

St. No.	State ID	$[\ell_1 \ell_2 q_1 p q_2]$	Δ_0	$\Delta_0 + \# g^2$	δ	$2\sqrt{\delta}\lambda^{1/4} - 2 + \frac{\#}{\sqrt{\delta}} \frac{1}{\lambda^{1/4}}$	d_1	j_1	Type	Degs.
72	$\frac{11}{2}[0 2 2 1 1 1 3 0]_1$	[2 3 1 0 0]	$\frac{11}{2}$	20	3	12.9		28.2	IV	73, 74, 75
73	$\frac{11}{2}[0 2 2 1 1 1 3 0]_2$	[2 3 1 0 0]	$\frac{11}{2}$	20	3	12.9		28.2	IV	72, 74, 75
74	$\frac{11}{2}[0 3 2 2 2 1 2 0]_1$	[3 2 0 0 1]	$\frac{11}{2}$	20	3	12.9		28.2	IV	72, 73, 75
75	$\frac{11}{2}[0 3 2 2 2 1 2 0]_2$	[3 2 0 0 1]	$\frac{11}{2}$	20	3	12.9		28.2	IV	72, 73, 74

Table 31. States in our database with $\delta = 3$ and $(\ell_1 \ell_2) = (2 3)$ or $(\ell_1 \ell_2) = (3 2)$.

In table 31, the entries shaded with

belong to one of the 2 [2 3; 0 1], belong to one of the 2 [3 2; 0 1].

The 2 states with Lorentz spin labels (3 3), are displayed in table 32. They are

St. No.	State ID	$[\ell_1 \ell_2 q_1 p q_2]$	Δ_0	$\Delta_0 + \# g^2$	δ	$2\sqrt{\delta}\lambda^{1/4} - 2 + \frac{\#}{\sqrt{\delta}} \frac{1}{\lambda^{1/4}}$	d_1	j_1	Type	Degs.
214	$6[0 3 2 2 1 1 3 0]_1$	[3 3 0 1 0]	6	$\frac{35}{2}$	3	12.00	12	27	II	215
215	$6[0 3 2 2 1 1 3 0]_2$	[3 3 0 1 0]	6	$\frac{35}{2}$	3	12.00	12	27	II	214

Table 32. States in our database with $\delta = 3$ and $(\ell_1 \ell_2) = (3 3)$.

In table 32, the entries shaded with

belong to one of the 2 [3 3; 1 0].

The 1 state with Lorentz spin labels (0 4) and 1 state with Lorentz spin labels (4 0) are displayed in table 33. They are

St. No.	State ID	$[\ell_1 \ell_2 q_1 p q_2]$	Δ_0	$\Delta_0 + \# g^2$	δ	$2\sqrt{\delta}\lambda^{1/4} - 2 + \frac{\#}{\sqrt{\delta}} \frac{1}{\lambda^{1/4}}$	d_1	j_1	Type	Degs.
138	$6[1 1 1 1 1 1 4 0]_1$	[0 4 0 0 0]	6	22	3	16.0000	16	36	III	216
216	$6[0 4 2 2 2 2 1 1]_1$	[4 0 0 0 0]	6	22	3	16.0000	16	36	III	138

Table 33. States in our database with $\delta = 3$ and $(\ell_1 \ell_2) = (0 4)$ or $(\ell_1 \ell_2) = (4 0)$.

In table 33, the entries shaded with

belong to [0 4; 0 0], belong to [4 0; 0 0].

We didn't find any states with Lorentz spin labels (1 4) and (4 1), exactly as expected by [99] through (D.1). The 1 state with Lorentz spin labels (2 4) and 1 state with Lorentz spin labels (4 2), are given in table 34, they are

St. No.	State ID	$[\ell_1 \ell_2 q_1 p q_2]$	Δ_0	$\Delta_0 + \# g^2$	δ	$2\sqrt{\delta}\lambda^{1/4} - 2 + \frac{\#}{\sqrt{\delta}} \frac{1}{\lambda^{1/4}}$	d_1	j_1	Type	Degs.
209	$6[0 2 1 1 1 1 4 0]_1$	[2 4 0 0 0]	6	$\frac{64}{3}$	3	15.000	15	36	III	218
218	$6[0 4 2 2 2 2 2 0]_1$	[4 2 0 0 0]	6	$\frac{64}{3}$	3	15.000	15	36	III	209

Table 34. States in our database with $\delta = 3$ and $(\ell_1 \ell_2) = (2 4)$ or $(\ell_1 \ell_2) = (4 2)$.

In table 34, the entries shaded with belong to [2 4; 0 0], belong to [4 2; 0 0]. We didn't find any states with Lorentz spin labels (3 4) and (4 3), exactly as expected by [99] through (D.1). The 1 state with Lorentz spin labels (4 4) is given in table 35. We have

St. No.	State ID	$[\ell_1 \ell_2 q_1 p q_2]$	Δ_0	$\Delta_0 + \# g^2$	δ	$2\sqrt{\delta\lambda^{1/4}} - 2 + \frac{\#}{\sqrt{\delta}} \frac{1}{\lambda^{1/4}}$	d_1	j_1	Type	Degs.
219	${}_6[0\ 4\ 1\ 1\ 1\ 1\ 4\ 0]_1$	$[4\ 4\ 0\ 0\ 0]$	6	$\frac{98}{5}$	3	13.0000	13	36	I	

Table 35. The states in our database with $\delta = 3$ and $(\ell_1 \ell_2) = (4\ 4)$.

In table 35, the entries shaded with

belong to $[4\ 4; 0\ 0]$.

To conclude, we observe matching with the counting at strong coupling for $\delta = 2$ and $\delta = 3$. In addition, we break degeneracies of KK-towers using the sub-leading Casimir j_1 which as we notice is a good classifier.

Open Access. This article is distributed under the terms of the Creative Commons Attribution License ([CC-BY4.0](https://creativecommons.org/licenses/by/4.0/)), which permits any use, distribution and reproduction in any medium, provided the original author(s) and source are credited.

References

- [1] N. Gromov, V. Kazakov and P. Vieira, *Exact Spectrum of Planar $\mathcal{N} = 4$ Supersymmetric Yang-Mills Theory: Konishi Dimension at Any Coupling*, *Phys. Rev. Lett.* **104** (2010) 211601 [[arXiv:0906.4240](https://arxiv.org/abs/0906.4240)] [[INSPIRE](#)].
- [2] B. Basso, *An exact slope for AdS/CFT*, [arXiv:1109.3154](https://arxiv.org/abs/1109.3154) [[INSPIRE](#)].
- [3] N. Gromov, D. Serban, I. Shenderovich and D. Volin, *Quantum folded string and integrability: From finite size effects to Konishi dimension*, *JHEP* **08** (2011) 046 [[arXiv:1102.1040](https://arxiv.org/abs/1102.1040)] [[INSPIRE](#)].
- [4] R. Roiban and A.A. Tseytlin, *Semiclassical string computation of strong-coupling corrections to dimensions of operators in Konishi multiplet*, *Nucl. Phys. B* **848** (2011) 251 [[arXiv:1102.1209](https://arxiv.org/abs/1102.1209)] [[INSPIRE](#)].
- [5] B.C. Vallilo and L. Mazzucato, *The Konishi multiplet at strong coupling*, *JHEP* **12** (2011) 029 [[arXiv:1102.1219](https://arxiv.org/abs/1102.1219)] [[INSPIRE](#)].
- [6] N. Gromov and S. Valatka, *Deeper Look into Short Strings*, *JHEP* **03** (2012) 058 [[arXiv:1109.6305](https://arxiv.org/abs/1109.6305)] [[INSPIRE](#)].
- [7] S. Frolov, *Scaling dimensions from the mirror TBA*, *J. Phys. A* **45** (2012) 305402 [[arXiv:1201.2317](https://arxiv.org/abs/1201.2317)] [[INSPIRE](#)].
- [8] N. Gromov, F. Levkovich-Maslyuk, G. Sizov and S. Valatka, *Quantum spectral curve at work: from small spin to strong coupling in $\mathcal{N} = 4$ SYM*, *JHEP* **07** (2014) 156 [[arXiv:1402.0871](https://arxiv.org/abs/1402.0871)] [[INSPIRE](#)].
- [9] Á. Hegedús and J. Konczer, *Strong coupling results in the AdS_5/CFT_4 correspondence from the numerical solution of the quantum spectral curve*, *JHEP* **08** (2016) 061 [[arXiv:1604.02346](https://arxiv.org/abs/1604.02346)] [[INSPIRE](#)].
- [10] C. Marboe and D. Volin, *The full spectrum of AdS_5/CFT_4 I: Representation theory and one-loop Q -system*, *J. Phys. A* **51** (2018) 165401 [[arXiv:1701.03704](https://arxiv.org/abs/1701.03704)] [[INSPIRE](#)].

- [11] C. Marboe and D. Volin, *The full spectrum of AdS_5/CFT_4 II: Weak coupling expansion via the quantum spectral curve*, *J. Phys. A* **54** (2021) 055201 [[arXiv:1812.09238](#)] [[INSPIRE](#)].
- [12] A. Cavaglià, N. Gromov, J. Julius and M. Preti, *Integrability and conformal bootstrap: One dimensional defect conformal field theory*, *Phys. Rev. D* **105** (2022) L021902 [[arXiv:2107.08510](#)] [[INSPIRE](#)].
- [13] A. Cavaglià, N. Gromov, J. Julius and M. Preti, *Bootstrability in defect CFT: integrated correlators and sharper bounds*, *JHEP* **05** (2022) 164 [[arXiv:2203.09556](#)] [[INSPIRE](#)].
- [14] S. Caron-Huot, F. Coronado, A.-K. Trinh and Z. Zahraee, *Bootstrapping $\mathcal{N} = 4$ sYM correlators using integrability*, *JHEP* **02** (2023) 083 [[arXiv:2207.01615](#)] [[INSPIRE](#)].
- [15] A. Cavaglià, N. Gromov, J. Julius and M. Preti, *Integrated correlators from integrability: Maldacena-Wilson line in $\mathcal{N} = 4$ SYM*, *JHEP* **04** (2023) 026 [[arXiv:2211.03203](#)] [[INSPIRE](#)].
- [16] M. Alfimov, N. Gromov and V. Kazakov, *Chapter 13: $\mathcal{N} = 4$ SYM Quantum Spectral Curve in BFKL Regime*, in *From the Past to the Future*, J. Bartels et al. eds., World Scientific (2021), p. 335–367 [[DOI:10.1142/9789811231124_0013](#)] [[arXiv:2003.03536](#)] [[INSPIRE](#)].
- [17] N. Beisert and M. Staudacher, *Long-range $\mathfrak{psu}(2,2|4)$ Bethe Ansatz for gauge theory and strings*, *Nucl. Phys. B* **727** (2005) 1 [[hep-th/0504190](#)] [[INSPIRE](#)].
- [18] N. Beisert, B. Eden and M. Staudacher, *Transcendentality and Crossing*, *J. Stat. Mech.* **0701** (2007) P01021 [[hep-th/0610251](#)] [[INSPIRE](#)].
- [19] E. Quinn and S. Frolov, *Excited states in Bethe ansatz solvable models and the dressing of spin and charge*, *J. Phys. A* **46** (2013) 205001 [[arXiv:1211.5503](#)] [[INSPIRE](#)].
- [20] N. Gromov, V. Kazakov, S. Leurent and D. Volin, *Quantum Spectral Curve for Planar $\mathcal{N} = 4$ Super-Yang-Mills Theory*, *Phys. Rev. Lett.* **112** (2014) 011602 [[arXiv:1305.1939](#)] [[INSPIRE](#)].
- [21] N. Gromov, V. Kazakov, S. Leurent and D. Volin, *Quantum spectral curve for arbitrary state/operator in AdS_5/CFT_4* , *JHEP* **09** (2015) 187 [[arXiv:1405.4857](#)] [[INSPIRE](#)].
- [22] S. Leurent and D. Volin, *Multiple zeta functions and double wrapping in planar $N = 4$ SYM*, *Nucl. Phys. B* **875** (2013) 757 [[arXiv:1302.1135](#)] [[INSPIRE](#)].
- [23] C. Marboe and D. Volin, *Quantum spectral curve as a tool for a perturbative quantum field theory*, *Nucl. Phys. B* **899** (2015) 810 [[arXiv:1411.4758](#)] [[INSPIRE](#)].
- [24] N.B. Agmon, S.M. Chester and S.S. Pufu, *Solving M-theory with the Conformal Bootstrap*, *JHEP* **06** (2018) 159 [[arXiv:1711.07343](#)] [[INSPIRE](#)].
- [25] N. Gromov, F. Levkovich-Maslyuk and G. Sizov, *Pomeron Eigenvalue at Three Loops in $\mathcal{N} = 4$ Supersymmetric Yang-Mills Theory*, *Phys. Rev. Lett.* **115** (2015) 251601 [[arXiv:1507.04010](#)] [[INSPIRE](#)].
- [26] N. Gromov, F. Levkovich-Maslyuk and G. Sizov, *Quantum Spectral Curve and the Numerical Solution of the Spectral Problem in AdS_5/CFT_4* , *JHEP* **06** (2016) 036 [[arXiv:1504.06640](#)] [[INSPIRE](#)].
- [27] M. Alfimov, N. Gromov and G. Sizov, *BFKL spectrum of $\mathcal{N} = 4$: non-zero conformal spin*, *JHEP* **07** (2018) 181 [[arXiv:1802.06908](#)] [[INSPIRE](#)].
- [28] N. Gromov and F. Levkovich-Maslyuk, *Quantum Spectral Curve for a cusped Wilson line in $\mathcal{N} = 4$ SYM*, *JHEP* **04** (2016) 134 [[arXiv:1510.02098](#)] [[INSPIRE](#)].
- [29] N. Gromov and F. Levkovich-Maslyuk, *Quark-anti-quark potential in $\mathcal{N} = 4$ SYM*, *JHEP* **12** (2016) 122 [[arXiv:1601.05679](#)] [[INSPIRE](#)].

- [30] A. Cavaglià, N. Gromov and F. Levkovich-Maslyuk, *Quantum spectral curve and structure constants in $\mathcal{N} = 4$ SYM: cusps in the ladder limit*, *JHEP* **10** (2018) 060 [[arXiv:1802.04237](#)] [[INSPIRE](#)].
- [31] S. Giombi and S. Komatsu, *More Exact Results in the Wilson Loop Defect CFT: Bulk-Defect OPE, Nonplanar Corrections and Quantum Spectral Curve*, *J. Phys. A* **52** (2019) 125401 [[arXiv:1811.02369](#)] [[INSPIRE](#)].
- [32] D. Grabner, N. Gromov and J. Julius, *Excited States of One-Dimensional Defect CFTs from the Quantum Spectral Curve*, *JHEP* **07** (2020) 042 [[arXiv:2001.11039](#)] [[INSPIRE](#)].
- [33] J. Julius, *Modern techniques for solvable models*, Ph.D. thesis, King's College London, Strand, London, WC2R 2LS, U.K. (2021) [[INSPIRE](#)].
- [34] N. Gromov, J. Julius, Á. Hegedús and N. Sokolova, *Quantum Spectral Curve Solver for Full Spectrum of one-dimensional Wilson Line-defect Superconformal Field Theory*, to appear.
- [35] D. Bombardelli et al., *The full Quantum Spectral Curve for AdS_4/CFT_3* , *JHEP* **09** (2017) 140 [[arXiv:1701.00473](#)] [[INSPIRE](#)].
- [36] D. Bombardelli, A. Cavaglià, R. Conti and R. Tateo, *Exploring the spectrum of planar AdS_4/CFT_3 at finite coupling*, *JHEP* **04** (2018) 117 [[arXiv:1803.04748](#)] [[INSPIRE](#)].
- [37] D.H. Correa, V.I. Giraldo-Rivera and M. Lagares, *Integrable Wilson loops in ABJM: a Y-system computation of the cusp anomalous dimension*, *JHEP* **06** (2023) 179 [[arXiv:2304.01924](#)] [[INSPIRE](#)].
- [38] R.N. Lee and A.I. Onishchenko, *ABJM quantum spectral curve and Mellin transform*, *JHEP* **05** (2018) 179 [[arXiv:1712.00412](#)] [[INSPIRE](#)].
- [39] R.N. Lee and A.I. Onishchenko, *Toward an analytic perturbative solution for the ABJM quantum spectral curve*, *Teor. Mat. Fiz.* **198** (2019) 292 [[arXiv:1807.06267](#)] [[INSPIRE](#)].
- [40] R.N. Lee and A.I. Onishchenka, *ABJM quantum spectral curve at twist I: algorithmic perturbative solution*, *JHEP* **11** (2019) 018 [[arXiv:1905.03116](#)] [[INSPIRE](#)].
- [41] A. Cavaglià et al., *Quantum Spectral Curve for AdS_3/CFT_2 : a proposal*, *JHEP* **12** (2021) 048 [[arXiv:2109.05500](#)] [[INSPIRE](#)].
- [42] S. Ekhammar and D. Volin, *Monodromy bootstrap for $SU(2|2)$ quantum spectral curves: from Hubbard model to AdS_3/CFT_2* , *JHEP* **03** (2022) 192 [[arXiv:2109.06164](#)] [[INSPIRE](#)].
- [43] A. Cavaglià, S. Ekhammar, N. Gromov and P. Ryan, *Exploring the Quantum Spectral Curve for AdS_3/CFT_2* , *JHEP* **12** (2023) 089 [[arXiv:2211.07810](#)] [[INSPIRE](#)].
- [44] C. Marboe and E. Widén, *The fate of the Konishi multiplet in the β -deformed Quantum Spectral Curve*, *JHEP* **01** (2020) 026 [[arXiv:1902.01248](#)] [[INSPIRE](#)].
- [45] F. Levkovich-Maslyuk and M. Preti, *Exploring the ground state spectrum of γ -deformed $N = 4$ SYM*, *JHEP* **06** (2022) 146 [[arXiv:2003.05811](#)] [[INSPIRE](#)].
- [46] D. Grabner, N. Gromov, V. Kazakov and G. Korchemsky, *Strongly γ -Deformed $\mathcal{N} = 4$ Supersymmetric Yang-Mills Theory as an Integrable Conformal Field Theory*, *Phys. Rev. Lett.* **120** (2018) 111601 [[arXiv:1711.04786](#)] [[INSPIRE](#)].
- [47] V. Kazakov, *Quantum Spectral Curve of γ -twisted $\mathcal{N} = 4$ SYM theory and fishnet CFT*, [arXiv:1802.02160](#) [[DOI:10.1142/9789813233867_0016](#)] [[INSPIRE](#)].
- [48] R. Klabbers, *Quantum spectral curve for the η -deformed $AdS_5 \times S^5$ superstring*, Ph.D. thesis, Universität Hamburg, 22761 Hamburg, Germany (2017) [[arXiv:1804.06741](#)] [[INSPIRE](#)].

- [49] R. Klabbers and S.J. van Tongeren, *Quantum Spectral Curve for the eta-deformed $AdS_5 \times S^5$ superstring*, *Nucl. Phys. B* **925** (2017) 252 [[arXiv:1708.02894](#)] [[INSPIRE](#)].
- [50] T. Harmark and M. Wilhelm, *The Hagedorn temperature of AdS_5/CFT_4 at finite coupling via the Quantum Spectral Curve*, *Phys. Lett. B* **786** (2018) 53 [[arXiv:1803.04416](#)] [[INSPIRE](#)].
- [51] T. Harmark and M. Wilhelm, *Solving the Hagedorn temperature of AdS_5/CFT_4 via the Quantum Spectral Curve: chemical potentials and deformations*, *JHEP* **07** (2022) 136 [[arXiv:2109.09761](#)] [[INSPIRE](#)].
- [52] S. Ekhammar, J.A. Minahan and C. Thull, *The asymptotic form of the Hagedorn temperature in planar super Yang-Mills*, *J. Phys. A* **56** (2023) 435401 [[arXiv:2306.09883](#)] [[INSPIRE](#)].
- [53] L.F. Alday, T. Hansen and J.A. Silva, *AdS Virasoro-Shapiro from dispersive sum rules*, *JHEP* **10** (2022) 036 [[arXiv:2204.07542](#)] [[INSPIRE](#)].
- [54] L.F. Alday, T. Hansen and J.A. Silva, *AdS Virasoro-Shapiro from single-valued periods*, *JHEP* **12** (2022) 010 [[arXiv:2209.06223](#)] [[INSPIRE](#)].
- [55] F. Gliozzi, J. Scherk and D.I. Olive, *Supersymmetry, Supergravity Theories and the Dual Spinor Model*, *Nucl. Phys. B* **122** (1977) 253 [[INSPIRE](#)].
- [56] L. Brink, J.H. Schwarz and J. Scherk, *Supersymmetric Yang-Mills Theories*, *Nucl. Phys. B* **121** (1977) 77 [[INSPIRE](#)].
- [57] M.F. Sohnius and P.C. West, *Conformal Invariance in $N = 4$ Supersymmetric Yang-Mills Theory*, *Phys. Lett. B* **100** (1981) 245 [[INSPIRE](#)].
- [58] S. Mandelstam, *Light Cone Superspace and the Ultraviolet Finiteness of the $N = 4$ Model*, *Nucl. Phys. B* **213** (1983) 149 [[INSPIRE](#)].
- [59] P.S. Howe, K.S. Stelle and P.K. Townsend, *Miraculous Ultraviolet Cancellations in Supersymmetry Made Manifest*, *Nucl. Phys. B* **236** (1984) 125 [[INSPIRE](#)].
- [60] L. Brink, O. Lindgren and B.E.W. Nilsson, *$N = 4$ Yang-Mills Theory on the Light Cone*, *Nucl. Phys. B* **212** (1983) 401 [[INSPIRE](#)].
- [61] V.K. Dobrev and V.B. Petkova, *All Positive Energy Unitary Irreducible Representations of Extended Conformal Supersymmetry*, *Phys. Lett. B* **162** (1985) 127 [[INSPIRE](#)].
- [62] J.A. Minahan and K. Zarembo, *The Bethe ansatz for $N = 4$ superYang-Mills*, *JHEP* **03** (2003) 013 [[hep-th/0212208](#)] [[INSPIRE](#)].
- [63] G. 't Hooft, *A Planar Diagram Theory for Strong Interactions*, *Nucl. Phys. B* **72** (1974) 461 [[INSPIRE](#)].
- [64] E. Witten, *Baryons in the $1/n$ Expansion*, *Nucl. Phys. B* **160** (1979) 57 [[INSPIRE](#)].
- [65] M.B. Green, J.H. Schwarz and L. Brink, *$N = 4$ Yang-Mills and $N = 8$ Supergravity as Limits of String Theories*, *Nucl. Phys. B* **198** (1982) 474 [[INSPIRE](#)].
- [66] S. Rychkov, *EPFL Lectures on Conformal Field Theory in $D \geq 3$ Dimensions*, [arXiv:1601.05000](#) [[DOI:10.1007/978-3-319-43626-5](#)] [[INSPIRE](#)].
- [67] D. Simmons-Duffin, *The Conformal Bootstrap*, in the proceedings of the *Theoretical Advanced Study Institute in Elementary Particle Physics: New Frontiers in Fields and Strings*, Boulder, U.S.A., June 01–26 (2015) [[DOI:10.1142/9789813149441_0001](#)] [[arXiv:1602.07982](#)] [[INSPIRE](#)].
- [68] P. Di Francesco, P. Mathieu and D. Senechal, *Conformal Field Theory*, Springer-Verlag, New York (1997) [[DOI:10.1007/978-1-4612-2256-9](#)].

- [69] D. Poland, S. Rychkov and A. Vichi, *The Conformal Bootstrap: Theory, Numerical Techniques, and Applications*, *Rev. Mod. Phys.* **91** (2019) 015002 [[arXiv:1805.04405](#)] [[INSPIRE](#)].
- [70] L. Andrianopoli and S. Ferrara, *On short and long $SU(2, 2/4)$ multiplets in the AdS/CFT correspondence*, *Lett. Math. Phys.* **48** (1999) 145 [[hep-th/9812067](#)] [[INSPIRE](#)].
- [71] L. Andrianopoli, S. Ferrara, E. Sokatchev and B. Zupnik, *Shortening of primary operators in N extended $SCFT_4$ and harmonic superspace analyticity*, *Adv. Theor. Math. Phys.* **4** (2000) 1149 [[hep-th/9912007](#)] [[INSPIRE](#)].
- [72] S. Lee, S. Minwalla, M. Rangamani and N. Seiberg, *Three point functions of chiral operators in $D = 4$, $N = 4$ SYM at large N* , *Adv. Theor. Math. Phys.* **2** (1998) 697 [[hep-th/9806074](#)] [[INSPIRE](#)].
- [73] G. Arutyunov, S. Frolov and A.C. Petkou, *Operator product expansion of the lowest weight CPOs in $\mathcal{N} = 4$ SYM₄ at strong coupling*, *Nucl. Phys. B* **586** (2000) 547 [[hep-th/0005182](#)] [[INSPIRE](#)].
- [74] F.A. Dolan and H. Osborn, *On short and semi-short representations for four-dimensional superconformal symmetry*, *Annals Phys.* **307** (2003) 41 [[hep-th/0209056](#)] [[INSPIRE](#)].
- [75] N. Beisert, *The complete one loop dilatation operator of $N = 4$ superYang-Mills theory*, *Nucl. Phys. B* **676** (2004) 3 [[hep-th/0307015](#)] [[INSPIRE](#)].
- [76] M. Gunaydin and N. Marcus, *The spectrum of the S^5 Compactification of the Chiral $N = 2$, $D = 10$ Supergravity and the Unitary Supermultiplets of $U(2, 2/4)$* , *Class. Quant. Grav.* **2** (1985) L11 [[INSPIRE](#)].
- [77] I. Bars and M. Gunaydin, *Unitary Representations of Noncompact Supergroups*, *Commun. Math. Phys.* **91** (1983) 31 [[INSPIRE](#)].
- [78] N. Beisert, *The dilatation operator of $N = 4$ super Yang-Mills theory and integrability*, *Phys. Rept.* **405** (2004) 1 [[hep-th/0407277](#)] [[INSPIRE](#)].
- [79] N. Beisert, *The $su(2|3)$ dynamic spin chain*, *Nucl. Phys. B* **682** (2004) 487 [[hep-th/0310252](#)] [[INSPIRE](#)].
- [80] N. Gromov, F. Levkovich-Maslyuk and G. Sizov, *New Construction of Eigenstates and Separation of Variables for $SU(N)$ Quantum Spin Chains*, *JHEP* **09** (2017) 111 [[arXiv:1610.08032](#)] [[INSPIRE](#)].
- [81] J.M. Maillet and G. Niccoli, *On quantum separation of variables*, *J. Math. Phys.* **59** (2018) 091417 [[arXiv:1807.11572](#)] [[INSPIRE](#)].
- [82] P. Ryan and D. Volin, *Separated variables and wave functions for rational $gl(N)$ spin chains in the companion twist frame*, *J. Math. Phys.* **60** (2019) 032701 [[arXiv:1810.10996](#)] [[INSPIRE](#)].
- [83] J.M. Maillet and G. Niccoli, *Complete spectrum of quantum integrable lattice models associated to $Y(\mathfrak{gl}(n))$ by separation of variables*, *SciPost Phys.* **6** (2019) 071 [[arXiv:1810.11885](#)] [[INSPIRE](#)].
- [84] P. Ryan and D. Volin, *Separation of Variables for Rational $\mathfrak{gl}(n)$ Spin Chains in Any Compact Representation, via Fusion, Embedding Morphism and Bäcklund Flow*, *Commun. Math. Phys.* **383** (2021) 311 [[arXiv:2002.12341](#)] [[INSPIRE](#)].
- [85] J.M. Maillet, G. Niccoli and L. Vignoli, *On Scalar Products in Higher Rank Quantum Separation of Variables*, *SciPost Phys.* **9** (2020) 086 [[arXiv:2003.04281](#)] [[INSPIRE](#)].
- [86] A. Cavaglià, N. Gromov and F. Levkovich-Maslyuk, *Separation of variables and scalar products at any rank*, *JHEP* **09** (2019) 052 [[arXiv:1907.03788](#)] [[INSPIRE](#)].

- [87] N. Gromov, F. Levkovich-Maslyuk and P. Ryan, *Determinant form of correlators in high rank integrable spin chains via separation of variables*, *JHEP* **05** (2021) 169 [[arXiv:2011.08229](#)] [[INSPIRE](#)].
- [88] A. Cavaglià, N. Gromov and F. Levkovich-Maslyuk, *Separation of variables in AdS/CFT: functional approach for the fishnet CFT*, *JHEP* **06** (2021) 131 [[arXiv:2103.15800](#)] [[INSPIRE](#)].
- [89] N. Gromov, N. Primi and P. Ryan, *Form-factors and complete basis of observables via separation of variables for higher rank spin chains*, *JHEP* **11** (2022) 039 [[arXiv:2202.01591](#)] [[INSPIRE](#)].
- [90] C. Bercini, A. Homrich and P. Vieira, *Structure Constants in $\mathcal{N} = 4$ SYM and Separation of Variables*, [arXiv:2210.04923](#) [[INSPIRE](#)].
- [91] N. Gromov, *Introduction to the Spectrum of $\mathcal{N} = 4$ SYM and the Quantum Spectral Curve*, [arXiv:1708.03648](#) [[INSPIRE](#)].
- [92] S.S. Gubser, I.R. Klebanov and A.M. Polyakov, *Gauge theory correlators from noncritical string theory*, *Phys. Lett. B* **428** (1998) 105 [[hep-th/9802109](#)] [[INSPIRE](#)].
- [93] R. Roiban and A.A. Tseytlin, *Quantum strings in $AdS_5 \times S^5$: Strong-coupling corrections to dimension of Konishi operator*, *JHEP* **11** (2009) 013 [[arXiv:0906.4294](#)] [[INSPIRE](#)].
- [94] A.A. Tseytlin, *Quantum strings in $AdS_5 \times S^5$ and AdS/CFT duality*, *Int. J. Mod. Phys. A* **25** (2010) 319 [[arXiv:0907.3238](#)] [[INSPIRE](#)].
- [95] S. Frolov, *Konishi operator at intermediate coupling*, *J. Phys. A* **44** (2011) 065401 [[arXiv:1006.5032](#)] [[INSPIRE](#)].
- [96] F. Passerini, J. Plefka, G.W. Semenoff and D. Young, *On the Spectrum of the $AdS_5 \times S^5$ String at large λ* , *JHEP* **03** (2011) 046 [[arXiv:1012.4471](#)] [[INSPIRE](#)].
- [97] L.F. Alday, T. Hansen and J.A. Silva, *On the spectrum and structure constants of short operators in $\mathcal{N} = 4$ SYM at strong coupling*, *JHEP* **08** (2023) 214 [[arXiv:2303.08834](#)] [[INSPIRE](#)].
- [98] M. Bianchi, J.F. Morales and H. Samtleben, *On stringy $AdS_5 \times S^5$ and higher spin holography*, *JHEP* **07** (2003) 062 [[hep-th/0305052](#)] [[INSPIRE](#)].
- [99] L.F. Alday, T. Hansen and J.A. Silva, Private communication.
- [100] C. Cordova, T.T. Dumitrescu and K. Intriligator, *Multiplets of Superconformal Symmetry in Diverse Dimensions*, *JHEP* **03** (2019) 163 [[arXiv:1612.00809](#)] [[INSPIRE](#)].
- [101] F.A. Dolan and H. Osborn, *Superconformal symmetry, correlation functions and the operator product expansion*, *Nucl. Phys. B* **629** (2002) 3 [[hep-th/0112251](#)] [[INSPIRE](#)].
- [102] F.A. Dolan and H. Osborn, *Conformal partial waves and the operator product expansion*, *Nucl. Phys. B* **678** (2004) 491 [[hep-th/0309180](#)] [[INSPIRE](#)].
- [103] G.F. Chew and S.C. Frautschi, *Regge Trajectories and the Principle of Maximum Strength for Strong Interactions*, *Phys. Rev. Lett.* **8** (1962) 41 [[INSPIRE](#)].
- [104] L.F. Alday and T. Hansen, *The AdS Virasoro-Shapiro amplitude*, *JHEP* **10** (2023) 023 [[arXiv:2306.12786](#)] [[INSPIRE](#)].
- [105] S.M. Chester, R. Dempsey and S.S. Pufu, *Bootstrapping $\mathcal{N} = 4$ super-Yang-Mills on the conformal manifold*, *JHEP* **01** (2023) 038 [[arXiv:2111.07989](#)] [[INSPIRE](#)].
- [106] H. Paul, E. Perlmutter and H. Raj, *Integrated correlators in $\mathcal{N} = 4$ SYM via $SL(2, \mathbb{Z})$ spectral theory*, *JHEP* **01** (2023) 149 [[arXiv:2209.06639](#)] [[INSPIRE](#)].

- [107] L.D. Faddeev, *How algebraic Bethe ansatz works for integrable model*, in the proceedings of the *Les Houches School of Physics: Astrophysical Sources of Gravitational Radiation*, Les Houches, France, September 26 – October 06 (1995) [[hep-th/9605187](#)] [[INSPIRE](#)].